IJEST

ISSN: 0973-6255
Vol. 11 No.1
January - June 2017

Indian Journal of Engineering, Science, and Technology

A Refereed Research Journal









Published by

BANNARI AMMAN INSTITUTE OF TECHNOLOGY
(Autonomous Institution Affiliated to Anna University of Technology, Coimbatore -
Approved by AICTE - Accredited by NBA and NAAC with "A" Grade)
Sathyamangalam - 638 401 Erode District Tamil Nadu India
Ph: 04295-226340 - 44 Fax: 04295-226666
www.bitsathy.ac.in E-mail: ijest@bitsathy.ac.in

BANNARI AMMAN INSTITUTE OF TECHNOLOGY
Stay Ahead

Indian Journal of Engineering, Science, and Technology

IJEST is a refereed research journal published half-yearly by Bannari Amman Institute of Technology. Responsibility for the contents rests upon the authors and not upon the IJEST. For copying or reprint permission, write to Copyright Department, IJEST, Bannari Amman Institute of Technology, Sathyamanagalam, Erode District - 638 401, Tamil Nadu, India.

Indian Journal of Engineering, Science, and Technology

ISSN: 0973-6255

Volume 11 Number 1 **January - June 2017**

CONTENTS

Excerpt from the Proceeding of National Conference

Optimization of Mechanical Property of Automobile Components through Implementation of Super Hydrophobic Nano Colloid by Surface Finishing

A. Dineshkumar, S. Vasanthaseelan, S.Dineshkumar, R. Elavarsan, G. Vijay and K. Kavin Surya
Department of Automobile Engineering, SNS College of Technology, Coimbatore - 641 035, Tamil Nadu
E-mail: dineshau17@gmail.com, vasanthaseelan.s@gmail.com

Abstract

It is essential to product the chassis and other automotive parts from water, corrosion and mud, By using Nano composite with Superhydrophobic property. In this research static and dynamic analysis were carried out with the aid of CATIA for existing dimensions and analysis of chassis design by using through ANSYS before and after of coating superhydrophobic mater. Dynamic analysis states that varying the frequency in different point to find the deflection, that point will have standard load at any time. Static analysis state that load acting at a point any time in that point load will be applied. Then we have to make the colloid of polystyrene with Mangese oxide to form a superhydrophobic coating, this is to be formed in a correct ratio. By using the equipment's Goinmeter to find the exact contact angle and Scanning Electron Microcope (SEM) to find bonding were Nano particles are analysed. Mangese oxide polystyrene Nano composite solution has been ready to get superhydrophobic coating on the substrate. The centralized coating technique is used to coat the specimen surface using spin coating mechanism. Followed by various testing methods such as, corrosion test, impact test, hardness test (Brinell) and weight analysis are carried out to analysis the mechanical properties such as brittleness, ductility, shear strength, stiffness etc.

Keywords: *Corrosion test, Contact angle, Hardness test (Brinell), Manganese oxide, Nano, Polystyrene, SEM*

1. INTRODUCTION

In current research hydrophobic surface gained extreme interest among researcher because of its advantage over industrial application and micro structural physical properties. Biomimetic normally known as artificial material posing a characteristics similar to the natural material, for example superhydrophobic material has a special property of liquid repellent property due to its enhanced hydrophobicity property which is similar to Lotus leaf property of repelling water. This hydrophobicity property of superhydrophobic material drawn the high interest towards researcher and development of its application in automobile industries, space craft manufacturing. Also that property of anti-sticking, self-cleaning properties enhanced its vast application. Among the superhydrophobic material such as MnO/PS Nano composite, ZnO-PS Nano composite, precipitated Calcium carbonate, Carbon Nano-tube composite, potassium titanate whiskers and polyetheretherketone (PEEK), ZnO- PS composite drawn a favourable superhydrophobic properties since it has vase application in manufacturing rubbers, plastic, ceramic, glass due to its superhydrophobic property of water contact angle more than 150^{O}. The surface roughness and wettability also seemed will be more acceptable. Surface wetting behaviour can be take into four different regions less than 10^{O} to 90^{O}, 90^{O} to 150^{O} and above 150^{O}. up to 90^{O} water contact angle surface of the material is considered as hydrophilic due to its strong attraction towards water, whereas above 150^{O} posies superhydrophobic where the percentage of water attraction towards the surface of the material is very low. On taking the account of zinc oxide polystyrene Nano composite the advantage whereas follow its one of the most economical way of the creating superhydrophobic coating in numerous systematic way such as Gel based system, Aero sell spray and by dipping the object. In contrast on the effect of Zinc oxide polystyrene Nano composite has more durable property on gel based coating than other [3,4].

Cheng.et.al in their paper title fabrication of Superhydrophobic and Superoleophilic polystyrene surface by a facile one-step method discuss about preparation of superhydrophobic and Superoleophilic surface with the aid of polystyrene in the absence of any modification simultaneously, they discuss about microbeads and Nano fibre structure, preparation through electro spring method and property of oil sorbent [5].Wang.et.al in his research article The effect of self-

assembly modified potassium titanate whiskers on the friction and wear behaviours of PEEK composites discuss about self-assembling of Polytetrafluoroethylene (PTFE) polyetheretherketone (PEEK) in the presence of potassium titanate whiskers and n-octade cyltrichlorosilane (OTS). It discusses about tribological mechanical properties of PTFE and PEEK with respect to matrix formation dispersion and interfacial compatibility in which OTS seemed to be better self-assembling surface property [2].

In Corrosion behaviour of superhydrophobic surface; A review, Adel,et.al proposed a review on surface wetting and stability of superhydrophobic material with respect to specific surface material such as morphology, roughness and surface chemistry. Also he compared the theory superhydrophobic such as contact angle and young equation and rough surface with Wenzel and Cassic Baxter models. The competence technique for manufacturing superhydrophobic material such as sol-gel process, layer by layer self-assembly icing chemical and electro chemical deposing respectively. Finally, he concludes the stability of superhydrophobic surface with respect to solvent stability, Ph. stability, Thermal stability, Humidity stability and UV stability [1].

Lin.et.al in their paper Superhydrophobic surface from Natural to Artificial discuss about naval method to construct superhydrophobic surface with respect to high contact angle, multi scale structure that have significant effect of reduce angle of water droplets, on the other hand micro array structure have constant influence on Superhydrophobicity[6]. In the paper Superhydrophobic surface develop by Mimicking Hierarchical Surface Morphology of Lotus leaf discuss about the primitive property such as self-cleaning, anti- corrosion and non metability collecting known as lotus effect. It discusses with reference to high water contact angle of above 150^{O} and slow slide angle less that 10^{O} stance the major explosion of artificial superhydrophobic material. Also they briefly reviewed about Mimicking natural superhydrophobic property of lotus to artificial material with respect to micro and Nano structure using various polymers. In this current research MnO polystyrene was employed to evaluate superhydrophobic and subject to hardness, corrosion and SEM test and results were evaluated separately [7].

2.0. EXPERIMENTATION

2.1. Pre-processing of Coating Material

In pre-processing of coating material MnO was purchased from local vendor – Chennai of research quality. MnO employed in pre-processing of coating material is found to have 4.8 g/cm^3 density with high melting point at 1989^{O}C. Also it has high solubility range of 0.0004% at 17.8^{O}C and Refractive index of 2 [8,11]. Table 1 shows the property of MnO.

Manganese oxide obtained was in the form of crystalline, further processing involves grinding of MnO to powder form for subjection to UV testing in order to manipulate the crystal size. This crystal size graphing was recorded in order to fix the required size/acquire the required size for processing. Figure 1&2 represents the ultra violet spectroscopic for crystal size graphing of MnO.

Table 1 Properties of MnO.

Chemical Formula	MnO
Appearance	Brown solid
Density	4.8 g/cm^3
Melting point	1565^{O}C
Solubility in water	0.0004% (17.8^{O}C)
Refractive Index	2

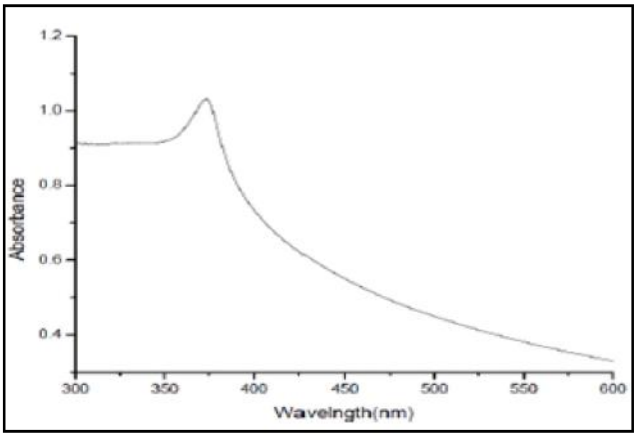

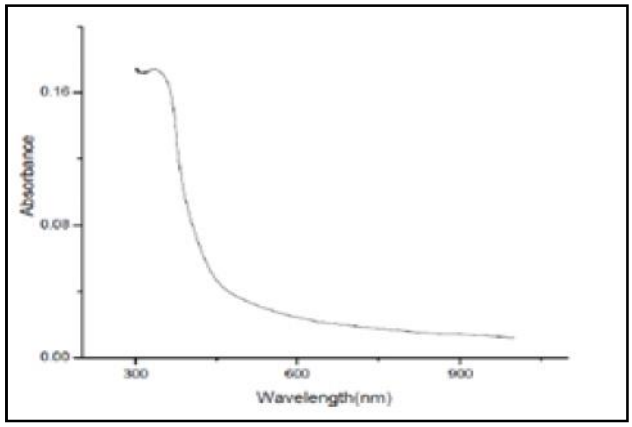

Fig. 1 & 2 UV spectrometer analysis for crystal size graphing of MnO.

Further MnO was surface washed in the presence of methanol in Ultracentrifuge (C.24 BL). Table 2 specifies the technical attributes of Ultracentrifuge used.

Table 2 Technical Specification of Ultracentrifuge

Maximum Capacity	3.0 Liter
Speed	20000 RPM
Weight	128kg
Timed Run	Up to 99 hours, 59 min
Rotor Capacity	4×750 mL
Electrical Requirements	60Hz, 120V

In Ultracentrifuge for varying the RPM between 2000-4000 RPM for the period of 20-30 mins MnO was subjected to surface wash with methanol. Resulting MnO obtained was sedimented in rotor tube at ultrapure stage.

2.2. Fabrication of MnOPS Composite Coating Material

In the process of fabrication ultrapure MnO obtained was mixed with polystyrene in the liquid state at 260^{O} to 270^{O}. Initially varying polystyrene ratio of 2 to 6 % of MnO was tested. In which 9.5:0.5 % of MnO to polystyrene stands the best and optimized colloidal mixture [9]. The mixing of MnO to Polystyrene was carried out in the presence of integrated thermocouple for generating heat and thermal magnetic stirrer. Properties of polystyrene was show in table 3.

Table 3 Properties of Polystyrene

Density	0.94-1.04g/cm^2
Melting Point	240^{O}C
Refractive Index	1.6
Young's Modulus	3000-3600 MPa
Tensile Strength	46-60 MPa
Specific Heat	1.3 kJ/(kg.K)

Specimen to be testing with superhydrophobic coating was initially surface grinding and cleaned with methanol. Various techniques intended for coating material on specimen were as follows get based system, aero-sol spray and by dipping the object [12,13]. Here gel- based system was employed because of its optimized usage of coating material and even spreading of coat on the surface. Technical specification for Spin coater machine NXG-P1 was illustrated in table 4.

Table 4 Technical Specification of Spin Coater

Maximum Speed	10000RPM
Acceleration/Deceleration	1-25.5 seconds
Weight	17.3kg
Vacuum Input	17 to 25 Hg
Power Input	115V, 230AC

Specimen to be coated is fixed on the holder at 20-35 bar pressure in order to avoid slipping of specimen during coating. Initially disc is rotated at the speed of 3000rpm for 30 seconds with acceleration during this process colloidal calculation is made to be dropped at the centre with the aid of micro pipette for the higher accuracy this step is again repeated for varying rpm for increasing time and constant acceleration for even coating of Superhydrophobic colloidal coat on the specimen at constant rate [10].

3.0. RESULT AND DISCUSSION

Specimen coated with Manganese oxide polystyrene composite coating to enhance the superhydrophobic property of the base material was subjected to hardness test, corrosion test and SEM test and results were summarised as below.

3.1. SEM test

Scanning Electron Microscope analysis was employed on powder zinc oxide. It was analysis of particle, failure analysis on mixing with polystyrene external morphologic characteristic and orientation of the material with respect to specimen. Here SEM instrument used for analysis has a capacity of X25 to X1,000,000 magnifications, maximum accelerating voltage of 30 kV with built in energy filter, aperture angle control lens and dictator and general beam. And figure 3, 4, 5, 6 shows the Nano structure of MnO at standard accelerating voltage of 20 kV was varying magnification resolution of X20K, X30K, X10K and X55K, it can be concluded at particle size is Nano structured enough to be coated on specimen. Technical specification of scanning electron microscope is shown in Table 5. The close size of the coated of the particle can be measure up to 15ØßmØßm, 0.55ØßmØßm 0.25ØßmØßm [14].

Table 5 Technical Specification of Scanning Electron Microscope

Magnification	25 to 1,000,000
Accelerating Voltage	0.1kV to 30kV
Digital Image	1280×960 pixels
Energy Filter	New r-filter
Aperture Angle Control Lens	Built-in
Detectors	Upper detector, Lower detector
Gentle Beam	Built-in
Rotation	360°

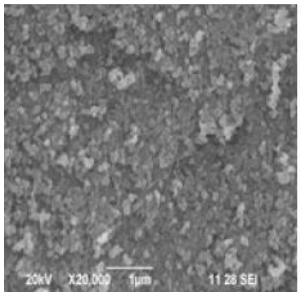

Fig.3 SEM image at 20K Optical Zoom

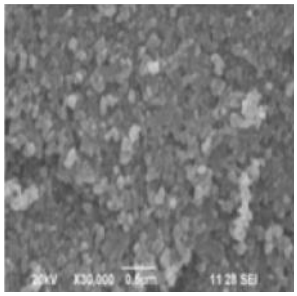

Fig.4 SEM image at 30K Optical Zoom

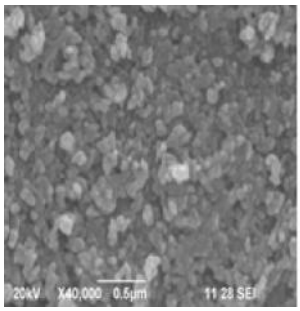

Fig.5 SEM image at 40K Optical Zoom

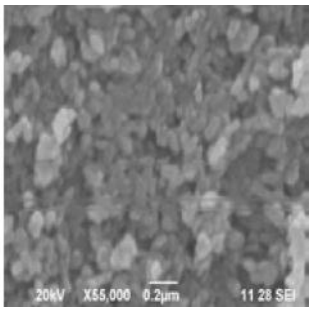

Fig.6 SEM image at 55K Optical Zoom

3.2 Hardness Test

Hardness test is experimented on coated and uncoated specimen (MnO/PS coating). This is carried out in order to explore the stiffness/temper or resistance of metal to plastic deformation commonly by indentation. Brinell hardness test is carried out in which indenter will standard ball diameter of 10mm was employed. Table 6 represents the technical specification of brinell hardness testing machine employed. Here load apply is 3000 N. Diameter of indentation on the specimen with coating and without coating was observed under microscopic environment. The trail was repeated for 3 times and average of Brinell hardness number (BHN) was found to be 391 for the specimen with coating on comparing with specimen without coating of 242 BHN, from this we can concluded the hardness of the material increases after coating due to the effect of MnO/PS composite coating [16]. Reading and calculations were shown in table 7.

Table 6 Technical Specification of Brinell Hardness Testing Machine

Maximum Load	3000 N
Size of base mm	165×425
Diameter of the Indenter	2.5mm, 5mm, 10mm
Machine Height	650mm
Maximum Test Height	225mm
Weight	65kg

Table 7 Calculation for Brinell Hardness Number

Sl. No.	Ball Diameter (mm)	Load Applied P in N	Diameter of Indentation 'd' (mm)		BHN	
			With Coating	Without Coating	With Coating	Without Coating
1	10	3000	4.6	5.3	370.46	237.21
2	10	3000	4.3	5.1	458.19	267.85
3	10	3000	4.7	5.4	346.45	223.43

3.4 Corrosion Test

Main aim of the experimental investigation is to reduce the rate of corrosion and to enhance the superhydrophobic property of material with aid of Nano composite coating. Here the specimen (coated and uncoated) is subject to corrosion under heavy water (of high salt and iron constant) and soft water (employed of laboratory purpose) observation were made at the internal of 6 hrs up to 56 hrs the experiment is repeated twice and the result shows rate of corrosion by formation rust over the specimen seems to the higher with uncoated specimen whereas specimen coated was stable and rate of corrosion seems to be very low [15]. Figures 5 & 6 shows that inference taken at 28 hrs of observation under hard water and soft water.

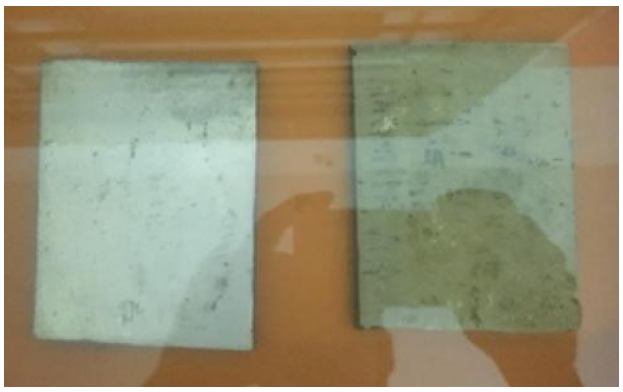

Fig.7 Observation in Hard water

Fig.8 Observation in Soft water

3.5 Contact Angle Measurement

Superhydrophobicity of the object is determined by its contact angle with water droplets. Here water is made fall on the specimen surface was illuminated with the aid of high beam light in order capture the water droplet and specimen with aid of high resolution camera. The image output obtain was subject to microscopically analysis. Figure 7 shows the contact angle measurement of image taken. In which the contact angle for superhydrophobic material [17].

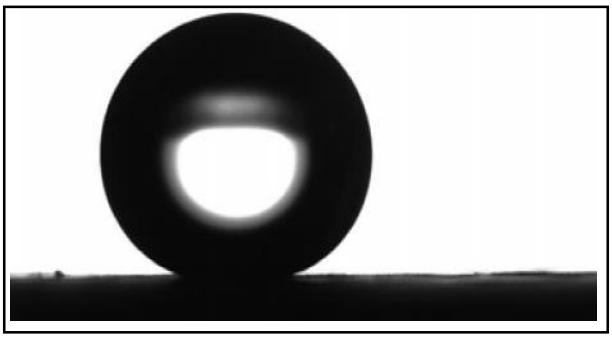

Fig.9 Contact angle measurement image

4. CONCLUSION

- Formulation of Nano composite coating (MnOPS) was carried water static experimental condition. Enhanced ratio of polystyrene zinc oxide was found to be 11:0.5 which is optimal mixing ratio for colloidal coating.
- Ultracentrifuge and spin coater were employed to purify the MnO and to make the superhydrophobic coating on the test specimen.
- SEM test was carried out between zooming of 20k to 55k at 20kV and molecule of microscope size 0.25ØßŠØZÜ to 15ØßŠØZÜ were found.

- Hardness test and corrosion test were carried out on specimen with coating and without coating in which specimen with Nano composite coat seems to have better Brinell hardness number and high corrosion resistance.
- Ultimate property of Superhydrophobicity i.e. contact angle between water drop and specimen was measured at the aid of Goniometer in which result obtained source contact angle of 154^{O}.

Above result were interconnected and interpreted to quantify the superhydrophobic layer coating on specimen and the result sources positive variation and better superhydrophobic layer formation.

REFERENCES

[1] Adel M.A. Mohamed, Aboubakr M. Abdullah, Nathalie A. Younan, "Corrosion Behaviour of Superhydrophobic Surface: A Review", Arabian Journal of Chemistry, 2014, http://dx.doi.org/10.1016/j.arabjc.2014.03.006

[2] Wang Huaiyuan, Zhu Yanji, Feng Xin, Lu Xiaohua, "The Effect of Assembly Modification Potassium Titanate Whiskers on the Friction and Wear Behaviour of PEEK Composites", Wear 269, 2010, pp.139-144.

[3] Sanjay Subhash Latthe, Annaso Basavraj Gurav, Chavan Shridhar Maruti, Rajiv Shrikant Vhatkar, "Recent Progress in Preparation of Superhydrophobic Surface: A Review", Journal of Surface Engineered Materials and Advanced Technology, Vol.2, 2012, pp.76-94.

[4] Emiliano Lepore, Nicola Pugno, "Super hydrophobic Polystyrene by Direct Copy of a Lotus Leaf", BioNanoSci., Vol.1, 2011, pp.136-143.

[5] Cheng-Wei Tu, Chia-Hua Tsai, Chih- Feng Wang, Shiao-Wei Kuo, Feng-Chih Chang, "Fabrication of Superhydrophobic and Superoleophilic Polystyrene Surface by a Facile One- Step Method", Macromolecular Journals, Vol.28, 2007, pp.2262-2266.

[6] Lin Feng, Shuhong Li, Yingshum Li, Huanjun Li, Lingjuan Zhang, Jin Zhai, Yanlin Song, Biqian Liu, Lei Jiang, Daoben Zhu, "Super-Hydrophobic Surface: From Natural to Artificial", Adv. Mater. 17 Dec 2002, Vol.14, No.24.

[7] Sanjay S. Latthe, Chiaki Terashima, Kazuya Nakata and Akira Fujishima, "Superhydrophobic Surface Developed by Mimicking Hierarchical Surface Morphology of Lotus Leaf", Molecules, Vol.19,2014, pp.4256-4283.

[8] H.Q. Liu, *etal*, "Preparation of Superhydrophobic Coating on Zinc as Effective Corrosion Barriers", ACS Appl. Mater. Interfaces, Vol.1, No.6, 2009c., pp.1150-1153.

[9] C.H. Xue, *et al*, "Large-area Fabrication of Superhydrophobic Surface for Practical Application: A Overview", Sci. Technol. Adv. Mater., Vol.11, No.3, 2010.

[10] R.K. Goyal, A.N. Tiwari, U.P. Mulik, Y.S. Negi, "Novel High Performance Al_2O_3/poly(ether ether ketone) Nanocomposite for Electronic Application", Compos. Sci. Technology, Vol.67 2007, pp.1802-1812.

[11] J.Y. Kim, S.I. Han, D.K. Kim, S.H. Kim, "Mechanical Reinforcement and Crystallization Behaviour of Poly(ethylene 2, 6-naphthalate) Nanocomposite Induced by Modified Carbon Nanotube", Compos. A: Appl. Sci. Manuf., Vol.40 2009, pp.45-53.

[12] X. Zhang, F. Shi, J. Niu, Y.G. Jiang and Z.Wang, "Superhydrophobic Surface: From Structure Control to Functional Application", Journal of Materials Chemistry, Doi:10.1039/b711226b., Vol.18, No. 6, 2008, pp.621-633.

[13] V.V. Ganbavle, U.K.H. Bangi, S.S. Latth, S.A. Mahadik and A.V. Rao, "Self-cleaning Silica Coating on Glass by Single step Sol-gel Route", Surface and Coatings Technology, Doi:10.1016/j.surfcoat.2009.07.113, Vol. 205, No. 23-24, 2011, pp. 5338-5344.

[14] M. Nosonovsky and B. Bhushan, "Wetting of Rough Three-dimension Superhydrophobic Surfaces", Microsystem Technologies, Vol. 12, 2006, pp.273-281.

[15] X. Wu, L. Zheng, D. Wu, "Fabrication of Superhydrophobic Surface from Microstructured ZnO based Surface via A Wet-chemical Route", Langmuir, Vol.21, 2005, pp.2665-2667.

[16] A.Marmur,"The Lotus Effect:Super Hydrophobicity and Metastability", Langmuir 2004, Vol.20, pp.3517-3519.

Modeling and Simulation of A Conventional Powertrain Using Matlab/Simulink

T.Mahendran, J.Aiay Vishwas Anto, A. Kavidevan, K.C. Vetriselvan, K.Kirupa Shankar
Department of Automobile Engineering, S.N.S College of Technology, Coimbatore - 641 035, Tamil Nadu
E-mail: leomahe001@gmail.com

Abstract

This study discusses about modeling and simulation of the entire conventional power train. Modelling and simulation is carried out using MATLAB/SIMULINK package. This package involves the creation of components through visual programming technique as hierarchical sub systems. The powertrain simulation using simulink has an efficient support to optimize cost and duration of the whole engine in terms of technological developments. The series of steps involves the modeling of entire power train, simulation and obtaining the result graphically. Modeling is carried using the specifications of Maruti Alto. After modeling, power train is subjected to simulation process. Simulation results helps to determine the performance characteristics such as engine speed, torque developed for various gear ratios, power loss occurring inside the system and tire torque characteristics. The results are viewed graphically. These results will also establish the interaction between powertrain and vehicle dynamics factors contributing significantly to the vehicle handling and ride response characteristics. Using the results obtained for the conventional power train, modeling and simulation can be carried out for an electric hybrid vehicle. This helps the user to understand the technique and procedure which is involved in complete designing of a power train before the prototype construction begins.

Keywords:*MATLAB/SIMULINK, Simdriveline, Modeling, Simulation and Speed-Torque characteristics.*

1. INTRODUCTION

Computer modeling and simulation can be used to reduce the expense and length of design cycle of conventional vehicles by testing configurations and energy management strategies before prototype construction begins. MATLAB/SIMULINK is a system level modeling, simulation and analysis package to study issues related to conventional vehicle design such as energy efficiency, fuel economy and vehicle emissions.

Simulink is a program that runs as a companion to MATLAB, these programs are developed and marketed by the MathWorks limited. Simulink and MATLAB form a package that serves as a vehicle for modeling dynamic systems. Simulink provides a graphical user interface (GUI) that is used in building block diagrams, performing simulations, as well as analyzing results. Simulink is integrated with MATLAB, providing immediate access to an extensive range of tools that helps the user to develop algorithms, analyze and visualize simulations, create batch processing scripts, customize the modeling environment, and define signal, parameter, and test data.

In SimDriveline, one has an access to all Simulink functionality. Using sensor blocks, one can measure values for velocity, acceleration, and torque and pass these signals into standard Simulink blocks. Actuator blocks enable Simulink signals to define values for driving torques or prescribed motion parameters for shafts.SimDriveline can be used for a variety of automotive, aerospace, defence, and industrial applications. It is particularly suited to the development of controllers for automotive and aerospace industry.

The conventional internal combustion engine driven drive train was designed based on the specifications of a Maruti ALTO. It is a four-door hatch back five-passenger vehicle with a desired 0–60 mph in the 10-s range characteristic and a curb weight of 1580 kg.The vehicles five-speed manual transmission with a clutch retaining is modeled for the same overall gear ratios.

2. METHODOLOGY

2.1 Collected Data

The powertrain modeling and simulation is carried with the help of the standard values and specifications available for Maruti Alto. Engine torque and torque at

gear box for various gear ratios is calculated manually using the specifications and standard values. The table illustrating the specifications along with some standard vales is given below.

Table 1 Specifications and Standard Values of Maruti ALTO

Dimensions and Weights	Overall Length (mm)	3495
	Overall Width (mm)	1475
	Overall Height (mm)	1460
	Wheel Base (mm)	2360
	Ground Clearance (mm)	160
	Front Track (mm)	1295
	Rear Track (mm)	1290
	Kerb Weight (kg)	735
	Gross Vehicle Weight (kg)	1165
	No of Doors	5
Performance	Maximum Speed	137 kmph
	0-100kmph	21.5 s
	Engine Type/Model	FC engine
	Displacement cc	796
	Power (PS@rpm)	47PS @6200rpm
	Torque (Nm@rpm)	62Nm @3000rpm
	Compression Ratio	:1
	No of Cylinders (cylinder)	3
Transmission Data	Transmission Type	Manual
	Gears/Speeds	5Gears
	Gear ratios: first	3.52
	Second	2.16
	Third	1.33
	Fourth	0.9
	Final drive	4.5

2.2 Modeling Using Simdriverline

SimDriveline includes simple vehicle component library that helps the user to develop a complete powertrain model. These models enable early evaluation of overall system performance. Library includes a list of automotive components that can be clicked and dragged to the editor page as illustrated in the figure 2a. By double clicking the component, the necessary dialogue box is appears on the screen representing the appropriate data that can be entered with the help of the specifications.

2.3 Engine

The Gasoline Engine block in Simdriveline models a gasoline-fuel, spark-ignition engine with a speed governor. The engine runs at a variable speed that a user can control with a Simulink throttle signal. The throttle signal directly controls the output torque generated by an engine and indirectly controls the speed at which the engine runs. If the engine speed exceeds the maximum speed than specified by the user, the engine generates no torque.

The block accepts the throttle signal through a Simulink inport. This signal specifies the engine torque as a fraction of the maximum torque possible in a steady state at a fixed engine speed and should lie between 0 and 1. A throttle signal below zero is interpreted as zero and greater than one, as one.

2.4 Clutch

Modeling of clutch involves dragging of friction clutch to the editor page. It is connected to the output of engine through the connector available. By double clicking the clutch model a necessary dialogue box appears which involves certain parameters regarding the type of clutch material. Since the type of clutch material is not mentioned in the manufacturer's catalogue, the standard clutch material is taken from Design Data book. The following table shows the different properties of commonly used clutch materials.

2.5 Gear Box

The purpose of a gear set is to transfer rotational motion and torque at a known ratio from one driveline axis to another. The type of gear box can be selected according to the passenger vehicle from simulink library. By dragging the component, the selected gear box is bought to the editor page. The clutch output and the gear box can be joined using the connector. By double clicking the gear box, a dialogue box specifying the necessary gear ratio is obtained.

The choice of signs indicates that the gears can spin in the same or in opposite directions. If the gears are external to one another (rotating on their respective outside surfaces), they rotate in opposite directions. If the gears are internal to one another (rotating with the outside of the smaller gear meshing with inside of the larger gear), they rotate in the same direction.

2.6 Torque Sensor

The Torque Sensor block measures the torque transferred along a driveline axis at the point where the Torque Sensor is inserted. A positive torque is transferred from the base (B) axis to the follower (F) axis at that point if the follower axis accelerates positively with respect to the base and if no other torques are applied to the follower-connected inertias. The torque is output as a Simulink signal in newton-meters.

2.7 Differential

The Differential block represents a differential gear that couples rotational motion about the longitudinal axis to rotational motion about two lateral axes. Any one of the lateral axis can be considered as an input. In normal use, the longitudinal shaft is the input, and motion, torque, and power flow out through the lateral shafts. The output axes, in general, have different angular velocities. The longitudinal motion is divided by the drive gear ratio that a user can specify and then split between the two lateral shafts.

2.8 Tires

The Tire block models a vehicle tire in contact with the road. The driveline port transfers the torque from the wheel axis to the tire. The user must specify the vertical load Fz and vehicle longitudinal velocity Vx as Simulink input signals. The model provides the tire angular velocity Ω and the longitudinal force Fx on the vehicle as Simulink output signals. The convention for the Fz signal is positive downward.

3. MODELING A POWER TRAIN

A power train is a system of mechanical parts in a vehicle that first produces energy, then converts it in order to propel it, whether it be an automobile, boat or other machinery. The model includes engine, transmission system, differential unit and rotating tires. Longitudinal vehicle dynamics is also added in order to carry out the real time simulation. Inertia is added to all rotating components including gear box, differential components and tires.

Signal builder model is used to generate the input signals to the engine and clutch. Input signal of the engine includes the throttling conditions such as part or full throttle operations. Clutch pressure required for engaging

and disengaging is indicated using the signal builder block. From clutch the torque is transmitted to the gear box. The torque is increased or decreased depending upon the gear ratio mentioned in the parameter block of a gear box. The torque sensor is used to measure the torque available at the output transmitted to the differential and to the road tires.

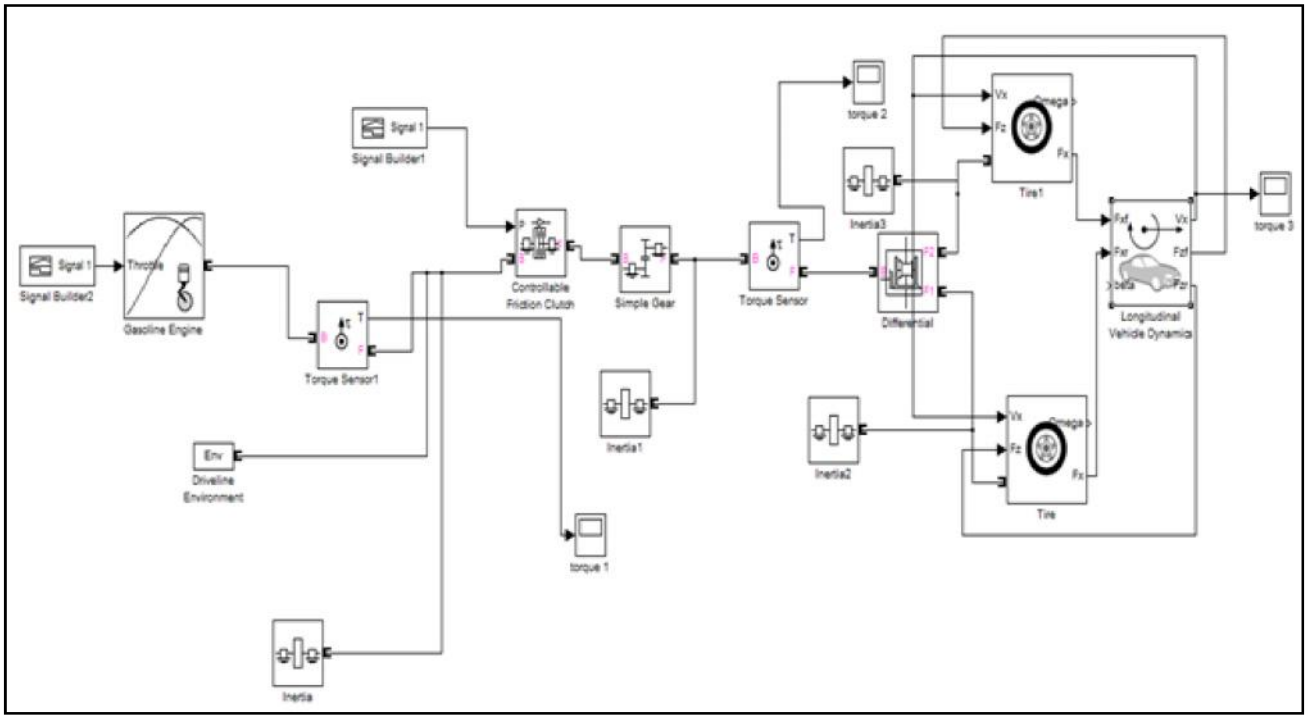

Fig.1 Layout of powertrain model in simdriveline environment

4. SIMULATION OF A POWER TRAIN

Once the powertrain model is modeled in a model editorial page, the user can specify the parameters on the configuration parameter dialogue box as mentioned earlier. The user can start the simulation by selecting the start button that is available on the model toolbar.

5. RESULTS AND DISCUSSIONS

Conventional power train is simulated with the specifications available for the given vehicle, to illustrate the performance potential. The modeled power train is simulated for different throttling conditions and gear ratios. The simulation time ranges from 0-10 seconds. Maximum simulation is taken as 10seconds because of available system configuration. Extended period of simulation requires a system with very high system configuration or should be connected with a super computer. The output of the simulation is viewed graphically with time in x-axis and varying parameter in y-axis. The results obtained during the simulation are as follows:

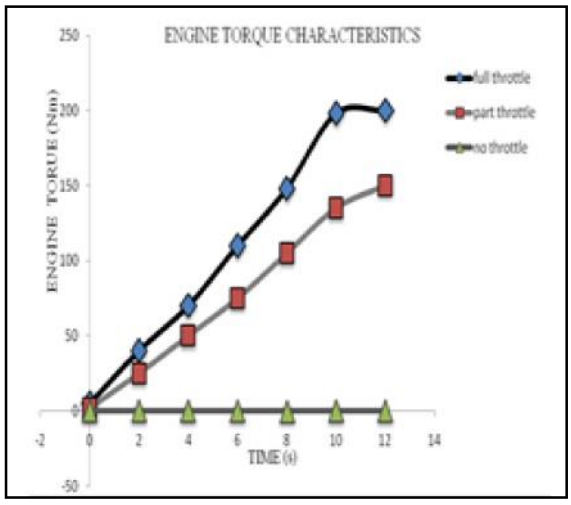

Fig.2 Engine torque characteristics

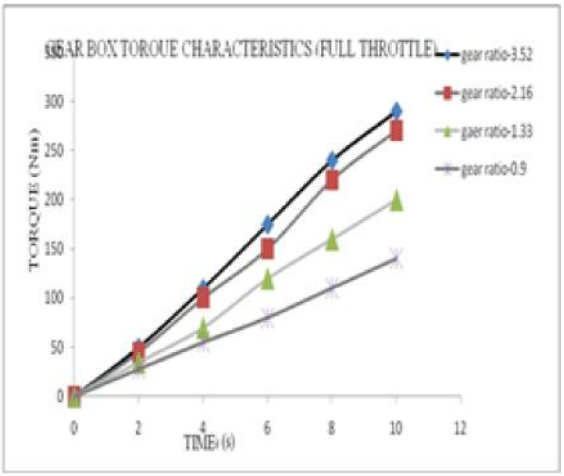

Fig.3 Gearbox torque characteristics

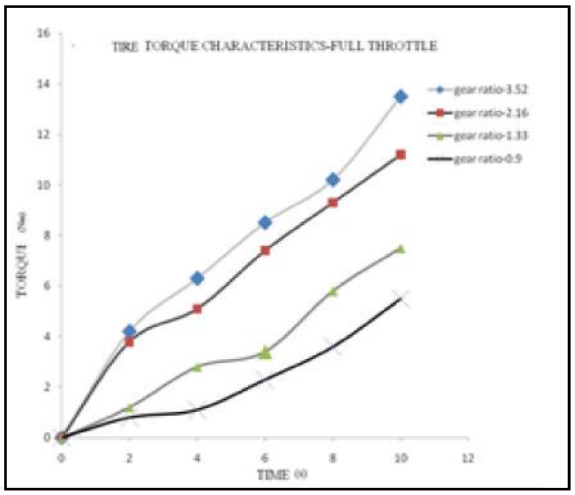

Fig. 4 Tire torque characteristics

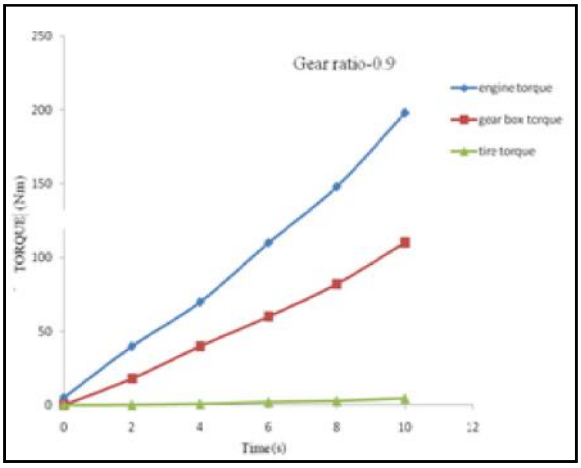

Fig. 5 Torque characteristics at a gear ratio of 0.9

6. CONCLUSION

In this study,powertrain model was developed to simulate for different throttling and gear ratios using Matlab/Simulink package. Simulation study helps us to determine the performance parameters of the powertrain such as engine torque for various operating conditions, gear box torque characteristics for variuos gear ratios, power loss due to inertia of rotating components and tire torque respectively. Also the simulated value is compared with the calculated and experimental values helping the user to interrupt the losses occuring inside the system. This interruption indicates that simulated values vary largely with the calculated values. This is mainly due to mechanical losses occuring inside the system along with the inertia of rotating components.This can be avoided by adding the mechanical or transmission efficiency in simdriveline model. Longitudinal vehicle dynamics factors can also be changed depending on the requirement of the vehicle. This enables the user to design a new drivetrain with increased efficiency and decresed power loss.

REFERENCES

[1] Karen L Butler, " A Matlab based Modeling and Simulation Package", IEEE Transactions on VEHICULAR TECHNOLOGY, Vol.48, No.6, November 1999.

[2] J. R. Bumby *et al.*, "Computer Modeling of the Automotive Energy Requirements for Internal Combustion Engine and Battery Electric-powered Vehicles", Proc. Inst. Elect. Eng., Vol.132, No.5, 1985, pp. 265–279.

[3] "Matlab/simulink," Version 4.2c.1/1.3c, The Mathworks Inc., Natick,MA.

[4] R. Noons, J. Swann and A. Green, "The Use of Simulation Software to Assesses Advanced Powertrains and New Technology Vehicles", in Proc.Electric Vehicle Symulation. 15, Brussels, Belgium, Oct. 1998.

[5] B. Bates, "On the Road with a Ford HEV", IEEE Spectrum, July 1995, pp. 22-25.

[6] Gisbert Lechner and Harald Naunheimer, "Automotive Transmissions", Fundamentals, Selection, Design and Application, Springer-Verlag Berlin Heidelberg 1999.

Optimization of Leaf Spring Production Rate through Automated GANTARY Robot System with the Aid of PLC

S. Vasanthaseelan, E.K. Aswin, R. Harish, R. Mohanraj and N. Sakthivel
Department of Automobile Engineering, S.N.S College of Technology, Coimbatore - 641 035, Tamil Nadu
E-mail:Vasanthaseelan.s@gmail.com

Abstract

Leaf Spring manufacturing includes series of process which also includes hardening, in which the mechanical property of the leaf spring is optimized for application followed by hot chambering, in which the human was employed to handle the leaf spring from the furnace and transformed to cambering dye. In this project, during the process material handling by human at 950°C, creates the more ill effect for the human. The overheat forces the employees to change their shift which leads to time lag in the production. This time lag affects the total production rate. To rectify and overcome this problem, Gantry robot is employed between the furnace and hot cambering dye to replace humans. The Gantry robot simultaneously replace the human also increases the production rate of the leaf spring. In conventional method using labour, it takes 11 seconds to complete this operation, whereas it reduce to 4.22 seconds when gantry robot employed in operation. X and Y axis were controlled during gantry operation. The implementation of the gantry robot significantly produces considerable reduction in error and increase in production rate. On another account investment on establishing the modern method can be recover through per capital income for the period of 13 months the comparison of human and gantry robot operation observed outcome of the implementation was as increased production rate by at least 1.75 times the conventional method followed by reduction in error %, very less human involvement, Decreased maintenance cost and activity, continuous work flow and reduced work time per work piece etc.

Keywords: *Cambering, Furnace, Gantry robot, Leaf Spring*

1. INTRODUCTION

Automation or automatic control, is the use of various control systems for operating equipment such as machinery, processes in factories, boilers and heat treating ovens, switching on telephone networks, steering and stabilization of ships, aircraft and other applications with minimal or reduced human intervention. Some processes have been completely automated. The biggest benefit of automation is that it saves labour; however, it is also used to save energy and materials and to improve quality, accuracy and precision. Fundamentally, there are two types of control loop; open loop control, and closed loop (feedback) control. In open loop control, thecontrol action from the controller is independent of the "process output" (or "controlled process variable"). A good example of this is a central heating boiler controlled only by a timer, so that heat is applied for a constant time, regardless of the temperature of the building. In closed loop control, the control action from the controller is dependent on the process output. In the case ofthe boiler analogy this would include a thermostat to monitor the building temperature, and thereby feedback a signal to ensure the controller maintains the building at the temperature set on the thermostat. A closed loop controller therefore has a feedback loop which ensures the controller exerts a control action to give a process output the same as the "Reference input" or "set point". For this reason, closed loop controllers are also called feedback controllers. [1,2,3] Oliver Sawodnyet.al, In the context of further automation of manufacturing processes, automated transportation of heavy weights using cranes becomes more and more important. Applying the skills of robots to crane automation, a wide market of new applications could be developed. The main idea is to interpret the crane as a large workspace-serving robot. The crane hook represents the effector of the robot. As an example, for the effector, an automated storageand retrieval unit for rack operations by a crane with three active auxiliary effector axes has been developed and integrated into the control concept. The control has been realized for a reconstructed 5-t-bridge crane with workspace dimensions of 30m*8.7m*7m. Eric Barnett Clement et.al Gosselin Although additive manufacturing (AM) is now a well-established industry, very few large-scale AM systems have been developed.

Here, we introduce a largescale 3D printer, which uses a six-degree-of-freedom cable-suspended robot for positioning, with polyurethane foam as the object material and having foam as the support material. Cable-positioning systems provide large ranges of motion and cables can be compactly wound on spools, making them less expensive, much lighter, more transportable, and more easily reconfigurable, compared to the gantry-type positioning systems traditionally used in 3D printing. The 3D foam printer performance is demonstrated through the construction of a 2.16-m-high statue of Sir Wilfrid Laurier, at an accuracy of approximately 1 cm,mwhich requires 38 hours of printing time. The system advantages and drawbacks are then discussed, and novel features such as unique support techniques and geometric feedback are highlighted. Finally, a description of the planned system modifications is provided. [4,5] S.B.Choi et.al, S.S.Han, K.H.Kin, C.C.Cheong This paper presents new feedback actuators to achieve an accurate position control of a flexible gantry robot arm The translational motion in the plane is generated by two dc motors and controlled by electro logical clutch actuators.

The generated motion can be continuously controlled by controlling the intensity of electric fields imposed to the ER fluiddomains of bidirectional rotating ER clutches On the other hand during control action of the translational motion a flexible arm attached to the moving part produces undesirable oscillations due to its inherent flexibility. The oscillations are actively suppressed by employing feedback voltage to the piezo ceramic actuator bonded on the surface of the flexible arm. Consequently an accurate position control at the endpoint of the flexible arm can be achieved. In order to accomplish this control target the governing equations of the proposed system are derived and rewritten as transfer functions to design a robust controller. The control electric fields to be applied to the ER clutch and the control voltage for the piezo ceramic actuator are determined via the loop shaping design procedures LSDP in the control technique. Control results of position regulating and tracking are provided to evaluate the effectiveness of the proposed methodology. [6, 7]

2. MATERIALS AND METHODS

The Material for the frame is selected based on its property, the material is stainless steel grade 316.The density of the material is 8.07mg/m3 ,the melting point of the material is 1673k,the hardness of the material is 2200mpa,the Poisson ratio ism0.275,the young's modulus is 205mpa,the loss of coefficient is 0.00148 and the thermal conductivity is 17w/mk. Table 1 shows the material property of frame. [8]

Table 1 Property of Frame

Variant grade	316
Density	8.07Mg/m^3
Melting Point	1673 K
Hardness	2200Mpa
Poisson ratio	0.275
Young's Modulus	205 Mpa
Loss Co efficient	0.00148
Thermal Conductivity	17w/m.K

The stepper motor of the robot is 22Kg torque,2.5 volts. The model no of the PLC Controller is 6ES72141AD230XB8 and 13 no. of memory is used. The compressor has a power of 2.5hp, Speed of 2850 rpm, Pressure of 115psi/8bar and capacity of 192 L/min. The Infrared sensor 1 memory stick, has a electronic range of 3-7cm and has a 2.54mm of breadboard compatibility. Table 2 shows the specification of stepper motor. [9]

Table 2 Specification of Stepper Motor

Stepper Motor	22kg torque, 2.5volts, 2.5amps.
PLC Controller	No. of Memory Sticks- 13, SIEMENS. Model No.:6ES72141AD230XB8
Compressor	Power-2.5hp, Speed:2850 rpm, Pressure:115psi/8 bar, Capacity:192
Infrared sensor	No. of Memory Sticks:1, Electronics with a range of 3-7 cm, 2.54mm with breadboard compatibility

3. RESULTS AND DISCUSSION

Using the human employee, the company can finish their 1 job at 11 to 12 seconds and 10 jobs at 110 to 120 seconds.1 shift of the work is 20 minutes.85 to 90 pcs are done per shift and total shift for 1 day is 15. Total pieces done in 1 day is 850 to 900 pieces. Table 3 shows the job calculation for human. Using the robot, the company can finish their 1 job at 6 seconds and 10 jobs at 60 seconds,218pcs are done per one shift and total shift per day is 15. Totally 2000 pcs are done per day. Table 4 shows the job calculation for robot. Figure 1 depicts the comparison of human and machine comparison. [10].

Table 3 Job Calculation with Human Jobs Time in Seconds

One job	11-12
10 jobs	110-120
One shift	72000(20 minutes)
Total job per shift	85-90 pcs
Total shift 15 Total pcs per day	850-900 pcs

Table 4 Job Calculation with Robot Job Time in Seconds

One job	6
10 jobs	60
One shift	72000(20 minutes)
Total job per shift	218 pcs
Total shift 15 Total pcs per day	2000 pcs

REFERENCES

[1] Y. Li, Y. Yu and S. Tsujio, "An Analytical Grasp Planning On Given Object With Multi Fingered Hand", In Proc. Int. Conf. Robot. Automat., 2002, pp.3749-3754.

[2] Z.Li and S.S. Sastry, "Task-ori Ented Optimal Grasping by Multifingered Robot Hands", IEEE J. Robot. Automat., Vol.4, No.1, 1988, pp.32-44.

[3] L. Magialardi, G. Mantriota and A. Trentadue, "A Three-Dimensional Criterion for the Determination of Optimal Grip Points", Robot. Computer-Integrated Man., Vol.12, No.2, 1996, pp.157-167.

[4] X. Markenscoff and C.H. Papadimitriou, "Optimum Grip of a Polygon", Int. J. Robot. Res., Vol.8, No.2, 1989, pp. 17–29.

[5] T. Murakami, N. Oda, Y. Miyasaka and K. Ohnishi, "Force Sensor less Impedance Control by Disturbance Observer", In Proc. of Power Conv. Conf., 1993, pp.352-357.

[6] Y. Nakamura, K. Nagai and T. Yoshikawa, "Dynamics and Stability in Coordination of Multiple Robotic Mechanisms", Int. J. Robot. Res., Vol. 8, No.2, 1989, pp.44-61.

[7] V. Nguyen, "Constructing Force-closure Grasps", Int. J. Robot. Res., Vol.7, No.3, 1988, pp.3-16.

[8] T. Omata, "Fingertip Positions of a Multifingered Hand", In Proc. IEEE Int. Conf. Robot. Automat., 1990, pp.1562-1567.

[9] T. Omata, "Finger Position Computation for 3-Dimentional Equilibrium Grasp", In Proc. IEEE Int. Conf. Robot. Automat., 1993, pp.216-222.

[10] J.K. Salisbury and B. Roth, "Kinematic and Force Analysis of Articulated Hands", ASME J. mech.Transmissions, Automat., Vol.105, No.1, 1983, pp.35-41.

Development of Green Sense Ferro Geopolymer Technique for the Construction of the Chaise Lounge

K. Siddharth, P.T. Ayswariya Lakshmi, Dr. V. Sreevidya
Assistant Professor, Department of Civil Engineering,
Hindusthan College of Engineering and Technology, Coimbatore - 641 032, Tamil Nadu

Abstract

Geopolymer mortar is a green sense composite material for construction. Silica fume blended with geopolymer mortar helps in easy blending and improves the cohesion and mechanical properties. Geopolymer is a low carbon dioxide cementitious material when compared to Ordinary Portland Cement. The binder used in geopolymer is sodium based alkaline activators. Ferro cementitious construction have taken a great development in constructing various shapes of structure, which paved way for the development of green sense ferro geopolymer chaise lounge, that can enhance the aesthetic of a garden lawn. The ferro geopolymer chaise lounge is well planned, designed and analyzed using computing applications like Auto CADD, 3Ds Max and STADD Pro. The analyzed lounge is moulded and casted into designed shape. Finished chaise lounge is tested for non-destructive tests and loading tests. And thus introduced for use of personage.

Keywords: *Alkaline solution, Ferro cement construction, Geopolymer, Low carbon dioxide*

1. INTRODUCTION

Cement is a fundamental raw material used in construction. As a greener alternative, calculated percentage of cement can be replaced by other materials such as fly ash, rice husk ash, metakaolin, silica fume etc. Fly ash is one of the most normally preferred substitutes for cement because concrete workability and durability are enhanced by fly ash by their small size and round shape. Silica fume as a blender to flyash enhance the strengthening property of the mortar. Geopolymer fits into an emerging class of cementitious materials that utilize „fly ash , one of the most abundant industrial by-products on earth, as a substitute for Portland cement. The development of geopolymer material is an important step towards the production of eco-friendly materials.
Geopolymer is an inorganic alumino-silicate compound, synthesized from materials of geological origin or from by-product materials such as fly ash, rice husk ash, etc., that are rich in silicon and aluminium. Fly ash is one of the residues generated from the combustion of coal. Fly ash is generally captured from the chimneys of coal-fired power plants. Consumption of fly ash in the manufacture of geopolymer is an important strategy in making materials more environment friendly. For this reason, fly ash has been chosen as a base material for this project in order to utilize this industrial waste in a better way.

For this reason the present project aims at replacing cement with flyash using geopolymer technology and also blending silica fume so that the consumption of OPC is reduced and hence reduced CO_2 emissions.

1.1 Silica Blended Geopolymer

Fly ash is a fine powder recovered by electrostatic precipitation from the gases of burning coal during the production of electricity in thermal power plants. It is available abundantly worldwide. Presently, as per the Indian Ministry of Environment & Forest Figures, only a little percentages of fly Ash is being used in manufacturing cements, construction concrete, block & tiles and some are disposed off in landfills and embankments but a huge amount of fly ash is unutilized.

Fly ash is rich in silica and alumina. Theoretically, any aluminosilicate material can be used as a base material to produce geopolymer binder. The various aluminosilicate materials such as metakaolin, Fly ash, GGBS, Silica fume etc. have been used by many researchers as base material to make geopolymer. The fly ash, a solid waste generated in thermal power plants, if used properly has full potential to use as one of the base material for producing geopolymer binder.

Again, the trends in early strength across a particular group of fly ashes do not match the trends in final strength

for the same ashes. Therefore, producing the flyash based geopolymers with consistent physical and mechanical properties despite the variability in the raw materials is a challenging issue. Here comes the concept of blending of some supplementary material like silica fume as it is being done successfully in case of traditional cement based concrete. Addition of some supplementary materials like silica fume, which itself is capable enough to form Geopolymer binder in similar condition, as blending material with fly ash may be beneficial in this field to supplement the ultimate product properties. In case of producing blended fly ash based geopolymer, thorough understanding of synthesizing parameters and their effect on microstructure and macroscopic properties is essential for optimizing processing parameters and product properties efficiently.

1.2 Ferro-Cement As Ferro-Geopolymer

Ferro-cement (thin-shell concrete, **ferro**-concrete) is a system of reinforced mortar or plaster (lime or **cement**, sand and water) applied over layers of metal such as chicken wire or woven or expanded metal mesh or fibers and possibly closely spaced small-diameter steel rods such as rebar. **Ferro-geopolymer** is a similar system of ferro-cement where cement is eliminated and filled with geopolymer composite.

2. MATERIALS USED

Flyash : Flyash of Class F from Mettur Thermal Power Plant (MTPP) was used. Flyash used are confirming to IS 3812-1981.

Silica Fume : Silica fume used was obtained from Coimbatore. It used as per the Silica Fume
User s Manual.

Fine aggregate : Clean and dry river sand available locally was used. Sand passing through IS
4.75 mm sieve was used for casting all the specimens. Fine aggregate used are confirming to IS
383-1970.

Water : Castings of specimens were done with the potable water.

Alkaline Solution : Sodium Hydroxide and Sodium Silicate are used to prepare the geopolymer mortar.

Wire Mesh : Chicken mesh or hexagonal wire mesh is used to cover the skeleton.

TMT Rods for Skeleton : 8mm TMT rods are used as the entire skeleton of the ferro geopolymer chaise lounge.

3. PRODUCT LAUNCH-FERRO GEOPOLYMER CHAISE LOUNGE

The designed ferro geopolymer chaise lounge is well planned and analysed using various computer applications and explained in detailed.

3.1 Pre Process- Stage 1

3.1.1 Planning & Drawing

The ferro geopolymer chaise lounge is planned and detailed using Auto CADD.

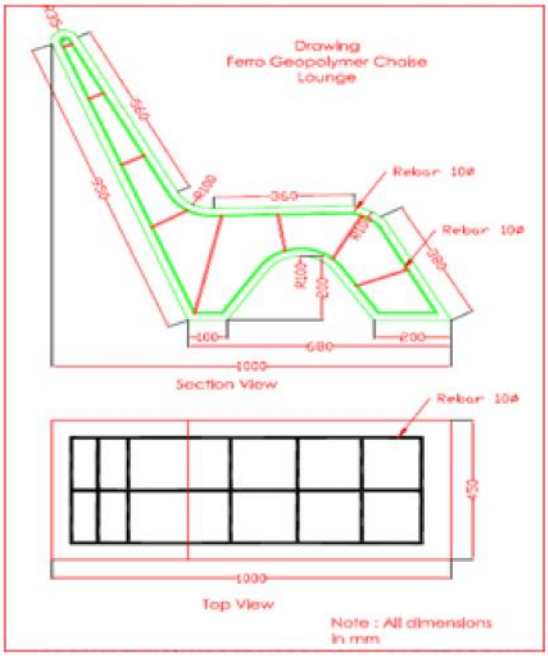

Fig.3.1 Section View-Ferro Geopolymer Chaise Lounge

3.1.2 3D Modelling

The ferro geopolymer chaise lounge is modeled using 3Ds Max.

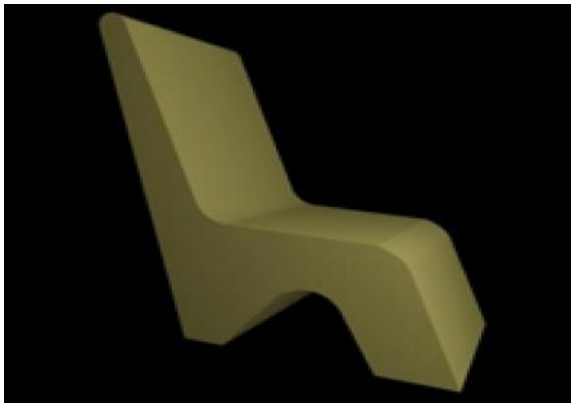

Fig. 3.2 3D Model

3.1.3 STADD Analysis

The ferro geopolymer chaise lounge analysed using STADD Pro. Its is analysed for required support and loading conditions. For which the bending moment, shear force and deflection are analysed and studied.

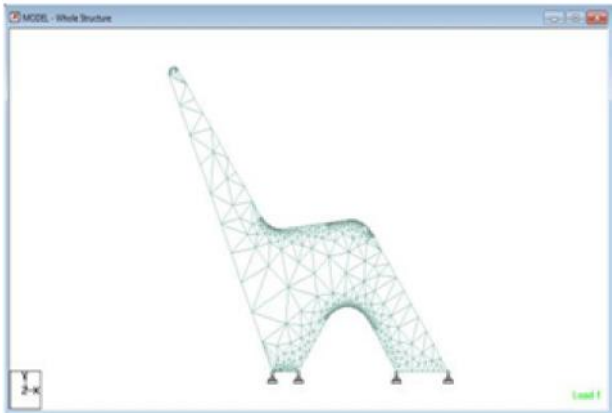

Fig. 3.3 Model & Support Condition

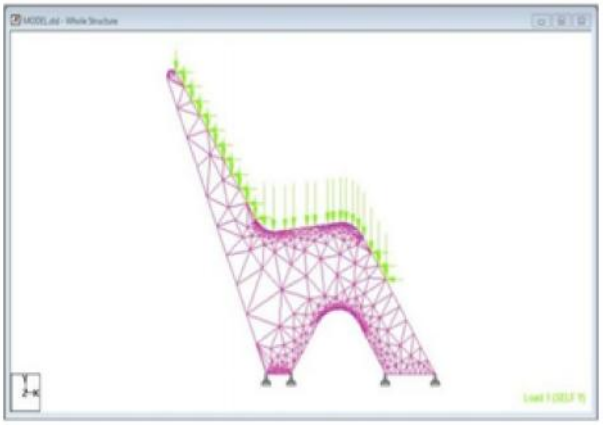

Fig.3.4 Loading Condition

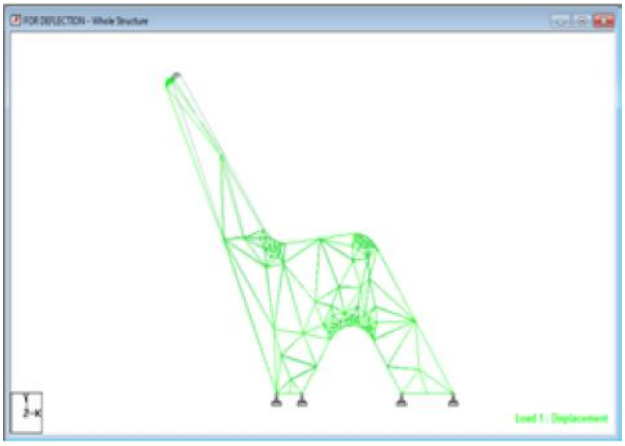

Fig. 3.5 Deflection

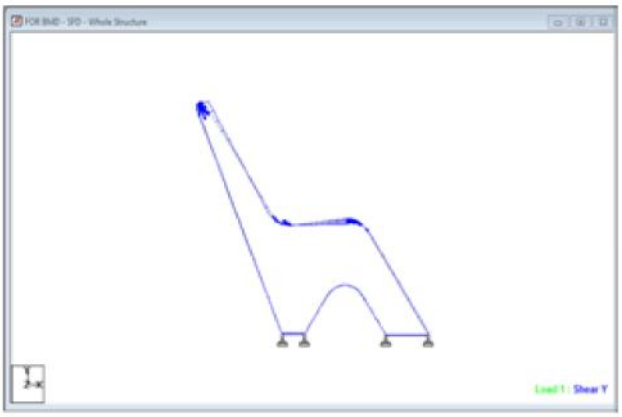

Fig. 3.6 Shear force

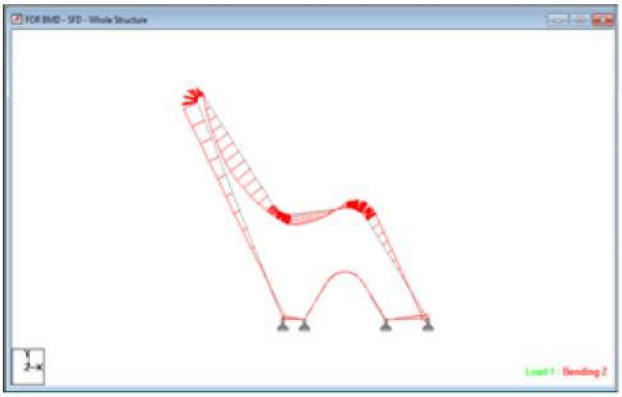

Fig. 3.7 Bending Moment

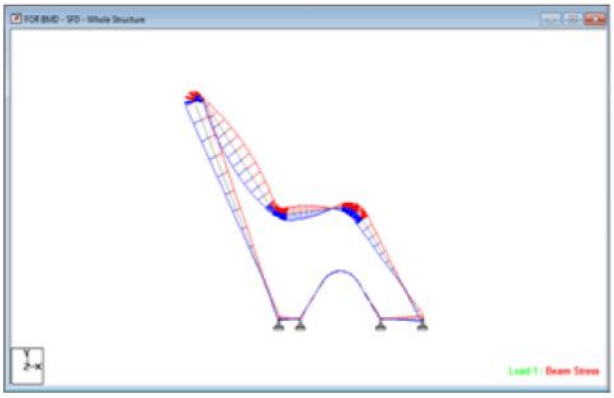

Fig. 3.8 Stress

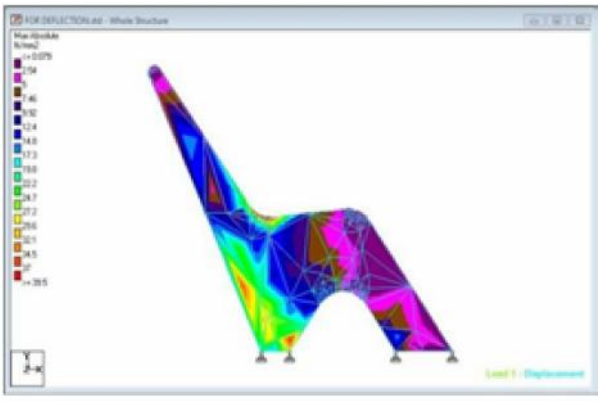

Fig.3.9 Stress Intensity

3.1.4. ANSYS Analysis

The ferro geopolymer chaise lounge analysed using ANSYS.

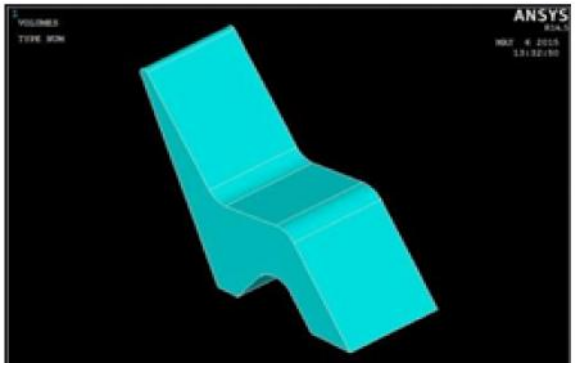

Fig. 3.10 Modelling

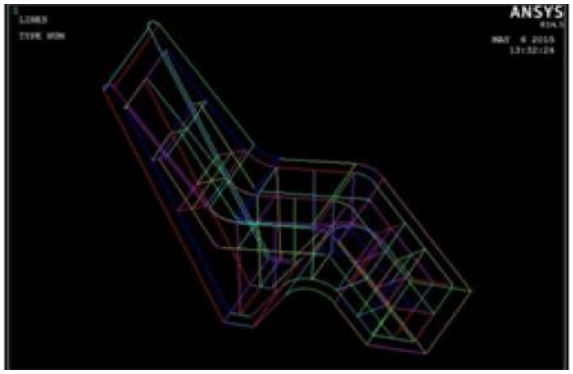

Fig. 3.11 Reinforcement

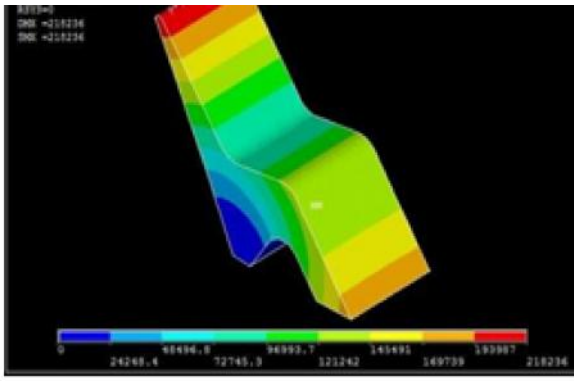

Fig. 3.12 Average Displacement

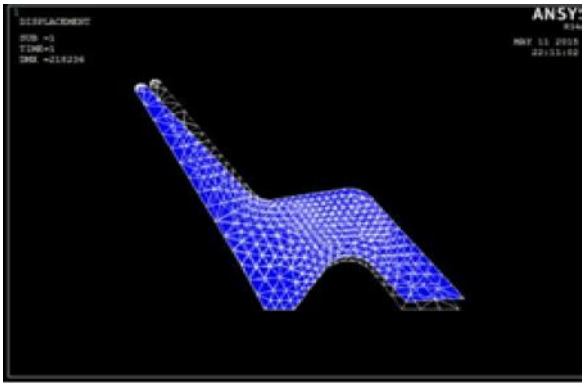

Fig. 3.13 Deflection

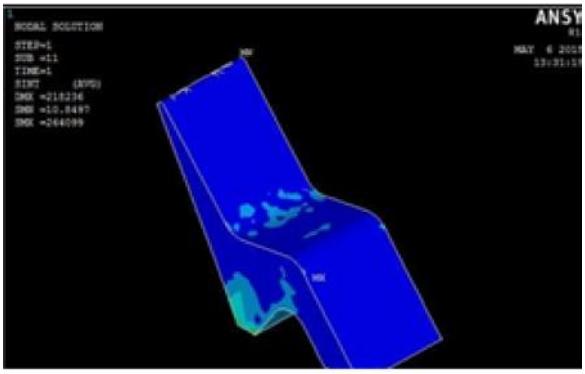

Fig. 3.14 Stress Intensity

3.2 Pre Process - Stage 2

3.2.1 Preperation of Mould

The mould was designed and manufactured from am industry in SIDCO, Coimbatore. It was made of mild steel and was fixed with bolts.

Fig.3.15 Mould Designed

Fig. 3.16 Mould Position

3.2.2 Formation of the Skeleton

TMT Rod of 10mm diameter was used as skeletal reinforcement and the mesh was wound around it with binding wires.

Fig. 3.17 Welding of bars

Fig. 3.18 Skeletal Reinforcement

3.3 Post Process – Construction of Ferro Geopolymer Chaise Lounge

3.3.1 Mix Ratio 1:2 (Flyash-Silica Fume Blend:Sand)

Binder - Alkaline solution (Sodium Hydroxide & Sodium Silicate) Blend - Flyash (FA) & Silica fume(SF)
NaOH = 9.6% of binder
Na_2SiO_3 = 2.5 times of NaOH = 24% of binder

Table 3.1 Mix Ratio

Mix	Mix Constituents			Binder-Blend Ratio	Na_2SiO_3/NaOH
	FA	SF	Sand		
Geopolymer Mortar 7.5% silica fume	0.925	0.075	2	0.34	2.5

3.3.2 Preparation Of Blended Geopolymer Mortar

- The flyash and river sand were first mixed dry for about 3-5 minutes.
- To this dry mix the alkaline liquid is added and mixed thoroughly for about 4 minutes.
- The fresh mortar were cast into the molds immediately after mixing and compacted properly.

Fig. 3.19 Dry materials

Fig. 3.20 Activated mortar

3.3.3 Setting the Mould with Rebar and Mesh

The mould is well greased and is placed with the mesh wounded rebar. Cover blocks were set where ever required. The well mixed geopolymer mortar is perfectly poured into the mould and proper compaction is provided.

Fig. 3.21 Mould with rebar & mesh

Fig. 3.22 Mould with mortar

3.3.4 Curing

The ferro geopolymer chaise lounge is well demoulded as left ambient curing.

Fig.3.23 Demoulded Chaise Lounge

Fig. 3.24 Ambient Curing

4. TESTING OF FERRO GEOPOLYMER CHAISE LOUNGE

4.1 Non Destructive Test (NDT) – Rebound Hammer

Table 4.1 Rebound Number

Average	27.3
Standard Deviation	2.49
Variance	6.23

Fig. 4.1 Rebound hammer test

4.2 Loading Test

Loading test is performed on the lounge by providing it with a load of 150kg sand bag. Loading test was just conducted to check whether it could carry the designed load without forming cracks.

Fig. 4.2 Loading Test

4. METHODOLOGY & EXECUTION

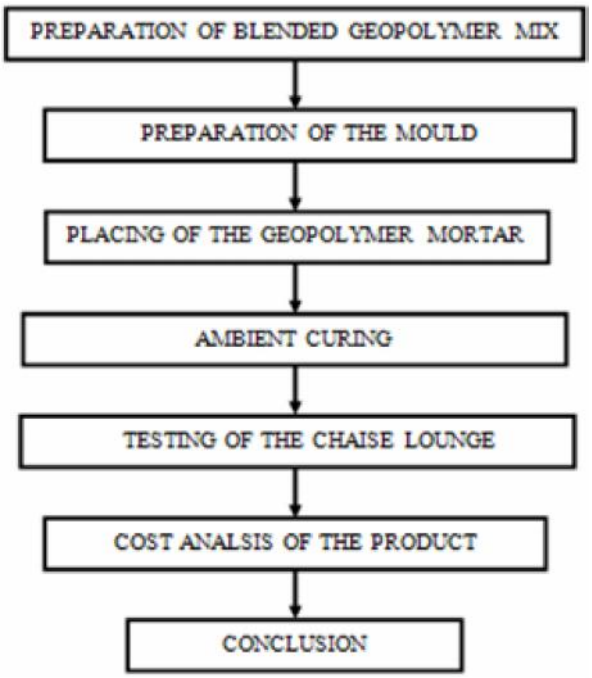

5. CONCLUSION

The overall procedure of this construction of ferro geopolymer chaise lounge paved a good experience and a satisfied result.

- The rebound number with respect to the compression test of the cube sample was found satisfied.
- The ferro geopolymer chaise lounge was able to withstand a load of 150 kg.

6. SCOPE FOR FUTURE WORK

- The design can be modified for various other shapes.
- The technique along with the composite can be applied in various other applications.

REFERENCES

[1] Djwantoro Hardjito, Chua Chung Cheak & Carrie Ho Lee Ing, "Strength and Setting Times of Low Calcium Fly Ash-based Geopolymer Mortar", Modern Applied Science, Vol.2, No.4, 2008, pp 9-18.

[2] B. V. Rangan, Pan, Zhu, Sanjayan and G. Jay, "An Investigation of the Mechanisms for Strength Gain or Loss of Geopolymer Mortar after Exposure to Elevated Temperature", Journal of Material Science. Vol.44, No.7, 2009, pp.1873-1880.

[3] Thanush Thampi, V. Sreevidya and R. Venkatasubramani, "Strength Studies on Geopolymer Mortar for Ferro Geopolymer Water Tank", International Journal of Advanced Structures and Geotechnical Engineering, Vol. 3, No.02, 2014, pp.102-105

[4] Dr. N. K. Patil and Dr. K B.Prakash, "Effect of Alternate Wetting and Drying on Impact Strength of Fibrous Ferrocement Using Round Steel Fibers", New Building Materials & Construction World, 2010.

[5] P.T.Ayswariya Lakshmi, Dr.V.Sreevidya and Dr.R.Venkatasubramani, "Strength Studies on Geopolymer Mortar By Blending Silica Fume With Flyash", (Annexure – II) International Journal of Applied Engineering Research ISSN 0973-4562 Vol.10, No.19, 2015, pp.13899-13902.

[6] M.S. Shetty, "Concrete Technology", 15th Edition, S.Chand& Company Ltd. , New Delhi, 2005.

[7] A.M. Neville, "Concrete Technology", 2nd Edition, Pearson Education Ltd., England, 2010.

[8] M.L. Gambhir, "Concrete Technology", 5th Edition, TataMcGraw-Hill, New Delhi, 2006.

Influences of Tool Pin Profile on Tensile Strength of Friction Stir Welded Aa7075 and Aa6061 Aluminium Alloy Dissimilar Joint

K.P. Yuvaraj, P. Ashoka Varthanan, M. Navin Kumar and B. Gunanidhi
Department of Mechanical Engineering,
Sri Krishna College of Engineering and Technology, Coimbatore – 641008, Tamil Nadu
E-mail: cadyuva94@gmail.com, ashokavarthanan@skcet.ac.in

Abstract

Aluminium Alloy AA6061 and AA7075 have gathered wide range of acceptance in the fabrication of light weight structures requiring a high strength-to-weight ratio and good corrosion resistance. Compared to other fusion welding processes that are frequently used for joining structural aluminium alloys, Friction stir welding (FSW) process is an emerging solid state joining process in which the material does not melt and recast can be welded. This process consists of non-consumable tool to generate frictional heat in between the tool and work surface. The welding parameters such as tool rotational speed, welding speed, axial force, etc., and tool pin profile play a vital role in deciding the weld quality. In this research work an attempt has been made to study the influence of tool pin profile on tensile strength of friction stir welded AA6061 and AA7075 aluminium alloy joint. Three different tool pin profiles (Cylindrical, triangular and square) with constant shoulder diameter 20mm have been used to fabricate the dissimilar joints. The formation of FSP zone has been analysed with help of optical microscope. Tensile properties of the joints have been evaluated and correlated with the FSP zone formation. From this experimental investigation it is found that the square pin profiled tool produced mechanically sound and metallurgically defect free welds compared to other tool pin profiles.

Keywords: *Friction Stir Welding, Tool Pin Profile, Tensile Strength*

1. INTRODUCTION

The problems faced for making high-strength, fatigue and fracture resistant welds in aerospace aluminum alloys, such as highly alloyed 2XXX and 7XXX series, has long inhibited the wide use of welding for joining aerospace structures. These aluminum alloys are generally defined as non-weldable one because of the poor solidification microstructure and porosity occurs in the fusion zone of welding. Also, the deviation in mechanical properties when compared to the base material is very significant one. These constraints make the joining of these alloys by conventional welding processes not successive one. Some aluminum alloys can be resistance welded, but the surface preparation is costlier, with surface oxide being a major problem.

Friction stir welding (FSW) was invented at The Welding Institute (TWI) of UK in 1991 as a solid-state joining technique, and initially it was applied to aluminum alloys. The basic concept of FSW is remarkably simple. A non-consumable rotating tool with a specially designed pin and shoulder is inserted into the abutting edges of sheets or plates to be joined and traversed along the line of joint (Fig. 1). The tool serves two primary functions: (a) heating of workpiece, and (b) movement of material to produce the joint. The heating is accomplished by friction between the tool and the workpiece and plastic deformation of workpiece. The localized heating softens the material around the pin and combination of tool rotation and translation leads to movement of material from the front of the pin to the back of the pin. As a result of this process a joint is produced in 'solid state'. Because of various geometrical features of the tool, the material movement around the pin can be quite complex. During FSW process, the material undergoes intense plastic deformation at elevated temperature, resulting in generation of fine and equiaxed recrystallized grains. The fine microstructure in friction stir welds produces good mechanical properties.

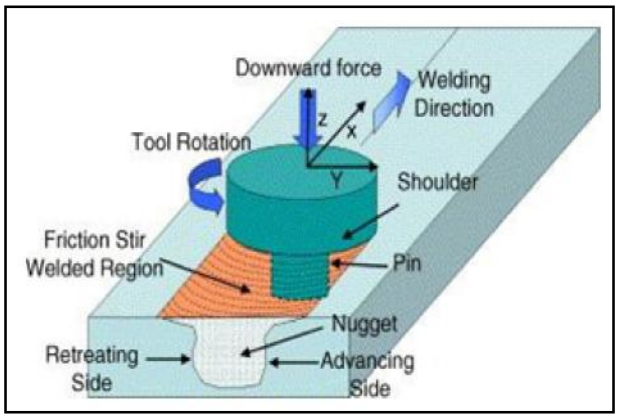

Fig .1 Schematic of the friction stir welding and tool shape

2. PROCESS PARAMETERS

FSW/FSP involves heat generation due to friction between tool and shoulder, complex material movement and plastic deformation. Welding parameters, geometry of tool, and joint design exert significant effect on the temperature distribution and material flow pattern, thereby influencing the microstructural evolution of material. In this research work, an attempt has been made to study the influence of tool pin profile on tensile strength of friction stir welded AA6061 and AA7075 aluminium alloy joint. The FSW process parameters which are used for the experimental run is mentioned below in the table 1.

Table 1 Parameters and its Level

Sl. No.	Parameter	Level 1	Level 2	Level 3
1	Toolpin profile (A)	Square	Cylindrical	Triangular
2	Speed (RPM) (B)	1000	1500	2000
3	Feed (mm/min) (C)	20	40	60

3. FSW PROCESS MODELING

Friction stir welding process results in intense plastic deformation and temperature increase within and around the stirred zone of weld. Due to this, there is a significant microstructural evolution, including grain size, grain boundary character, dissolution and coarsening of precipitates, breakup and redistribution of dispersoids, and texture. An understanding of mechanical and thermal processes during Friction stir welding is needed for process parameters optimization and controlling microstructure and properties of welds.

4. EXPERIMENTAL WORK

4.1 Machining set up

All friction stir welds were fabricated using a vertical milling machine as shown in the Figure 2 with a tilting head and and a typical FSW tool as per the design matrix framed. Prior to welding, base metal plates were cleaned with a degreaser and then clamped to a steel backing plate. The Aluminium 7075 and 6061 plates to be welded and FSW tool were fixed on the table and spindle respectively. The welds used in this investigation are all single pass, full penetration welds. Specimens of required size were cut from the welded plate to carry out mechanical and metallurgical studies. The specimens were polished using standard metallographic technique and observed using a optical microscope.

(a)

(b)

Fig.2 (a) (b) Experimental setup

4.2 FSW Tools

The rolled plates of 6 mm thickness, AA7075 and AA6061 aluminium alloy, have been cut into the required size by using power hacksaw cutting. The initial joint configuration is obtained by securing the plates in position using mechanical clamps. The direction of welding is

normal to the rolling direction. Single pass welding procedure has been followed to fabricate the joints. Non-consumable tools as shown in figure 3 made of high carbon steel with straight cylindrical,square and triangular pin have been used to fabricate the joints.

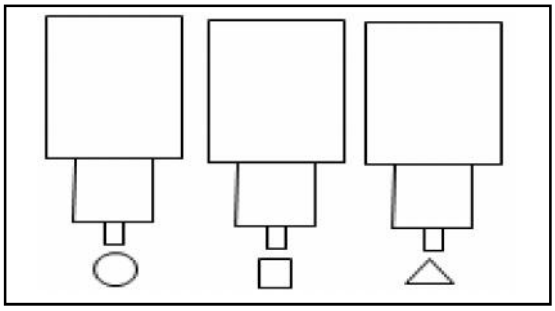

Straight round pin Square pin Triangular pin

Fig.3 FSW tools

4.3. Development of Design Matrix

The design matrix selected for the experimental run as shown in Table 2 is framed with Response Surface Methodology (RSM). It consists of three factor three level central composite rotatable design consisting of 20 sets of coded conditions composed of 6 centre points. It is framed with the help of MINITAB software.

Table 2 Design of Experiments and Results

Exp. Run	A	B	C	Experimental Tensile Strength N/mm^2	Precicted Values Tensile Strength N/mm^2
1	-1	-1	-1	138.251	134.8537
2	1	-1	-1	113.127	110.5374
3	-1	1	-1	136.119	132.6409
4	1	1	1	92.565	84.20259
5	-1	-1	1	107.523	105.3726
6	1	-1	1	100.482	96.18429
7	-1	1	-1	166.265	168.8288
8	1	1	1	134.458	135.5185
9	-1.68179	0	0	151.896	149.8318
10	1.68179	0	0	120.241	121.0185
11	0	-1.68179	0	124.565	126.7728
12	0	1.68179	0	144.589	145.3335
13	0	0	-1.68179	110.893	112.8185
14	0	0	1.68179	126.423	123.7359
15	0	0	0	139.756	134.3691
16	0	0	0	136.298	134.3691
17	0	0	0	130.842	134.3691
18	0	0	0	138.121	134.3691
19	0	0	0	138.233	134.3691
20	0	0	0	140.811	134.3691

4.4 Conducting Experiment as Per Design Matrix

The experiments are conducted with the help of the vertical milling machine as shown in the Figure 4 as per the design matrix framed. The Aluminium 7075 and 6061 plates to be welded and FSW tool were fixed on the table and spindle respectively. Specimens of required size were cut from the welded plate to carry out metallurgical studies.

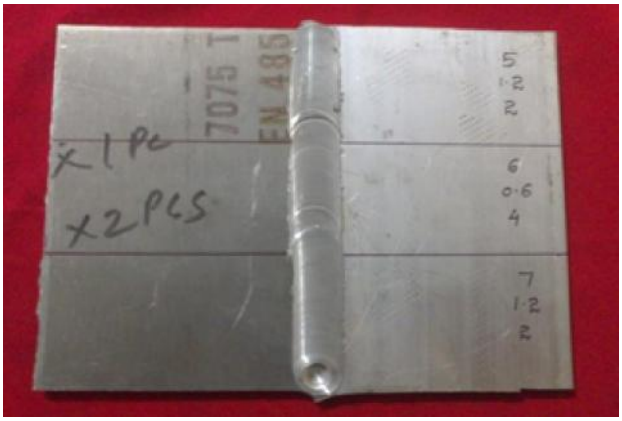

Fig.4 Sample of friction stir welded plate

4.5 Recording of responses

According to American Society for Testing of Materials (ASTM E8) standard and transverse tensile properties such as ultimate tensile strength of the FS welded joints were evaluated using the computerized universal testing machine as shown in the figure 9. For each experimental run, a specimen is prepared and tested.

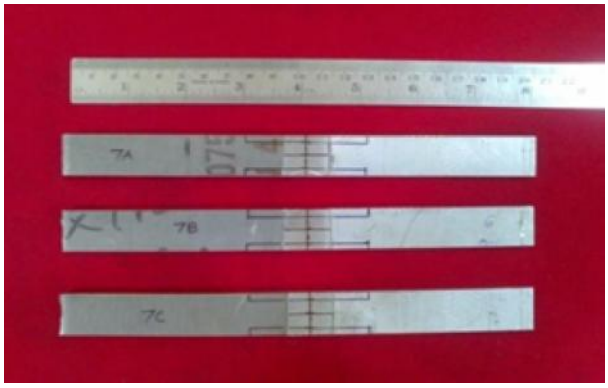

Fig.5 Preparation of tensile specimen from Friction stir welded plate

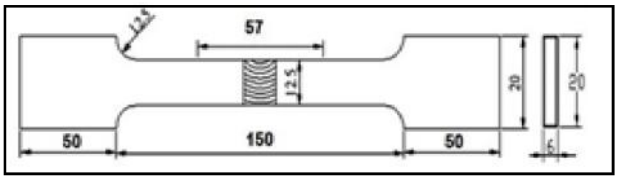

Fig 6. ASTM Standard ASTM E8M-04

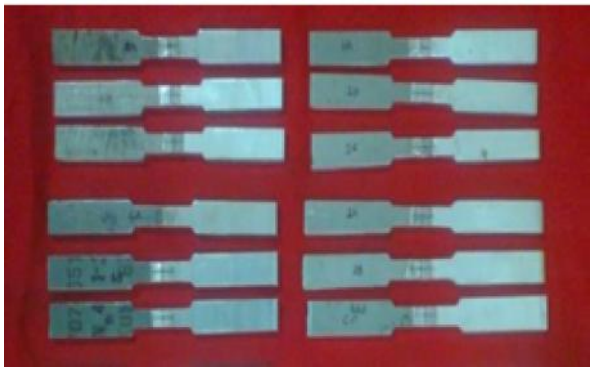

Fig.7 Tensile specimens before fracture

Fig 8 Tensile specimen after fracture

Fig.9 Computerized Universal Testing Machine

4.6 Microstructure

The specimens with good tensile strength can be found and the additional pieces available in the experimental run are cut, prepared and polished. Finally it can be etched with Wecks reagent which has 4g of $KMnO_4$, 1g of NaOH and 100 ml of water. The specimen was immersed for 20 seconds in room temperature. It has been observed that, 7075 flow well inside the 6061 region due to the stirring action.

Fig.10 Preparation of Wecks Reagent

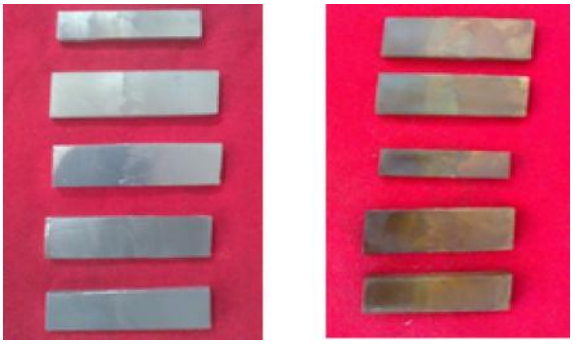

Fig 11 Specimen before and after applying etchant

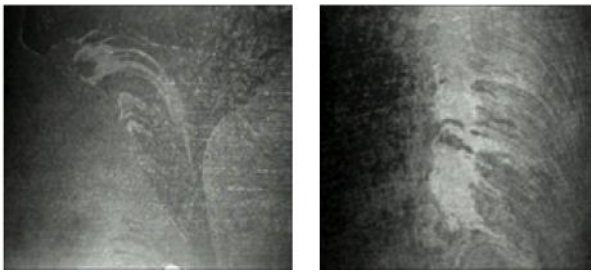

Fig.12 Microscopic view

5. RESULTS AND DISCUSSION

5.1 Tensile Strength

The tensile results show that the maximum failures were found to occurring near weld zone and at the advancing side of AA 6061. Among the different tool pin profile, squarepin yields the maximum tensile strength for all the other parameters. The tensile strength for triangular tool pin diameter was found to be lowest. And the roundtool pin diameter gives the moderate value of the tensile strength. The tool speed of 1500 rpm yields higher tensile results and the tool speed of 1000 rpm yields the lowest. In case of weld feed, 20 mm/min gives the maximum tensile strength and 60 mm/min yields the lowest. In dissimilar welding, due to difference in mechanical properties, the failure of the tensile specimen will always occur at the weaker of the two metals.

The ultimate tensile strength of base metal AA7075 is of 575 MPa whereas AA6061 was of 350 MPa. Higher welding tool feed results in insufficient heat input per unit length of the weld joint and faster cooling rate, affecting the plastic flow of the material during stirring resulting in kissing defect. But the lower tool feed results in higher heat input per unit length affecting the vertical movement of the material. Increase in tool speed results in pin hole with piping and tunnel defect due to insufficient heat generation and metal transfer. Thus for the current experimental run the process range which satisfies the welding conditions of the dissimilar AA7075 and AA6061 aluminium alloys were chosen.

5.2 Microhardness Results

Microhardness values were measured along the mid-thickness of the dissimilar AA7075 and AA6061 welded joint. The hardness distribution of the stir zone is found to be higher than that of the base metals. In the absences of the external defects, the tensile properties always follow the lowest hardness distribution. Most of the failure has taken place on the minimum hardness zone at the advancing side of AA6061 side.

6. CONCLUSION

The effect of process parameters for Friction stir welding of AA7075 and AA6061 aluminum alloy butt joint have been investigated. It is found that, square pin tool produced good tensile strength when compare to round and triangular pin. And also decrease in tool feed and increase in tool speed improves the tensile strength of the joint. From the microscopic view, it is found that square pin tool increases the tensile strength due to good flow of 7075 material in 6061 region. The Friction Stir Welding process parameters were optimized, and the optimum values of the process parameters were found to be square tool pin, 1500 tool speed, and 20 mm/min tool feed. Confirmation experiments were conducted at this optimum process condition to confirm the optimum value estimated by the statistical analysis. The average tensile strength at the optimal level was found to be 141.566 N/mm^2. Controlling tool pin profile, tool speed and tool feed may show good results on the machining process of FSW during various machining conditions.

REFERENCES

[1] R. Palanivel and P. Koshy Mathews, "Prediction and Optimization of Process Parameter of Friction Stir Welded Aa5083-H111 Aluminum Alloy Using Response Surface Methodology", Journal of Central South University of Technology, Vol.19, No.1, 2012, pp.1-8.

[2] A.Razal Rose, K.Manisekar and V. Balasubramanian, "Influences of Welding Speed on Tensile Properties of Friction Stir Welded AZ61A Magnesium Alloy", Journal of Materials Engineering and Performance, Vol.21, No.2, 2012, pp.257-265.

[3] M.Jayaraman, R.Sivasubramanian, V. Balasubramanian and S. Babu, "Influences of Process Parameters On Tensile Strength Of Friction Stir Welded Cast A319 Aluminium Alloy Joints", Metals and Materials International Vol.15, No.2, 2009, pp.313-320.

[4] A. Lakshminarayanan, V. Balasubramanian and K. Elangovan, "Effect of Welding Processes On Tensile Properties Of Aa6061 Aluminium Alloy Joints", The International Journal of Advanced Manufacturing Technology, Vol.40, No.3, 2009, pp.286-296.

[5] A.K. Lakshminarayanan and V. Balasubramanian. "Tensile and Impact Toughness Properties of Gas Tungsten Arc Welded and Friction Stir Welded Interstitial Free Steel Joints", Journal of Materials Engineering and Performance, Vol.20, No.1, 2011, pp.82-89.

[6] K. Elangovan and V. Balasubramanian, "Influences of Tool Pin Profile and Tool Shoulder Diameter on the Formation of Friction Stir Processing Zone in Aa6061 Aluminium Alloy", Materials & Design , Vol.29, No.2, 2008, pp.362-373.

[7] S. Gopalakrishnan and N. Murugan, "Prediction of Tensile Strength of Friction Stir Welded Aluminium Matrix TiC_P Particulate Reinforced Composite", Materials & Design, Vol.32, No.1, 2011, pp.462-467.

[8] Zadpoor, Amir Abbas, Jos Sinke and Rinze Benedictus, "Global and Local Mechanical Properties and Microstructure of Friction Stir Welds with Dissimilar Materials and/or Thicknesses", Metallurgical and Materials Transactions A, Vol.41, No.13, 2010, pp.3365-3378.

[9] S. Yazdanian, Z. W. Chen and G. Littlefair, "Effects of Friction Stir Lap Welding Parameters on Weld Features on Advancing Side and Fracture Strength of AA6060- T5 Welds", Journal of Materials Science, Vol.47, No.3, 2012, pp.1251-1261.

[10] A.R. Yazdipour and H. Jamshidi Aval, "An Investigation of the Microstructures and Properties of Metal Inert Gas and Friction Stir Welds In Aluminum Alloy 5083", Sadhana, Vol.36, No.4, 2011, pp.505-514.

[11] Aydin, Hakan, Mumin Tutar, Ali Durmus, Ali Bayram, and Tayfun Sayaca. "Effect of Welding Parameters on Tensile Properties and Fatigue Behavior of Friction Stir Welded 2014-T6 Aluminum Alloy", Transactions of the Indian Institute of Metals, 2012, pp.1-10.

[12] Cole, G. Edward, Axel Fehrenbacher, Edward F. Shultz, Christopher B.Smith, Nicola J. Ferrier, Michael R. Zinn, and Frank and E. Pfefferkorn, "Stability of the Friction Stir Welding Process in Presence of Workpiece Mating Variations", The International Journal of Advanced Manufacturing Technology, 2012, pp.1-11.

[14] M.Grujicic, G.Arakere, C-F.Yen and B.A. Cheeseman, "Computational Investigation of Hardness Evolution During Friction-stir Welding of AA5083 and AA2139 Aluminum Alloys", Journal of Materials Engineering and Performance, Vol.20, No.7, 2011, pp.1097-1108.

Patch Antenna Array for Medical Applications

S.Priyanka Gandhi and P.T.Bhuvana
Department of Electronics and Communication Engineering,
VSA Group of Institutions, Salem - 636 010, Tamil Nadu
E-mail: priyasiddhan@gmail.com

Abstract

In this paper, a compact and wearable antenna system is designed and tested for telemedicine applications. The telemedicine has a growing demand for remote monitoring and tracking of human health conditions. The telemedicine applications are also used for managing parameters such as Artificial Magnetic Conductor (AMC) which is introduced in the ground plane to isolate user's body from unwanted EM radiation. The proposed system is capable of operating at 2.4 GHz band. It is designed with JC cross frequency coverage for new evaluator applications.

Keywords: *Artificial Magnetic Conductor, Flexible and wearable Antennas, Printed Monopole, Telemedicine*

1. INTRODUCTION

In recent times monitoring a patient or health parameter of astronauts or athletes and recovery tracking of patients has become feasible due to telemedicine. It is a remote monitoring technology for human vital science. This type of health care of telemedicine technology can forward vital parameter of a patient to a remote station through wireless transmission. These parameters may include heart rate, blood pressure, body temperature, respiratory rate, ECG waveform and glucose level. The telemedicine provides better performance by using antenna which are compact, light weight and mechanically robust. The patch antennas are preferred since these provide high efficiency, have reliability and are conformal to the body shape. The most preferable antenna in telemedicine application is traditional microstrip antenna which minimizes the user's exposure to electromagnetic radiation due to its suitable characteristics in terms of unidirectional radiation patterns.

The low profile antenna has a spherical radiation pattern with low cost and has a relatively wide bandwidth. It is needed to be employed in telemedicine application. Some of the techniques lead to increase in the antenna height or these require complicated manufacturing process. It includes the use of observers and shielding planes. In order to overcome these limitations, a cavity slot antenna is normally used for body area network applications. This type of antenna is having relatively high profile and involves multilayer fabrication process and it shows that it is an efficient if tested on human phantom. The performance of this technique is based on the stack of multiple layers which are highly dependent on the ground plane size and it leads to complex profile system. In order to suppress the electromagnetic wave that is propagating towards the human body, a single negative metamaterial is used. The size of the antenna design is reduced by using the principles of AMC structure.

Artificial magnetic conductor is the single layer periodic array. It is found in the grounded dielectric substrate and it produces a reflection phase shift of zero degree incident waves. It presents a low profile microstrip antenna using AMC plane based on Jerusalem cross. AMC is used to isolate the user's body from harmful electromagnetic radiation. It has high gain microstrip patch antenna. The bandwidth and central frequency are analyzed for performance. A reduction of antenna profile is achieved through efficient technique.

Tunable metamaterial is an incident EM wave with a variable response. It is controlled by remote and can be incident with EM wave interaction with metamaterial. It is used to suppress the EM wave propagate through the human tissue in an effective manner. It is used to determine whether the EM wave is observed, reflected or transmitted. The structure of metamaterial is a type of lattice structure. The tunable metamaterial is adjusted by using real time and it is possible to reconfigure the device operation with the use of metamaterial. In this domain ongoing research paper includes EM band gap material (EMG) called photonic band gap (PBG).

The patch antenna is one of the types of radio wave antenna with low profile. It can be mounted on a

flat surface. It consists of square shaped microstrip patch antenna present over a metal called ground plane. A cavity slot is used for on body communication at the frequency of 2.4 GHz. It has a good efficiency and multiple layer fabrication process is done hence it has very high profile [1].

Cylindrical and rectangular patch antenna consists of two different types of frequencies. Cylindrical antenna operates at one frequency and rectangular operates at other frequency, hence both the antennas can stimulate the same substrate. This means that three different types of frequencies are obtained. It has high accuracy [2]. A wide band printed monopole antenna uses FR4 substrate. It is been designed on low cost and is easily available. These can be used for WLAN/WCDMA applications with good impedance matching properties [3]. In waveguide technology, inertial sensor node is used, on body communication, the outputs are sent to the data through node. It is easily configurable [4]. Readers may refer other important references which are listed from [5] to [12].

2. ANTENNA DESIGN

The proposed square shaped microstrip patch antenna is shown in Figure 1. The design is based on square shaped microstrip monopole patch antenna expected to operate with 2.4 GHz frequency band. It is integrated with Artificial Magnetic Conductor which offers a single layer fabrication process. Both the element of radiation and coplanar waveguide are printed on the FR4 substrate with thickness of 0.8 millimeter and dielectric constant 3.5 for telemedicine applications. AMC minimizes the antenna impedance and also achieves better impedance matching. The proximity of human tissues and the ground plane increase the front to back ratio. Figure 2 illustrates substrate layers and Table 1shows dimensions.

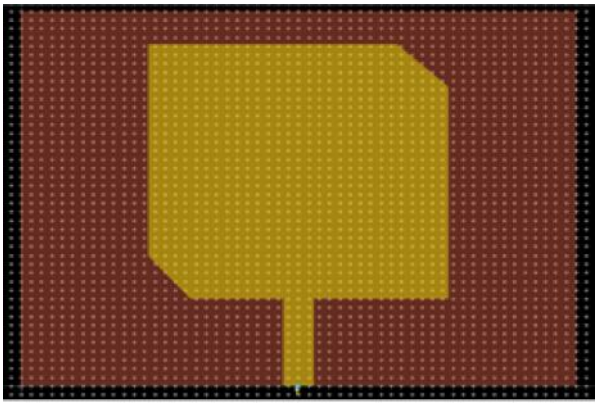

Fig.1 Square shaped microstrip patch antenna

The square shaped Microstrip patch antenna is well suited for telemedicine applications since these require compactness and light weight and ruggedness.

3. SUBSTRATE SPECIFICATIONS

The square shaped Microstrip patch antenna is designed with ground plane. The substrate is laid down over ground plane. Over the and above the substrate, a square shaped patch is incorporated by fabrication. Hence loss of an antenna can be minimized and the antenna input impedance is also minimized. It reduces the mismatches in the impedance. The antenna layout design has three layers. These are listed as follows.

- AMC ground plane
- Substrate
- Square shaped microstrip patch design

FR4 substrate is chosen as it is available easily and it also increases the gain. Fabrication process becomes easier and is very cost effective. FR4 offers an ultra low profile and the square shaped microstrip patch antenna with an AMC ground plane controlling the resonant frequency.

Table 1 Substrate Layer Specification

Sl. No	Parameter	Value
1	Ground plane	1mm
2	Dielectric medium	3.5
3	Substrate layer	1mm
4	Microstrip patch antenna	0.8mm

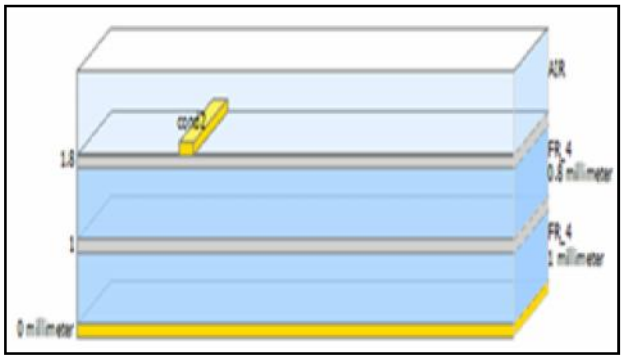

Fig. 2. Substrate layers of square shaped microstrip patch antenna

4. SIMULATED RESULTS AND DISCUSSION

The proposed antenna has been simulated by using Advanced Design System (ADS). The designed is based on square shaped microstrip monopole patch antenna operating at 2.4 GHz band. After the substrate designing

process, the frequency range can be selected between 2 GHz to 4 GHz. The reflection coefficient of antenna and the return loss can be obtained by determining S-parameters. The antenna resonates at a frequency of 2.4 GHz. It also offers very low return loss. It is estimated at about 29.58 dB. These are shown in Fig. 3.

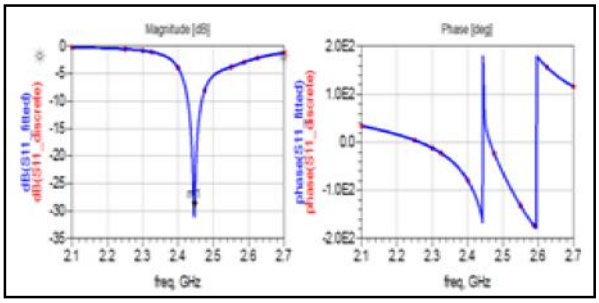

Fig.3 Return loss and phase shift of proposed square shaped microstrip patch antenna

5. RADIATION PERFORMANCE AND CURRENT DISTRIBUTION ANALYSIS

As illustrated in Figure 4, the radiation pattern can be stimulated by using square shaped microstrip patch antenna and its cut off frequency range is at about 2.4 GHz. This suits for telemedicine applications. The simulation tests are carried out on Advanced Design System software package. The stimulation of electromagnetic radiation and the current distribution directions are shown in the Figure 5 with 3D view for actual visual perception.

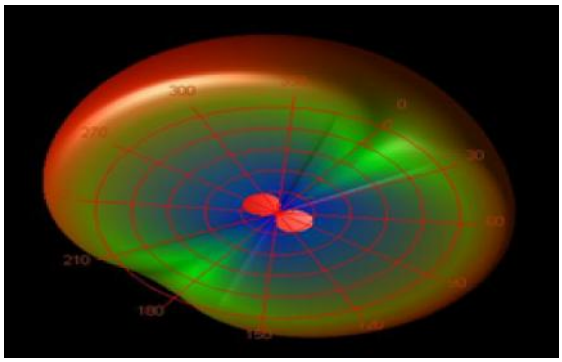

Fig. 4 Radiation pattern

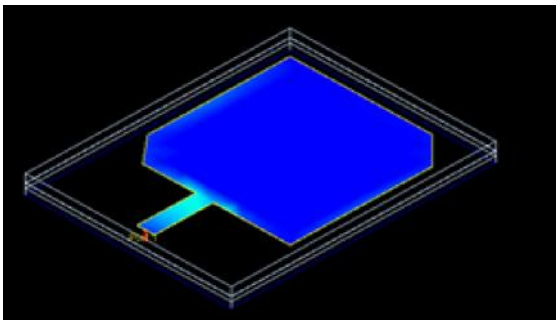

Fig. 5 Current distribution direction illustration

6. ANTENNA PARAMETERS AND RESULTS

The simulation tests have produced a gain of 6.20632 dBi for the proposed antenna. The directivity of the antenna is measured at 6.37373 dBi at 2.4 GHz. Antenna gain is a relative measure of an antenna's ability to direct or concentrate radio of the frequency energy in a particular direction or pattern. The measurement is typically measured in dBi (Decibels relative to an isotropic radiator) or in dBd (Decibels relative to a dipole radiator). The proposed antenna radiation efficiency is achieved by 96.21%. Figure 6 and Table II show various results.

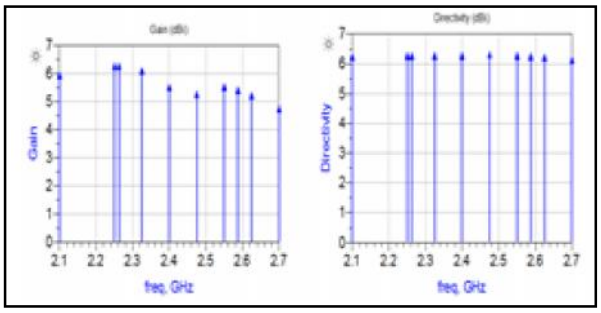

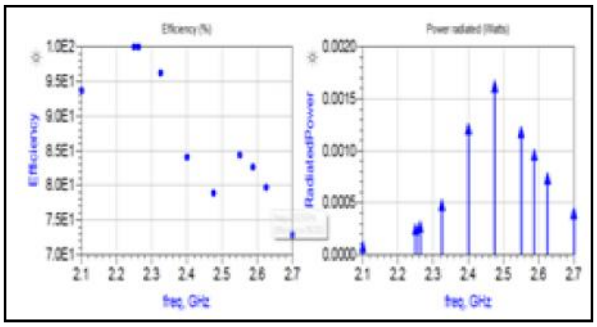

Fig. 6 Antenna parameters achieved Vs frequency opted

Table 2 List of Antenna Parameters

Sl. No.	Parameter	Value
1	Frequency (GHz)	2.4
2	Input (Watts)	0.00054298
3	Radiated power (Watts)	0.000522414
4	Directivity (dBi)	6.37373
5	Gain (dBi)	6.20632
6	Radiation efficiency (%)	96.2186
7	Maximum intensity (Watts)	0.000180377
8	Effective angle (Steradians)	2.89626
9	Angle of U Max (theta, phi)	90
10	E (theta) max (mag, phase)	71.0515
11	E (phi) max (mag, phase)	61.8346
12	E (x) max (mag, phase)	-118.165
13	E (Y) max (mag. phase)	71.0515
14	E (Z) max (mag, phase)	-108.948

The antenna parameters of rectangular patch such as gain, directivity, efficiency and radiated power which resonate at the frequency of 2.4 GHz are listed as shown in Table II. The gain of the antenna is closely related to the directivity. The antenna parameters include frequency, input power, radiated power, radiation efficiency, maximum intensity, angle of U max for both theta and phi, E (theta max), E (phi max), E (x max), E (y max), E (z max) and power. These parameters are estimated during simulation tests and are also listed in Table II. The analysis of these parameters shows that these are suitable for the telemedicine applications.

7. CONCLUSION

In this paper, Microstrip patch antenna is designed with Artificial Magnetic Conductor for telemedicine applications. The antenna gain is observed at about 6.20632 dBi and its directivity is estimated at about 6.37373dBi. The proposed antenna has a return loss at about -29 dB. Thus the efficiency of radiation is achieved at about 96.21%. By varying dimensions of patch, radiation efficiency of the antenna can be improved in future.

REFERENCES

[1] N. Haga, K.Saito, M. Takahashi and K.Ito, "Characteristics of Cavity Slot Antenna for Body-Area Networks", IEEE Trans. Antennas Propagation, Vol.57, No. 4, Apr. 2009, pp. 837-843.

[2] K-M. Luk, K.-F. Lee, and J. S. Dahele, "Analysis of the Cylindrical Rectangular Patch Antenna", IEEE Trans. Antennas Propag., Vol. 37, No.2, Feb. 1989, pp.143–147.

[3] M. N. Suma, P. C. Bybi and P. Mohanan, "A Wideband Printed Monopole Antenna for 2.45GHz WLAN Applications", Microw. Opt. Technol. Lett., Vol.48, No.5, May 2006, pp.871-873.

[4] R. Moro, S. Agneessens, H. Rogier and M. Bozzi, "Wearable Textile Antenna in Substrate Integrated Waveguide Technology", Electron. Lett., Vol.48, No.16, Aug 2012, pp. 985-986.

[5] Q. Fang, S. Lee, H. Permana, K. Ghorbani and I. Cosic, "Developing A Wireless Implantable Body Sensor Network Inmics Band", IEEE Trans. Inf. Technol. Biomed., Vol.15, No.4, 2011, pp.567-576.

[6] G. Conway and W. Scanlon, "Antennas for Over Body-Surface Comm. At 2.45 GHz", IEEE Trans. Antennas Propagat., Vol.57, No.4, Apr 2009, pp. 844-855.

[7] Y. Ouyang, D. Love and W. Chapel, "Body-worn Distributed MIMO System", IEEE Trans. Veh. Technol., Vol.58, No.4, May 2009, pp.16-22.

[8] L. Liu, S. Zhu and R. Langley, "Dual-band Triangular Patch Antenna with Modified Ground Plane", Electron. Lett., Vol.43, No.3, Feb. 1, 2007, pp.140-141.

[9] W. Rowe and R. Waterhouse, "Reduction of Backward Radiation for CPW Fed aperture Stacked Patch Antennas on Small Ground Planes, IEEE Trans. Antennas Propagat., Vol.51, No.6, Jun 2003, pp.1411-1413.

[10] C. T. Islam, M. Faruque and N.Misran, "Reduction of Specific Absorption Rate (SAR) in the Human Head with Ferrite Material and Metamaterial", Prog. Electromagn. Res. C, Vol.9, No.4758, 2009.

[11] S. Zhu and R. Langley, "Dual-band Wearable Textile Antenna on An EBG Substrate", IEEE Trans. Antennas Propagat., Vol.57, No.4, Apr 2009, pp.926-935.

[12] Y. P. Salonen, J. Kim and Y. Rahmat-Samii, "Dual-band E- shaped Patch Wearable Textile Antenna", in IEEE Antennas Propagat. Soc. Symp., Vol. 1, 2004, pp.466-469.

Highly Efficient Linear Power Amplifier for QPSK Amplification

S. Thulasi and V. Ezhilya
Department of Electronics and Communication Engineering,
VSA Group of Institutions, Salem - 636 010, Tamil Nadu
E-mail: s.thulasi.thulasi@gmail.com

Abstract

Power amplifiers are one of the main elements in a telemetry transmitter. Overall efficiency of the power amplifier varies according to the type of transistor device used for operation, bias point selection and type of modulation for carrier signal. For a launch vehicle application, a carrier signal, to be modulated with QPSK technique, linear operation of power amplifier with high efficiency is necessary. The application of this project designing comes in the RF telemetry system which operates in the S band frequency range of 2.2 to 2.3GHz. Device capable of operating at high frequency range with high efficiency and gain is necessary for such applications. In this paper, a unique design of a highly efficient and linear power amplifier with QPSK amplification is discussed. The circuit and layout designing is done on Advanced Design System (ADS) software.

Keywords: *GaN HEMT, Power amplifier, QPSK modulation*

1. INTRODUCTION

Telemetry involves the collection of data from sensors on board of the spacecraft and relay this information to the ground. The telemetry carrier modulation is Frequency Shift Keying (FSK) or Phase Shift Keying (PSK), with telemetry channel transmitted in a Time Division Multiplexing (TDM) format. There are two types of modulation techniques, linear and non linear. Linear modulation techniques include all forms of Quadrature Amplitude Modulation (QAM) and Phase Shift Keying (PSK) such as Binary Phase Shift Keying (BPSK), Quadrature Phase Shift Keying (QPSK), 8 PSK and 16QAM. These techniques are less bandwidth than non linear modulation techniques such as Frequency Shift Keying (FSK) and Minimum Shift Keying (MSK). However, for linear modulation technique, amplifiers are more expensive and less efficient than those of non linear modulation. In PSK modulation, the carrier always remains at the same amplitude and frequency. When the incoming signal channel varies from a 0 or a 1 or vice versa, the phase of the carrier shifts. PSK is very resistant to interference, since little in nature can produce such a phase shift.

In order to amplify a signal and generate the required Radio Frequency (RF) power that allows transmission of signal on to the appropriate range, a power amplifier is necessary. Efficiency and linearity depends on the class of operation of the power amplifier. various classes of operation such as class A, B, AB, C, D, E and F are available. Each class is limited to a specified portion of the input signal during which current flows in the amplifying device. Linear amplifiers preserve both amplitude and phase, whereas non linear amplifiers only preserve phase information. Thermal management and DC power consumption of a power amplifier determines its efficiency. Linearity and efficiency are two contradict factors. As linearity increases, efficiency decreases due to conductive and dielectric losses, which in turn increases the heat dissipation. A compromise between linearity and efficiency of a power amplifier is necessary for a carrier modulated with QPSK.

Gallium Nitride High Electron Mobility Transistor (GaN HEMT) is one of the latest technique in transistor technology for high power applications that operate at high frequencies such as RF power amplifier in telemetry launch vehicle applications. It reduces current and power losses in the power supply. Since GaN contains semiconductors such as GaN and AlN, which are sensitive in nature, it reduces the temperature rise in the device. For high power Rf subsystems, where thermal management and power losses is a greater problem, semiconductor channel temperature must be low enough for reliable operation. GaN provides such a reliable operation at higher temperature than GaAs and Sillicon. GaN is used when high gain, signal level and efficiency at a particular frequency is needed. It also reduce the number of stages using high gain power.

This paper discusses about the power amplifier design

for QPSK amplification with high efficiency and linearity. Section II describes about the QPSK linear amplification and section III about power amplifier theory. Section IV discusses about GaN HEMT technology. Remaining sections describes about various steps in the power amplifier designing along with simulation results and finally the conclusion.

2. QPSK LINEAR AMPLIFICATION

For satellite communication, the choice of modulation play an important role to transmit data through the channel without any degradation. It helps the transmission of message signals at the carrier frequency and can be used to provide multiple access to the radio frequency bands at frequency domain. During digital transmission the satellite link conditions may change and the altitude of transmission also changes with link conditions. It is difficult to use Amplitude Modulation (AM) in such situations. Frequency Modulation (FM) is also difficult to implement on bandwidth utilization. PM has ease of implementation compared to other modulation techniques. Phase Shift Keying (PSK) is the most communication system for transmitting and receiving high speed digital information over satellites to have a trade off among power, frequency and implementation efficiency. Since the application of this project comes in the launch vehicle, PSK is preferred. It has the advantage of constant envelope and in comparison with FSK, it provides better spectral efficiency, which is defined as the ratio of the transmitted bit rate to the bandwidth occupied by the carrier. The bandwidth occupied by the carrier depends on the spectrum of the modulated carrier and filtering it undergoes. Both BPSK and QPSK are very efficient in the way bandwidth and power are used. Higher level modulation schemes other than QPSK, can be used to increase the capacity, but it subjects the signal to greater degradation from the repeater. When higher data rate modulation schemes like QPSK, is used, it requires a linear power amplifier to faithfully reproduce the amplitude and phase information. As the data rate becomes higher, peak to average power ratio (PAR) will also be high. High peaks can cause the power amplifier to move towards saturation, causing intermodulation distortion which generate spectral regrowth., which is a condition that interfaces with signals in the adjacent frequency bands. Due to its linear amplification feature, QPSK is able to maintain low spectral side lobes; thus providing good adjacent channel performance.

3. POWER AMPLIFIER THEORY

RF power amplifiers are used in many applications such as wireless communications, TV transmissions, radar applications, etc. Efficiency of a power amplifier is an important factor in the transmitter section since it accounts for the thermal dissipation and DC power consumption. For wireless communication, thermal dissipation and DC power consumption should be less. Power that is not converted to useful signal is dissipated as heat. Power amplifiers with low efficiency will have high levels of heat dissipation. This will be a limiting factor while design a power amplifier.

A power amplifier can be operated in various classes of operation such as class A, B, AB, C, D, E and F. Here, efficiency increases from A to F and linearity increases from F to A. The most linear class A amplifier can reproduce the exact input signal at the output, with a conduction angle of 360º, but the efficiency is too low with a theoretical value of 25%. Class B power amplifier has better efficiency than class A of 70% with a conduction angle of 180º but with lower linearity due to cross over distortion. Class AB operation has better linearity than class B operation. It has a conduction angle between 180º and 360º with efficiency greater than 70%. Class C amplifiers are having better efficiency, with a theoretical value of 100%. The conduction angle is less than 180º. Classes D, E and F are called as switched mode power amplifiers. They have efficiency of 100% but with poorest linearity. Various linearization techniques have to be incorporated when such amplifiers are used for design. Since, in the designing of QPSK amplifier linearity is the main criteria; switched mode power amplifiers cannot be used. In order to incorporate both efficiency and linearity together, selection of class of operation comes in the conduction angle based classes. Among those classes, class AB has significant efficiency as well as linearity.

The class of operation for power amplifier design determines the bias point selection, which in turn the device selection. To provide voltage and current at various points of the electronic circuit, biasing circuit is necessary for a transistor. Bias circuit designing plays an important role in establishing stable operation of the device. Instability of power amplifier causes oscillations at almost every frequency and will damage or destroy the transistor.

4. GALLIUM NITRIDE FIELD EFFECT TRANSISTOR

Field Effect Transistors (FET) are those kind of transistors used to amplify the weak signals such as wireless signals. In a FET, current flows along a semiconductor path, known as the channel. At one end of the channel is an electrode called the source, and at the other end of the channel is an electrode called the drain. Electrical current can be modified by applying a voltage to a control electrode called the gate. Small changes in gate voltage can cause a large variation in the current from the source to the drain. Because the power required to control the channel is much smaller than the power the transistor can deliver to a load, the FET can amplify a radio frequency (RF) signal. FETs can be constructed from different semiconductors such as Silicon, Gallium Arsenide (GaAs), Gallium Nitride (GaN), Indium Gallium Arsenide (InGaAs) and Indium Phosphide (InP). Compared to other semiconductor structures, GaN has lower capacitances, so that an amplifier can design with wider bandwidth, lower combining losses which we can have higher efficiency, gain and thus power. These features make GaN structure to be used in satellite communication, radar applications which require higher frequency, higher bandwidth, high power and high efficiency. GaN can deliver higher current than other semiconductors because it has a high charge capacity in the channel and a high saturation velocity. It can also sustain higher breakdown fields among common semiconductors due to its large band gap. That's why GaN can deliver the highest RF power density among semiconductors. GaN FET has two structures, the vertical semiconductor structure and horizontal device structure. The vertical semiconductor structure contains, gate, barrier, channel, buffer and substrate. Horizontal structure consists of source electrode, source access region, gate controlled channel region, drain access region and drain electrode. The most important part of GaN HEMT is the gate. It's size determines the speed of the device. Smaller the gate, faster the electron flow through the gate controlled channel and the device will be faster. The gates of GaN has a length of 0.1 to 0.5µm.

RF3931 from RFMD, GaN HEMT is used for the amplifier design. It is a 48V, 30W high power discrete amplifier which has a Power Added Efficiency of 62% at 2.14GHz. It is an unmatched power transistor packaged in a hermetic, flanged ceramic package. It has a maximum RF input power of 37dBm, drain voltage of 48V, gate voltage of - 2.5V and maximum output power of 47dBm.

5. DC LOAD LINE ANALYSIS

The load line gives the every possible operating point for circuit. It is drawn on the I-V characteristics of the device. In order to operate the power amplifier in a suitable class of operation, bias point selection plays an important role. Load line is drawn with saturation point and cut off point. Saturation point gives the maximum possible drain current (ID) and cut off point gives the maximum voltage across drain and source (V_{DS}). For class AB operation, the bias point is preferred near to the cut off region. The voltages to be applied to gate and drain terminals are obtained from the load line after fixing the bias point. Fig.2 shows the DC I-V characteristics curve of the devic. The voltages at gate and drain are obtained as -3.5V and 48V respectively from the load line. The device capable of operating at 12dB gain

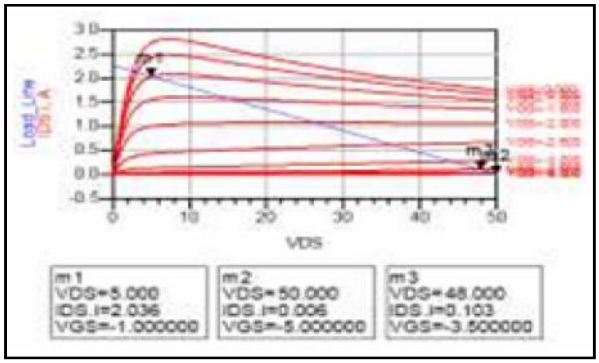

Fig.1 DC IV characteristic curve

6. BIASING CIRCUIT AND STABILITY ANALYSIS

It is important to check the stability of the device, in order to ensure that it may not function as an oscillator. So that biasing circuits plays an important role in the amplifier design. Among the three terminals gate, drain and source of the FET device, biasing circuits are provided to gate and drain and source is grounded. Fig.3 shows the entire biasing circuit provided to the device.

The gate current is negligible in comparison to the drain current. Dual supply is provided to FET such that, negative voltage for gate and a positive voltage for drain. Since gates do not draw appreciable currents, gates can be biased through low current chokes or л/4 transformers or resistors. Resistors are always used in the gates to improve stability as well as to improve isolation between

the stages. In the present scenario, the gate is biased through resistors, capacitors and an RF choke[1]. Biasing as well as coupling capacitors are provided to the device. Coupling capacitors are used to decouple Dc and Ac signals, so that the quiescent point is not changed, when Ac signals are passed to the device. That is, coupling capacitors block DC and pass AC signals to the device by providing a high impedance value. Bypass capacitors are used to force signals currents to the elements connected in the device by providing a low impedance path at the designed frequency. High impedance value is selected to be 100&! and low impedance is provided as 10^{-6}&!. Corresponding capacitor values are found by using the formula

$X_C = 1/(2pfC)$ (1)

where f= 2.25GHz. Thus the value of bypass capacitors is found as 22µF, 47µF and 1pF. The impedance value to calculate coupling capacitor is selected as 100&!. Thus the value of coupling capacitor is found to be 0.8pF. The inductor value is found by equating it to an impedance value of 1000&!. Equation to find inductance value is

$X_L = 2pfL$ (2)

The drain side is biased through л/4 transformers or RF chokes with minimum resistance value. Here, the drain biasing is done through л/4 transformers and coupling and biasing capacitors are also provided. The capacitor values are designed as did in the gate side.

Stability analysis is done on the circuit after biasing circuit is added at drain and gate of the FET device. Equation used to find the stability values are:-

Stability factor, $K = 1 - |S11|^2 - |S22|^2 + |D|^2 / (2|S21 S11|)$ (3)

Where, $D = S11S22 - S21S12$ (4)

A device will be unconditionally able if K>1 and Δ >0.

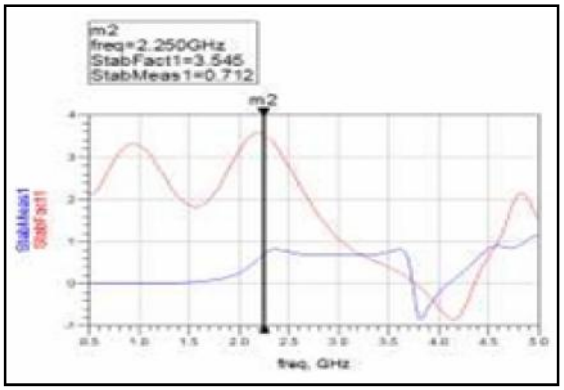

Fig.2 Stability factor and stability measure values

Figure3 shows the stability values of the device after biasing circuit is provided. Stability factor, K has a value of 3.545 and stability measure, ? has a value of 0.712, so that the device is unconditionally stable. The microstrip lines provided in the biasing circuit are used to provide smooth transition from the transistor to the external circuit. The length and width of the transmission lines are found using the LinCalc option available in the ADS software. Microstrips along with taper lines, Mtee elements and Mcross elements are used to complete the design of the biasing circuit at the drain and gate of the device. The source is grounded to have common source configuration. The substrate, RTDuroid 6010 parameters used is as shown in Figure 4.

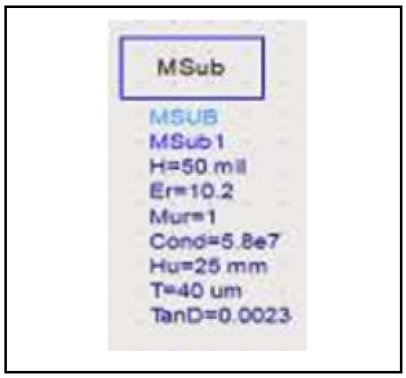

Fig.3 Substrate parameters of RTDuroid 6010

7. LOAD PULL ANALYSIS

./ Load Pull simulation is frequently used by power amplifier designers to determine, the load impedance to be provided for device or amplifier in order to achieve a particular power delivered, power-added efficiency, intermodulation distortion level, adjacent-channel leakage ratio, and other specifications. The amplifier is provided with a constant available source power and the load reflection coefficient is swept in a circular region of the Smith Chart. Thus the appropriate smith chart region is found and then suitable impedance matching circuit for the transistor is designed. [2]

Bias voltages at gate and drain along with frequency of operation and input power is provided as input for the analysis. The fundamental source impedance is initially set to a default value of 15+j*0. After performing load pull analysis, the fundamental source impedance is changed to the input impedance value corresponding to maximum power. Fig.4 shows the load pull contours in which the input impedance value is obtained as 23.750-j*4.490. Corresponding output impedance value is obtained as 22.108+j*5.025. These impedance values are then matched to 50&!.

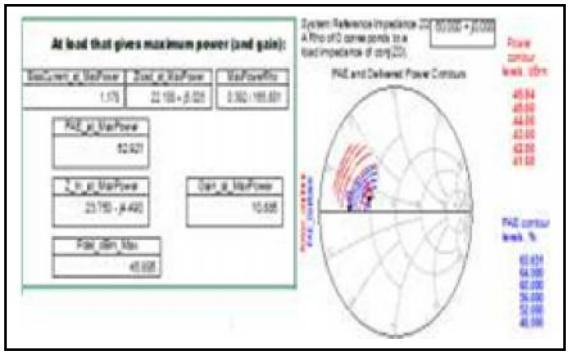

Fig.4 Load pull contours

8. IMPEDANCE MATCHING

Maximum power transfer is the main objective of every circuit. Matching at the both ends helps to attain this goal. Impedance matching is performed to transfer energy from generator to device and from device to load. In order to have maximum power the source impedance and load impedance should have conjugate match, that is, resistive part should be the same and imaginary part with same magnitude and opposite polarity. The matching network design depends on the frequency of operation used for the device[5]. Since the frequency is greater than 1GHz range, transmission line matching was chosen at the input and output side. Various methods are available to perform matching, where; smith chart, which is one of the simplest methods is used here. A smith chart is a circular plot with lot of interlaced circles on it. If we have a complex impedance of a+ib or a-ib form, then the resistive part (a) is matched to 50&! and reactance part (b) is made to zero. Smith chart contains both admittance circles as well as impedance circles. It also reflects the relationship among the normalized impedance, reflection coefficient and VSWR.

The input impedance and output impedance calculated from the load pull analysis for maximum power, gain and PAE is given at the input and output side respectively and they are matched to 50&!. Input impedance 23.750-j*4.490&! and output impedance 22.108+j*5.025&! are matched to 50+j*0&! respectively. Combination of series transmission line and open stubs are used to match source and load impedance. Fig 5 and 6 shows the input and output matching network respectively.

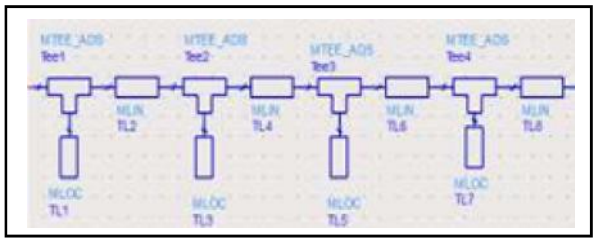

Fig.5 Input matching network

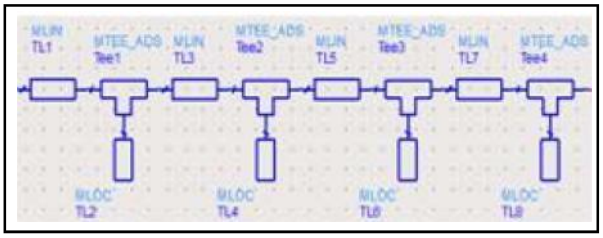

Fig.6 Output matching network

9. CIRCUIT ANALYSIS

Analysis of the entire circuit is done with biasing and impedance matching network connected to the device along with a Dc source of gate voltage -3.5V and a drain voltage of 48V respectively. The S parameter values are plotted in order to compare the improvement in gain S(2,1), reverse transmission coefficient S(1,2), reverse reflection coefficient S(2,2) and reflection coefficient S(1,1).

Figure7 shows the values after matching is provided at input and output. An improvement of gain value from 8.9dB to 11.86dB is observed. The circuit is then optimized with goals provided with PAE greater than 67% and output voltage minimum limit of 45dBm. The values after optimization is as shown in Fig.9. It shows an improvement of PAE to 67.038% and output of 45.259dBm.

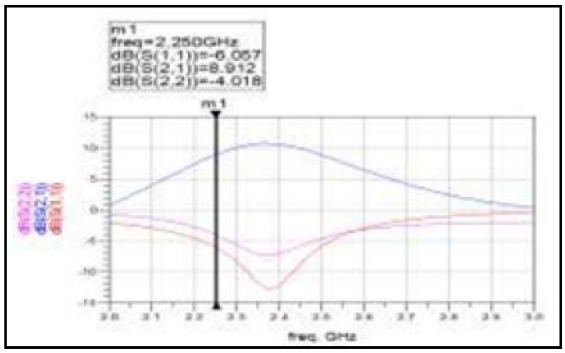

Fig.7 S parameter values before matching

Figure8 shows the S parameter values before matching circuit is provided for the device. It shows a lower gain of 8.912dB. To improve gain, matching at input and output side is provided.

PAE when biasing and matching is provided to the device. PAE was observed to be 57.258%. as shown in figure. Input power of 35dBm was provided and obtained an output power of 45.288dBm. in order to increase PAE, optimization for the input and matching circuit is done. Only the lengths of transmission lines at both the sides were selected to provide optimization, since changing the width will alter the frequency of operation of the device.

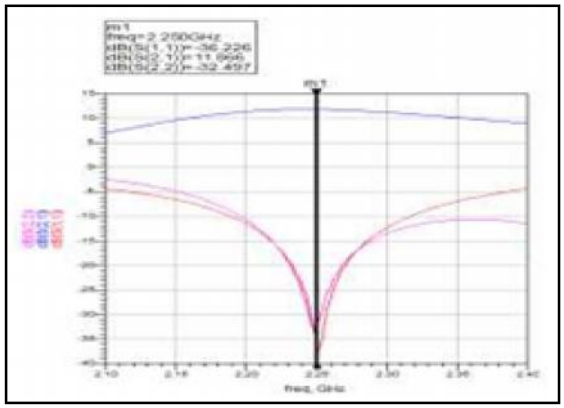

Fig. 8 S parameter values after matching

The optimization goals were provided while simulation was done such as minimum efficiency limit of 60% and minimumoutput power of 45dBm. Fig.9 shows the PAE and output power values when optimization is done for the transmission lines. Theoretically class AB power amplifier has an efficiency of 78.5% and practically between 60% to 70%. The From the designed power amplifier, an improvement in efficiency from 57.258% to 67.038% is obtained after optimization is done.

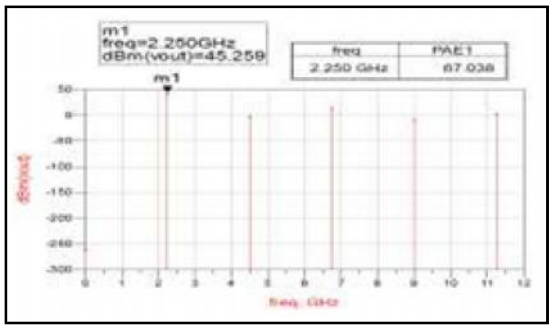

Fig.10 PAE and output power after optimization

10. MODULATED SIGNAL ANALYSIS

Next step is to provide modulation to the power amplifier. Modulation is the process of varying some aspects of the carrier wave with respect to the modulating signal. Modulation is necessary to shift the spectral content to an operating frequency band that is easily transmitted and received, to make the signal less vulnerable to noise and interference and to support multiple acces techniques. Fig.10 shows the circuit used for the modulated signal analysis. The input from data is split to two parts to have I and Q components. Two low pass Root Raised Cosine (RRC) filters are used before giving modulation[8]. This is to ensure about zero ISI condition for the channel. QPSK modulation is provided as the input to the power amplifier using QAM_Mod. Using spectrum analyzer components, the QPSK spectrum before and after amplification is plotted.

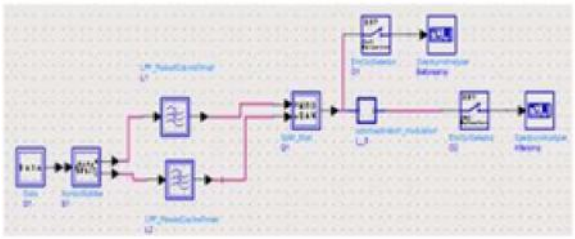

Fig.11 ADS schematic diagram of Modulated signal analysis

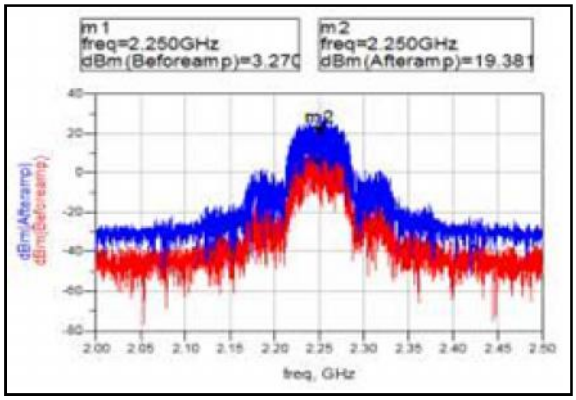

Fig.12 QPSK power spectrum

Figure 13 shows the QPSK spectrum when modulation is provided to the device. An amplification from 3.270dBm to 19.381dBm is observed.

11. LAYOUT CO-SIMULATION

Layout designing and co-simulation of the simulated circuit is done for visualizing the effects of layout on the simulated results. Fig 13 shows the layout design and fig.14 shows the S parameter values obtained when layout is simulated. Apart from the simulated results, the gain is obtained as 8.528dB, which is a lower value. This is due to the inclusion of the EM model.Fig.15 shows the corresponding circuit co-simulation in which the designed capacitors, resistors and inductors are provided.

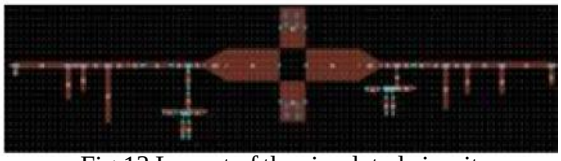

Fig.13 Layout of the simulated circuit

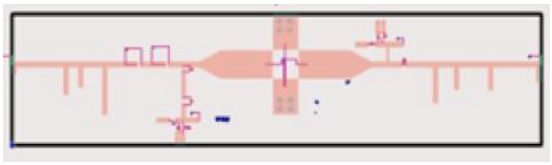

Fig.14 Circuit co-simulation

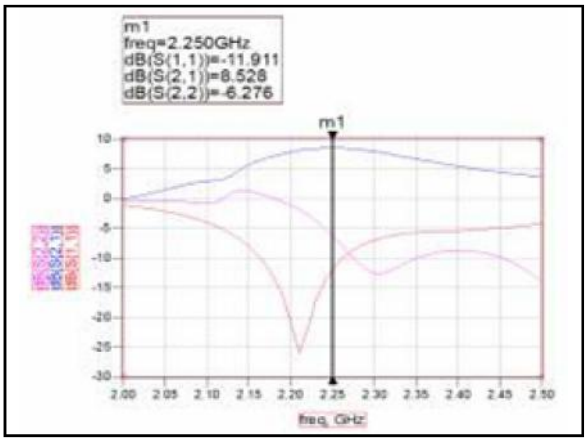

Fig.15 S parameter values of layout

12. CONCLUSION

In this paper class AB power amplifier was designed with QPSK amplification. It was subjected to operate in S band frequency of 2.25GHz. Biasing circuit was applied according to the class of operation and matching networks were designed according to the input and output impedance values obtained from the load pull analysis. The matched design showed an improved performance gain of 11.866dBm at the desired frequency range. QPSK amplification is also achieved with a less ACPR value.

REFERENCES

[1] Inder J Bahl, "Fundamentals of RF and Microwave Transistor Amplifiers", John Wiley and Sons Publications, 2009.

[2] Jose C. Pedro, Luis C. Nunes and Pedro M. Cabral, "Simple Method to Estimate the Output Power and Efficiency Load–Pull Contours of Class-B Power Amplifiers", IEEE Transactions On Microwave Theory And Techniques, Vol. 63, April 2015.

[3] Jin Shao, David Poe, Han Ren, Bayaner Arigong, Mi Zhou, Jun Ding, Rongguo Zhou, Hyoung Soo Kim and Hualiang Zhang, "Dual- Band Microwave Power Amplifier Design Using GaN Transistors", IEEE 2014.

[4] Soumya Ranjan Ghosh and Kamran Khan, "A Low Power Adaptive Bias Fully Differential Operational Amplifier", International Conference on Advanced Communication Control and Computing Technologies, IEEE 2014.

[5] David M Pozar, "Microwave Engineering", John Wiley and Sons, 2012.

[6] Sunil Kumar Khahl, Pallavi Singh Sweta Rabra, Richa Saxena and Tapas Chakarvarty, "Broadband Impedance Matching Technique for Microwave Amplifiers", , IEEE 2007.

[7] Gyan Prakash Pal, Anuj Kumar Shrivastav, "High Electron Mobility Transistor (HEMT)", International Journal of ScientificResearch Engineering &Technology (IJSRET), Vol.1, No.1, March 2012, pp 043-046.

[8] A. S.Kang and Vishal Sharma, "Pulse Shape Filtering in Wireless Communication-A Critical Analysis", International Journal of Advanced Computer Science and Applications, (IJACSA), Vol. 2, No.3, March 2011.

[9] Snehasis Despande, I. V. Prasanna and S K Panda, "An Efficient Impedance Matching Technique for Improving Narrowband Power Line Communication in Residential Smart Grids", International Journal of Advanced Research in Electrical, Electronics and InstrumentationEngineering, Vol.2, No.7, July 2013.

Experimental Investigation and Optimization of Process Parameters in WEDM on Machining of H13 Steel Using Response Surface Methodology

R. Arunbharathi, P. Ashoka Varthanan, M. Akilesh, R. Abinash Raju and G.B. Aravind Kumar
Department of Mechanical Engineering,
Sri Krishna College of Engineering and Technology, Coimbatore - 641 008, Tamil Nadu
E-mail: arunpsg09@gmail.com, ashokavarthanan@skcet.ac.in

Abstract

The main objective of the present work is to optimize the process parameters of wire electrical discharge machining process on machining AISI H13 die steel by considering the significant effect of input parameters viz. pulse on time, peak current, pulse off time and wire tension in order to get the desired outcome such as maximizing material removal rate, better surface finish and reduced kerf width. H13 steel is chosen as the specimen based on the wide usage in industrial applications like making of Hot punches and dies for blanking, bending, swaging and forging operations, hot extrusion dies for aluminium cores, ejector pins, inserts and nozzles for aluminium, tin and lead die casting. In this work a brass wire of 250ġm diameter is used as wire tool electrode and De-ionized water as the dielectric fluid. 30 experimental runs were carried out on the specimen based on the full factorial central composite design using response surface methodology. The performance characteristics viz., Material Removal Rate, Surface Roughness and Kerf Width were measured and analyzed using Minitab software analytically as well as graphically in order to evaluate the performances of the wire electrical discharge machining process. Mathematical model is developed for predicting the values of responses in terms of interactive and higher order input process parameters. The Analysis of variance (ANOVA) is performed to find the significant process parameters for material removal rate, surface roughness and Kerf width. The adequacy of the above proposed model is also tested using ANOVA. Response surface plot for the responses were plotted by considering the significant parameters. Finally optimal combination of process parameters were obtained through desirability function approach for this multi-objective optimization problem to maximize material removal rate, better surface finish and reduced kerf width by using Response Optimizer plot.

Keywords: *Desirability Function, H13 Steel, Kerf Width, Response Surface Methodology*

1. INTRODUCTION

WEDM process is usually used in combination with CNC and will only work when a part is to be machined completely through. The melting temperature of the parts to be machined is an important parameter for this process rather than strength or hardness. The surface quality and material removal rate (MRR) of the machined surface by wire EDM will depend on different machining parameters such as applied peak current, pulse on time, pulse off time, wire tension and wire materials. WEDM process is commonly conducted on submerged condition in a tank fully filled with dielectric fluid; nevertheless it also can be conducted in dry condition. During the WEDM process, the material is eroded ahead of the wire by using the channel of plasma generated by electric sparks between two conductive materials (i.e. electrode and the work piece), this channel of plasma converted into thermal energy at a temperature range of 8000 to 12000şC at a pulsating direct current supply of 20000 to 30000 Hz. The electrode and work piece are separated by a small gap being immersed in dielectric fluid, an electric spark is produced in between this small gap and the work piece material is eroded, as the pulsating current is turnedoff, the plasma breaks down which leads to sudden reduction in the temperature and the eroded material is flushed away with the help of dielectric fluid in the form of microscopic debris. With each electric spark discharge a small crater is formed on both the work piece and the electrode which is a prime decider in the final surface quality. As there is no direct contact between the work piece and the wire, eliminating the mechanical stresses during machining.

2. LITERATURE REVIEW

Aniza Alias *et al* [1], has reported that, improper electrical parameters settings can affect the processing

efficiency and surface roughness due to arcing phenomenon that lead by discharge focal point. Objective of the paper is to find the influence of three different machine rates which are 2 mm/min, 4 mm/min and 6 mm/min with constant current (6A) with WEDM of Titanium Ti-6Al-4V. The effects of various process parameters on the cutting width, material removal rate, surface roughness and surface topography are also discussed.

Farnaz Nourbakhsh *et al* [2], investigated the influence of zinc-coated brass and high speed brass wire on the performance of wire electro-discharge machining of titanium alloy. The process parameters including cutting speed, wire rupture and surface integrity are obtained by considering input parameters like pulse width, servo voltage, pulse current and wire tension. A Taguchi L18 design of experiment has been applied. It was also found that the cutting speed increases with peak current and pulse off time. Surface roughness was found to increase with pulse width and decrease with pulse interval. The Analysis of Variance table is carried out for all process parameters to determine the significant ones. Compared with high-speed brass wire, zinc-coated brass wire results in elevated cutting speed and even surface finish. Also, SEM photographs validated that uncoated wire produces a surface finish with more cracks, craters and melted drops.

Jaganjeet Singh *et al* [3], described the optimization of the WEDM process using Taguchi methodology. It was found that the Taguchi's parameter design is a simple, systematic, reliable, and more efficient tool for optimization of the machining parameters. The effects of different machining parameters such as pulse-on time, pulse-off time, peak current, servo voltage, wire tension and wire feed has been studied though machining of H13 hot work steel. An attempt has been made to optimize the machining conditions for surface roughness based on (L18 Orthogonal Array) Taguchi methodology.

Max Schwade [4], stated that EDM is time consuming especially for the application of new materials or in the case of unfavorable machining conditions. Due to the large number of influencing factors and their interdependencies it is difficult to foretell the machining conditions only by interpretation of the used generator parameters. In this study the actual physical values for current and voltage as well as pulse on-time and off-time of each discharge was found by monitoring the electrical process signals.

G. Harinath Gowd [5], optimized the wire EDM process parameters for machining SS304. After conducting pilot experiments and literature survey, the influencing parameters were identified. The effect of input parameters such as pulse-on time, pulse-off time, wire tension and water pressure on surface roughness and material removal rate while machining the stainless steel 304 material is analysed.

Sivaprakasam *et al* [6], investigated the influence of three different independent parameters such as voltage, capacitance and feed rate of micro wire electrical discharge machining performances of material removal rate (MRR), Kerf width (KW) or cutting width and surface roughness (SR) utilising response surface methodology with central composite design (CCD). The experiments are carried out on titanium alloy (Tie6Ale4V). Analysis of variance (ANOVA) was executed to find out the significant impact of each factor. The model evolved using genetic algorithm (GA) was used to determine the optimal machining conditions using multi-objective optimization technique.

Ugrasen *et al* [7], has established statistically significant machining parameters and the percentage contribution of these parameters on accuracy, surface roughness and MRR. Each experiment has been performed using L16 orthogonal array under different cutting conditions of pulse-on, pulse-off, current, and bed speed. Among various process parameters voltage and flush rate were persistent. Based on this analysis, process parameters are optimized. ANOVA is performed to calculate the relative magnitude of the each factor on the objective function. Evaluation and comparison of responses was done using artificial neural network.

3. EXPERIMENTAL DETAILS

3.1 Experimentation

The experiments were carried out on a five axis Electronica Sprintcut 734 CNC Wire cut machine. Sprintcut 734 provides full flexibility to the operator in choosing parameter values with in a wide range. The WEDM setup is shown in Figure 1. A brass wire of 250μm diameter is used as the tool material. De-ionized water is used as the dielectric fluid.

Fig.1 Wire EDM setup for experimentation

3.2 Work Piece

In this work, H13 hot work tool steel is used for the experimentation. The material has high hot tensile strength, hot wear-resistance, toughness, good thermal conductivity and insensitiveness to hot cracking. H13 type grade offers a good for experimentation, resistance to softening up to 600ºC, combined with good stability in hardening and high toughness, making it suitable not only for hot die applications but also plastic moulds. The composition of metal is shown in Table 1. In this work H13 tool steel plate of 100mm x 50mm x 15mm is used. The machined work pieces with cut pieces is shown in Figure 2.

Table 1 Composition of Workpiece Material

Element	C	Mn	P	Cr	Vn	Mb
%	0.316	0.338	0.0125	4.956	1.09	1.285

Fig. 2 Machined work piece with cut pieces

3.3 Design of Experiments with CCD

Using the response surface methodology, the different combinations of input parameters to conduct the experiments and their corresponding responses are tabulated in Table 2. The central composite design is adopted for creating 30 runs.

3.4 Monitoring of Output Responses

3.4.1 Material Removal Rate

The metal removal rate (mm3/min) is calculated from the cutting speed data directly displayed by the machine tool with the help of the Eq. 1. Values of the cutting speed are noted for certain distance from the initiation of cut along a particular axis. This is done to ensure that readings are to be noted only when the cutting is properly stabilized. The offset of the wire is set at zero.

Material removal rate = cutting speed x kerf width x height mm^3/min. (1)

3.4.2 Surface Roughness

Surface roughness of the workpiece was measured using MITUTOYO made surface roughness tester SJ-201P instrument having stylus radius of 3mm and its resolution is 0.1µm and it is shown in Figure 3. It is a shop–floor type surface roughness measuring instrument, which traces the surface of various machine parts and calculates the surface roughness based on roughness standards, and displays the results in µm.

Fig.3 Surface Roughness Tester

3.4.3 Kerf Width

Kerf width occurs during machining is measured using the tool maker microscope. It determines the dimensional accuracy of the finishing part, is of extreme importance. The internal corner radius to be produced in WEDM operations is also limited by the kerf.

Table 2 Design of Experiments and its Responses

STD Order	Ton	Toff	IP	WT	Responses		
					MRR	KW	SR
Unit	(µs)	(µs)	(amps)	(N)	(mm³/ min)	(mm)	(µm)
12	125	58	190	8	8.3292	0.279	2.20
8	125	58	210	6	9.4567	0.287	3.25
19	120	54	200	7	8.1218	0.273	2.52
2	125	50	190	6	12.725	0.285	2.56
10	125	50	190	8	12.470	0.289	2.41
15	115	58	210	8	5.0908	0.286	2.67
17	120	54	200	7	8.2913	0.275	2.94
13	115	50	210	8	7.7532	0.284	3.04
20	120	54	200	7	8.2913	0.275	2.94
1	115	58	190	6	7.0343	0.269	1.87
3	115	58	190	6	4.8655	0.263	1.72
4	125	58	190	6	8.7354	0.276	2.56
7	115	58	210	6	4.7912	0.273	2.75
9	115	50	190	8	6.8753	0.267	1.94
18	120	54	200	7	8.2474	0.281	2.97
14	125	50	210	8	13.875	0.300	3.47
6	125	50	210	6	13.813	0.299	3.58
5	115	50	210	6	7.3437	0.273	2.87
11	115	58	190	8	4.7038	0.265	1.61
16	125	58	210	8	9.9056	0.302	3.04
21	110	54	200	7	5.5136	0.267	2.14
22	130	54	200	7	14.229	0.306	3.37
30	120	54	200	7	8.1696	0.276	2.64
27	120	54	200	5	8.358	0.280	2.54
24	120	62	200	7	5.6592	0.259	2.76
25	120	54	180	7	7.6362	0.267	1.98
23	120	46	200	7	13.370	0.286	2.87
29	120	54	200	7	8.2225	0.275	2.7
26	120	54	200	7	9.0244	0.293	3.12
28	120	54	200	9	8.7822	0.287	2.64

4. RESULTS AND DISCUSSION

The experiments were framed and conducted by employing response surface methodology (RSM). The selection of appropriate model and the development of response surface models have been carried out by using Minitab 17 software. The regression equations for the selected model were obtained for the response characteristics, viz., Material Removal Rate, Kerf Width and Surface Roughness. These regression equations were developed using the experimental data and were plotted to investigate the effect of process variables on various response characteristics. The analysis of variance (ANOVA) was implemented to statistically analyze the results.

4.1 Analyis of Variance

Analysis of variance is carried out to statistically analyze the results. ANOVA checks the values of R^2 as it explains the ratio of the variability explained by the model to the total variability inherent in the observation data of experiments. It also shows adequate precision which calculates signal to noise ratios. A ratio greater than 4 shows that the model to be fit. Process variables having p-value < 0.05 are considered significant terms for the given response parameters. The backward elimination process eliminates the insignificant terms to adjust the fitted quadratic models and in the present work backward elimination process with α to exit = 0.05 is used to eliminate the insignificant terms.

4.1.1 ANOVA for Surface Roughness

Surface roughness is an important process criterion, which dictates the condition of the surface component which has to be machined. The Analysis of Variance of surface roughness is given in Table. 3. Based on analysis of variance as shown in Table. 3 the Values of 'Prob.> F' less than 0.05 indicates that model terms are significant at 95% confidence level. F-value of model is 12.62 and the associated p-value is lower than 0.05 and it indicates that the model is significant. The p-value for lack of fit is 0.494 suggesting that this model adequately fits the data. From ANOVA results, it could be observed that factors Ton, Toff and IP are significant and the other interaction factors are non-significant. Almost 84% of the total variation in the response data could be contributed to factors T_{on} and IP.

Table 3 Analysis of Variance of Surface Roughness

Source	DF	Adi SS	Adi MS	F-value	P-value
Model	15	6.87227	0.45815	12.62	0
Blocks	1	0.00641	0.00641	0.18	0.681
Linear	4	6.52083	1.63021	44.89	0
Ton	1	2.07682	2.07682	57.19	0
Toff	1	0.1944	0.1944	5.35	0.036
IP	1	4.2336	4.2336	116.58	0
WT	1	0.01602	0.01602	0.44	0.517
Square	4	0.21538	0.05383	1.48	0.26
Ton*Ton	1	0.00943	0.00943	0.26	0.618
Toff*Toff	1	0.00034	0.00034	0.01	0.924
IP*IP	1	0.1336	0.1336	3.68	0.076
WT*WT	1	0.10643	0.10643	2.93	0.109
2-way Interaction	6	0.12965	0.02161	0.6	0.73
Ton*off	1	0	0	0	1
Ton*IP	1	0.02103	0.02103	0.58	0.459
Ton*WT	1	0.0484	0.0484	1.33	0.268
Toff*IP	1	0.0196	0.0196	0.54	0.475
Toff*WT	1	0.03423	0.03423	0.94	0.348
IP*WT	1	0.0064	0.0064	0.18	0.681
Error	14	0.50839	0.03631		
Lack-of-fit	10	0.37519	0.03752	1.13	0.494
Pure	Error	4	0.1332	0.0333	
Total	29	7.38067			
Model	Summary				
S	R-sq	R-sq(adj)	R-sq(pred)		
0.19056	93.11%	85.735%	63.29%		

4.1.2 ANOVA for Material Removal Rate

From ANOVA results given in Table 4, it could be observed that factors T_{on}, Toff and IP are significant, in addition to that one higher order term T_{on}^2 and the other interaction factors are non-significant. It was observed from the F and P values that the factors Ton and Toff are most significant for MRR. This can also be observed from the values of percent contribution obtained for each source, which quantifies the contribution of a parameter towards the variation in response. Almost 88% of the total variation in the response data could be contributed to factors T_{on} and IP.

Table 4 Analysis of Variance for Material Removal Rate

Source	DF	Adi SS	Adi MS	F-value	P-value
Model	15	234.09	15.606	41.89	0
Blocks	1	1.189	1.189	3.19	0.096
Linear	4	226.36	56.592	151.89	0
Ton	1	137.62	137.62	369.38	0
Toff	1	75.413	75.413	202.4	0
IP	1	13.243	13.243	`35.54	0
WT	1	0.083	0.083	0.22	0.644
Square	4	3.859	0.965	2.59	0.082
Ton*Ton	1	2.858	2.858	7.67	0.015
Toff*Toff	1	1.498	1.498	4.02	0.065
IP*IP	1	0.22	0.22	0.59	0.455
WT*WT	1	0.192	0.192	0.51	0.485
2FI	6	2.68	0.447	1.2	0.362
Ton*off	1	1.332	1.332	3.57	0.08
Ton*IP	1	0.175	0.175	0.47	0.505
Ton*WT	1	0.191	0.191	0.51	0.485
Toff*IP	1	0.516	0.516	1.39	0.259
Toff*WT	1	0.458	0.458	1.23	0.286
IP*WT	1	0.007	0.007	0.02	0.89
Error	14	5.216	0.373		
Lack-of-fit	10	5.192	0.519	86.56	0
Pure	Error	4	0.024	0.006	
Total	29	239.31			
Model	Summary				
S	R-sq	R-sq(adj)	R-sq		
0.610405	97.82%	95.48%	85.66%		

4.1.3 ANOVA for Kerf Width

From ANOVA results found in Table 5, it could be observed that factors Pulse on time, Pulse off time, Current, Wire Tension and two higher order term TonI, WTI are significant and the other interaction factors are non-significant. It was observed from the F and P values that the factors T_{on} and IP are most significant for kerf width. This can also be observed from the values of percent contribution obtained for each source, which quantifies the contribution of a parameter towards the variation in response.

RSM is a statistical technique for calculating and representing the cause and effect relationship between true mean responses and input control variables. The main idea of RSM is to use a set of designed experiments to obtain an optimal response. In this work, response surface modelling is utilized for determining the relations between the various WEDM process parameters on the responses, i.e., Material Removal Rate (MRR), Surface Roughness (SR) and Kerf Width (KW).

4.2.1 Effect of Process Parameters on MRR

The regression coefficients of the second order equation are acquired by using the experimental values. The mathematical equation for the material removal rate as a function of four input process variables was developed using experimental data and is shown in Equation 2.

MRR = 174 - 2.41 Ton + 0.31 Toff - 0.307 IP - 6.45 WT + 0.01291 Ton*Ton + 0.01461 Toff*Toff + 0.00090 IP*IP + 0.084 WT*WT 0.01442 Ton*Toff + 0.00209 Ton*IP + 0.0219 Ton*WT - 0.00449 Toff*IP + 0.0423 Toff*WT + 0.0021 IP*WT (2)

The response surface is plotted to study the effect of process variables on the material removal rate and is shown in Figure 4a-4c. From Fig. 4a the material removal rate is found to have an rising trend with the increase of pulse duration and at the same time it decreases with the increase of pulse off time. From Figure 4b the terial removal rate is found to have an increasing trend with increase in pulse on time and kerf width. Figure 4c shows that the material removal rate increases with increase in peak current.

Table 5 Analysis of Variance for Kerf Width

Source	DF	Adi SS	Adi MS	F-value	P-value
Model	15	0.004011	0.000267	17.88	0
Blocks	1	0.000001	0.000001	0.09	0.768
Linear	4	0.003518	0.00088	58.8	0
Ton	1	0.001926	0.001926	128.77	0
Toff	1	0.00033	0.00033	22.07	0
IP	1	0.001107	0.001107	74.01	0
WT	1	0.000155	0.000155	10.37	0.006
Square	4	0.000342	0.000086	5.72	0.006
Ton*Ton	1	0.000206	0.000206	13.76	0.002
Toff*Toff	1	0.000016	0.000016	1.06	0.321
IP*IP	1	0.000034	0.000034	2.28	0.153
WT*WT	1	0.000109	0.000109	7.26	0.017
2-way	6	0.000149	0.000025	1.66	0.202
Ton*off	1	0.000033	0.000033	2.21	0.159
Ton*IP	1	0.000003	0.000003	0.2	0.658
Ton*WT	1	0	0	0	0.949
Toff*IP	1	0.000023	0.000023	1.51	0.24
Toff*WT	1	0.000023	0.000023	1.51	0.24
IP*WT	1	0.000068	0.000068	4.55	0.051
Error	14	0.000209	0.000015		
Lack-of-fit	10	0.000173	0.000017	1.89	0.282
Pure	Error	4	0.000036	0.000009	
Total	29	0.004221			
Model	Summary				
S	R-sq	R-sq(adj)	R-sq(pred)		
0.003867	95.04%	89.72%	69.26%		

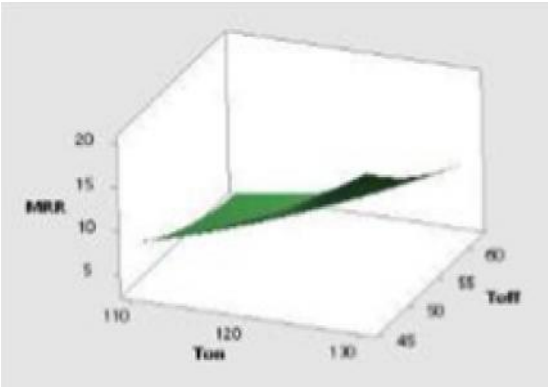

Fig. 4(a) Combined effect of Ton and Toff on MRR

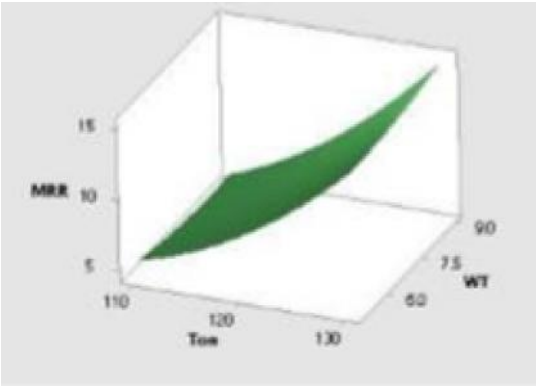

Fig. 4(b) Combined effect of Ton and WT on MRR

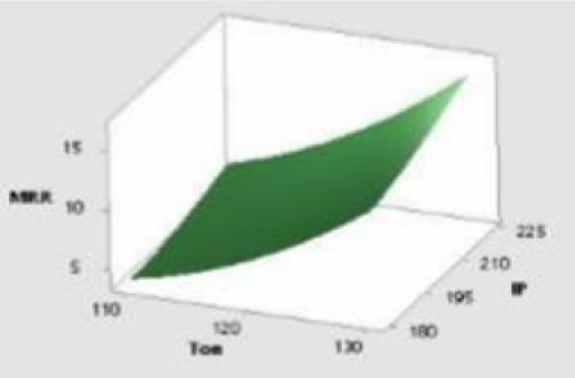

Fig. 4c Combined effect of Ton and IP on MRR

4.2.2 Effect of Process Parameters on KW

The regression equation for the kerf width as a function of four input process variables was developed using experimental data and is shown in Equation 3.

KW = 2.395 - 0.02229 Ton + 0.00482 Toff - 0.00788 IP - 0.0811 WT + 0.000110 Ton*Ton-0.000048 Toff*Toff + 0.000011 IP*IP + 0.001990 WT*WT - 0.000072 Ton*Toff + 0.000009 Ton*IP - 0.000012 Ton*WT + 0.000030 Toff*IP+ 0.000297 Toff*WT + 0.000206 IP*WT. (3)

The response surface is plotted to study the effect of process variables on the kerf width and is shown in Figure 5a-5c. From Figure 5a the kerf width is found to have an rising trend with the increase of pulse duration and at the same time it decreases slowly with the increase of pulse off time. It is observed from Figure 5b that the kerf width increases slightly with increase in peak current. The Figure 5c shows that kerf width not varied with increase in wire tension.

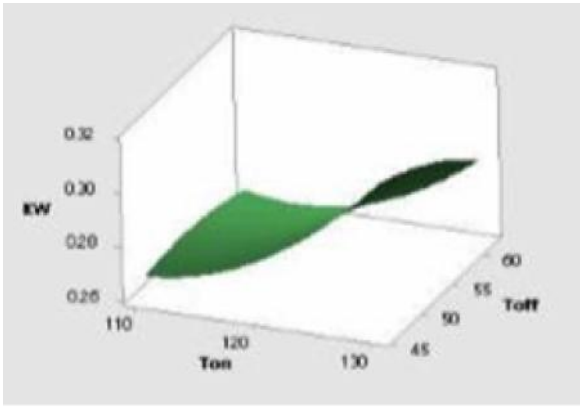

Fig. 5 (a) Combined effect of Ton and Toff on KW

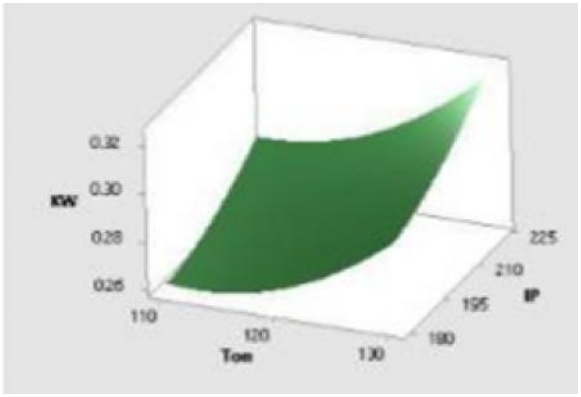

Fig. 5 (b) Combined effect of Ton and IP on KW

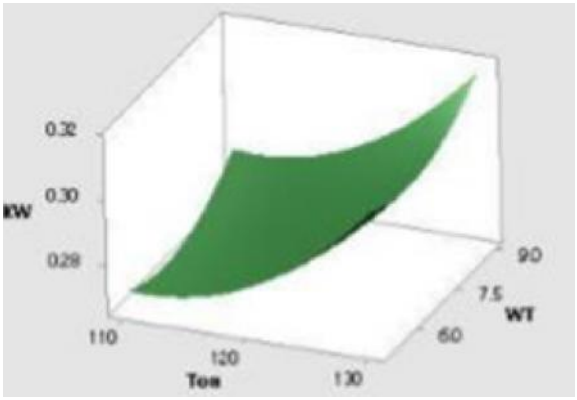

Fig. 5(c) Combined effect of Ton and WT on KW

4.2.3 Effect of Process Parameters on SR

The regression equation for the kerf width as a function of four input process variables was developed using experimental data and is shown in Equation 4.

SR = -91.2 + 0.459 Ton + 0.257 Toff + 0.441 IP + 2.39 WT 0.00074 Ton*Ton - 0.00022 Toff*Toff -0.000698 IP*IP - 0.0623 WT*WT + 0.00000 Ton*Toff - 0.000725 Ton*IP-0.01100 Ton*WT - 0.00087 Toff*IP 0.0116 Toff*WT + 0.00200 IP*WT. (4)

The response surface is plotted to study the effect of process variables on the surface roughness and is shown in Figure 6a-6c. From Figure 6a the surface roughness is found to have an rising trend with the increase of pulse duration and at the same time it declines slightly with the increase of pulse off time. It is observed from the Figure 6b that the surface roughness increases with increase in peak current. The Figure 6c shows that the surface roughness increases first and decreases with increase in wire tension.

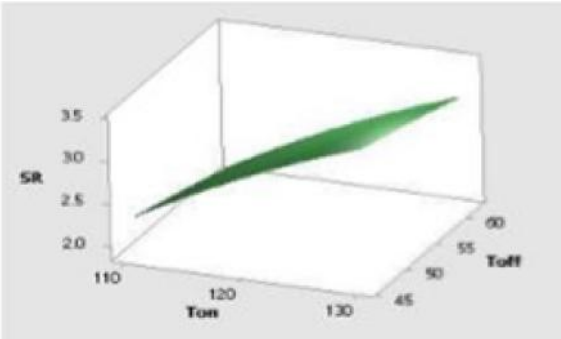

Fig. 6 (a) Combined effect of Ton and Toff on SR

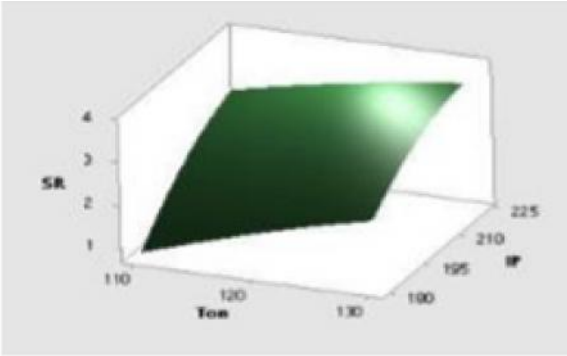

Fig. 6 (b) Combined effect of Ton and IP on SR

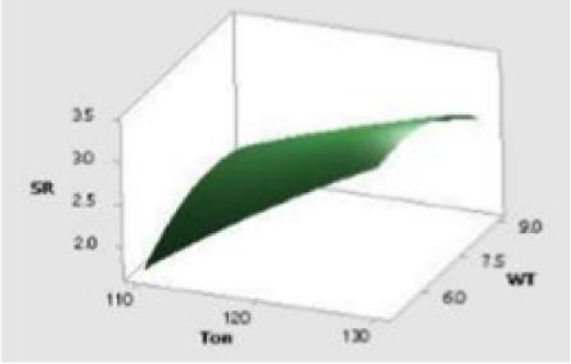

Fig. 6 (c) Combined effect of Ton and WT on SR

5. CONCLUSIONS

Experimental investigation on wire electrical discharge machining of H13 tool steel is performed with a view to correlate the process parameters with the responses such as material removal rate, kerf width and surface roughness. The process has been successfully modeled using response surface methodology (RSM) and model acceptability checking is also carried out using Minitab software. The central composite design is adopted for designing the experiments. The second-order response models have been checked with analysis of variance. Finally, an attempt has been made to identify the optimum machining conditions to provide the best possible responses within the experimental constraints.

This study can help researchers and industries for developing a robust, reliable knowledge base and early prediction of MRR, kerf width and surface roughness without experimenting with WEDM process for H13 steel.

- The present study develops MRR models for four different parameters namely pulse current, pulse on, pulse off and wire tension for WEDM process on H13 steel using response surface method. Ton and Toff are the most significant factors for material removal rate. The value of MRR increases with an increase of pulse on time and decreases with increase in pulse off time. WT has no significant effect on MRR.
- For kerf width, all the four parameters considered in this experiments are significant.
- Among these, pulse on time and peak current are the most significant. KW increases with increase in pulse on time and gradually increased with the increase in peak current.
- For surface roughness, pulse on time and peak current are the factors that most significant.
- Surface roughness value increases with increase in pulse on time and peak current and decreases slowly with increase in pulse off time.
- Finally, the obtained results are optimized to maximizing material removal rate and minimizing kerf width and surface roughness using desirability approach. The optimum parameter of combination setting is pulse on time 120 µs, pulse off time 46 µs, peak current 180 Amps and wire tension 8 N for maximizing MRR and minimizing SR and KW.

REFERENCES

[1] Aniza Alias, Bulan Abdullah, Norliana Mohd Abbas, “Influence of Machine Feed Rate in WEDM of Titanium Ti-6Al-4V with Onstant Current (6A) Using Brass Wire”, Proceeding Engineering, Vol.41, 2012, pp.1806-1811.

[2] Farnaz Nourbakhsh, K P Rajurkar, A P Malshe, Jain Cao, “Wire Electro-Discharge Machining Of Titanium Alloy”, Procedia CIRP, Vol.5, 2013, pp.1318.

[3] Jaganjeet Singh, Sanjeev Sharma, “Effects of Process Parameters on Material Removal Rate and Surface Roughness in WEDM of H13 Tool Steel”, International Journal of Current Engineering and Technology, ISSN 2277- 4106, Vol.3, No.5, 2013.

[4] Max Schwade, "Fundamental Analysis of High Frequent Electrical Process Signals for Advanced Technology Developments in WEDM", Procedia CIRP, Vol.14, 2014, pp.436-441.

[5] Harinath Gowd G, Gunasekhar Reddy M, Bathina Sreenivasulu, Manu Ravuri, "Multi Objective Optimization of Parameters in WEDM during Machining of SS304", Procedia Materials Science , Vol.5, 2014, pp.1408-1416.

[6] Sivaprakasam, P. Hariharan, S. Gowri, "Modeling and Analysis of Micro-WEDM Process of Titanium Alloy (Tie6Ale4V) Using Response Surface Approach", Engineering Science and Technology, An International Journal, pp.1-9.

[7] G. Ugrasen, H.V. Ravindra, G.V.Naveen Prakash, and R. Keshavamurthy, "Process Optimization and Estimation of Machining Performances Using Artificial Neural Network in Wire EDM", Procedia Material Science, Vol.6, 2014, pp.1752-1760.

Autodietary: A Smartphone Application for Food Recognition and Calories Estimation

V. Devisurya and Dr. S. Rathi
Government college of Technology, Coimbatore - 641 013, Tamil Nadu

Abstract

Now a days people are more interested in weight control, healthily eating and avoiding obesity. A system that can measure calories of foods may be very useful for them. Use of wearable sensors for food identification may be inconvenient to the users. Recently, due to ubiquity of mobile devices such as smart phones the health monitoring application is easily done by using built in camera present in it for food recognition in our plate. This application is very helpful in more regular and balanced diet, alerts on excessive snacking in a day, suggested intervals between meals, Medical auxiliaries in therapy of nutrition-related diseases etc. Image of a food has to be taken using smartphone camera before eating. After pre- processing image is segmented and various features like size, shape, colour and texture are calculated. Recognition of food is done by SVM classifier based on various extracted features. Using weight and food name the number of calories are calculated and saved in database with date and time. This proposed scheme provide accurate calories compared with other approaches.

Keywords: *Image processing techniques, SVM Classification.*

1. INTRODUCTION

Many people have already known that the food intake could affect our health. There are many reports that summarize about the suitable daily amount of calories. However, it is difficult to do it practically. The users, who lack of knowledge about nutrition, might be unable to know the amount of calories in each meal. Although they can ask experts to identify the amount of calories, it is not convenient and they could not aware of the amount of calories before meal. The easiest way is to take a note after each meal, then searching the detail of calories information from internet or asking some experts. Although this way is simple, users might be unable to get the required information in time. The users might record the wrong information about their meal. To overcome these problems, an automatic or semi-automatic system is required.

On the other hand, image recognition smartphone is much more promising in terms of availability, communication cost, delay, and server costs. Then, by taking advantage of rich computational power of recent smartphones as well as recent advanced object recognition techniques, we propose a real-time food recognition system which runs on a common smartphone. In this paper, image processing techniques are used. First, food area is segmented from the food image. Then, feature vector of such image is constructed by calculating various features like color, texture, shape and size. Then the image is segmented by using SVM classification algorithm.

2. RELATED WORK

Various methods are proposed to find calories of a food in different domains. Some of them are manual methods, Semi- automating methods, Image processing methods and sensors based methods.Sensors become more important in human life. For food recognition and calories calculation various sensors are used.

Yin Bi, Chen Song, Nan Guan, proposed a Wearable Acoustic Sensor based Food Intake Recognition System [1]. In this system Necklace like microphone was used for capturing vibrating signals, produced in our throat. Microphone convert vibrating signals into acoustic signals and sent to smartphone using Bluetooth. From continuous signals swallowing and chewing events are detected. Features are extracted and based on this values foods are recognized. Feature extraction is done by using HMM (Hidden Markov Model). Nutritional values are already need to be stored in database system and from that table calories for particular food item has to be taken. AutoDietary can help to reduce bowel disorders due to improper chewing and swallowing speed. Decision based tree is used for food classification.

Microphone was comfortable for the users compared with other wearable sensors. Each and every item was recorded and does not need any communication with users. But cost of microphone cannot be affordable for many people. It cannot able to detect foods of same sound frequency but differ in nature. Wearing necklace for whole day provides inconvenient to users.

Meyer *et al*. developed a methodology to study the ingestive behaviour by non- invasive monitoring of swallowing and chewing [2]. The main objective is producing volumetric and weight estimation of energy intake. The monitoring is conducted by a sound sensor located over laryngopharynx and by a bone conduction microphone detecting chewing through a below-the-ear sensor. Obviously, the composite microphone system reduces the wearability and comfortability.

Amft [3] presented an acoustic ear-pad sensor device to capture air-conducted vibrations of food chewing. To recognize the food types, Amft derived spectral features from all continuous chewing sounds, then averaged these features using multiple sliding windows. A combination of a Fisher discriminant filter and a naive Bayes classifier was used to perform feature reduction and food classification respectively. Use of Multiple classification for identifying foods which provide more accuracy.

A major drawback of their system is that it requires multiple microphones to collect acoustic signals and some of the microphones are placed in the ear canal. Therefore, wearing such a system is very unpleasant for the users. Also they focus only on four types of food items. Not possible to detect fluid intake.

Pabler and Wolff [4] recorded sound signals by miniature microphones in the outer ear canal. In this work hidden Markov models are used for the recognition of single chewing or swallowing events. Food intake cycles are modeled as event sequences in realized by a finite-state grammar decoder based on the Viterbi algorithm. The event detection accuracy is 83% and food recognition accuracy is 79%. Classification based only on HMM that produce less results compared with other techniques. Correct weight of a food cannot be calculated. Less comfortable to wear microphone because it is placed in ear canals for collecting sound signals.

Gao [6] used video analysis to record eating behavior of people. Typical food intake movements are tracked in video recordings. This solution is restricted to special locations where cameras are installed.

Also Wu and Yang [7] proposed intake of fast food was recorded using a wearable camera to recognize food by frequently taking images and comparing them with reference images in the database. Both system has common drawbacks that is if the recognition accuracy drops significantly with changing ambient light or incase relevant objects are hidden behind other objects. But provide accurate result when correct food is identified. Yoshiyuki Kawano developed a real time mobile food recognition system [9]. In this method to recognize food items, a user draws bounding boxes by touching the screen first, and then the system starts food item recognition within the indicated bounding boxes. To recognize them more accurately, segmentation of each food item region is done by using GrubCut, extract a color histogram and SURF based bag-of-features, and finally classify it into one of the fifty food categories with linear SVM and fast $\div 2$ kernel. In addition, the system estimates the direction of food region where the higher rate SVM output score is expected to be obtained, show it as an arrow on the screen in order to ask a user to move a smartphone camera. This recognition process is performed repeatedly about once a second. This system also depend on thumb based calibration technique or need to fix camera in the specified distance for calories estimation.

K-H Chang *et al*., [10] developed diet- aware dining table model. Radio frequency identification (RFID) tags on food packages are used to detect and distinguish how and what people eat. The amount of food eaten should be recorded by a dining table with integrated weight scales, which records bite weights and assigns these weights to each person at the table.

Main drawback of this approach is the restriction to only one location where meals could be recorded, which makes it impractical for eating monitoring under free living conditions. Moreover, the system is more expensive to deploy and requires extra efforts to attach RFID tags on every food package.

Zhou *et al*. presented a smart table surface system to dietary environment[11]. The system is based on a smart table cloth equipped with a fine grained pressure textile matrix and a weight sensitive tablet. Food intake

related actions, such as cutting, scooping, stirring, poking are detected and recognized. Based on these actions, the food content and weight can be estimated. The system not work well for the food type recognition and food amount estimation due to different food of similar types may lead to similar actions and need more cutting force to estimation food amount.

3. PROPOSED SYSTEM

User has to take a photograph of their food which is in a specific table. A load cell which is attached to the plate is responsible for weighting food items and send the values to the smartphone where recognition of food is done.

After food identification and calories estimation the values are stored in database and an application is developed based on the user needs. Mostly application is mainly focus on more regular and balanced diet, Alerts on excessive snacking in a day, Suggested intervals between meals and Suggestions on hydration intake. We can extend our application based on user requirements.

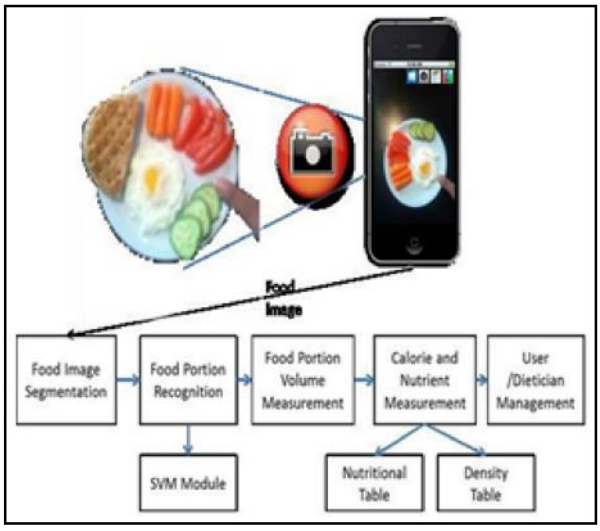

3.1 FOOD IMAGE IDENTIFICATION

User needs to take a photo of their meals before eating and then following processes are take place

3.1.1. Preprocessing

Simple transformation is need to get accurate result like cropping or padding. Noise present in the given image is eliminated.

3.1.2. Image Segmentation

The first step is to segment the food area from the input food image. Texture segmentation could be used to segment the food area from the input food image because food area should have a dense texture area. By using texture segmentation, mask image can be created and that can be used to segment the food area. Since the mask image is a binary image, simply multiple it with the input image to get the segmented image. Finally, crop the image to get rid of the black area of the segmented image.

3.1.3. Feature Extraction

After the food area is segmented from the input image extracting the feature vector from the input image has to be done. In our current study, our feature vector is constructed from 3 feature extraction techniques including of Bag-of-Features(BOF), Segmentation based Fractal Texture Analysis (SFTA) and Color Histogram.

Bag-Of-Feature:

Bag-Of-Words model has been used text processing for many years. Its characteristic is to extract the feature words from various document. Therefore, model each document with a histogram of feature words found in such document can be done. This is model for document classification. This idea has been applied for image recognition. Instead of extract the feature words, extracting the feature points from the input image has to be done. All feature points in the image are clustered into several groups, and the center of each cluster will be used to represented each group. SIFT is used to extract feature points in this system. K-Mean clustering method is used to cluster all extracted feature points into many groups.

Color Histogram:

It is obviously that color is another feature that can be used to distinct the type of food, so use of color histogram as another feature vector. Creating this histogram on RGB (Red, Green, Blue) channels.

4. SVM CLASSIFICATION

After the feature vector is constructed, support vector machine (SVM) a tool, to recognize the input image. Support vector machines are a set of related supervised learning methods used for classification and regression. They belong to a family of linear classifiers. In another terms, Support Vector Machine is a classification and regression prediction tool that uses machine learning theory to maximize predictive accuracy while automatically avoiding over-fit to the data. Support Vector machines can be defined as systems which use hypothesis space of a linear functions in a high dimensional feature space, trained with a learning algorithm from optimization theory. SVM compare all combination of feature and recognize food by using various training dataset.

Once the application performs the complete analysis of the image and the food portions, the user will get a suggestion of the type of food for each portion, and the user must then accept the suggestion made by the application, or correct the type of the food. The image will be shown to the user at the end of the recognition procedure.

4.1 Smartphone Application Development

After calculating calories we have to develop an application based on health monitoring system. For developing application Android studio has to be used. Food items are recorded in database using that datas various applications may be defined. Intimation to the users using messages for many types like need to be eat, over amount of calories are in taken today like that application can able to design.

5. IMPLEMENTATION

First the food items in the plate has to segmented. For this we need some preprocessing method. Using graphcut method the food item can be separated.

FOOD ITEM SEGMENTATION

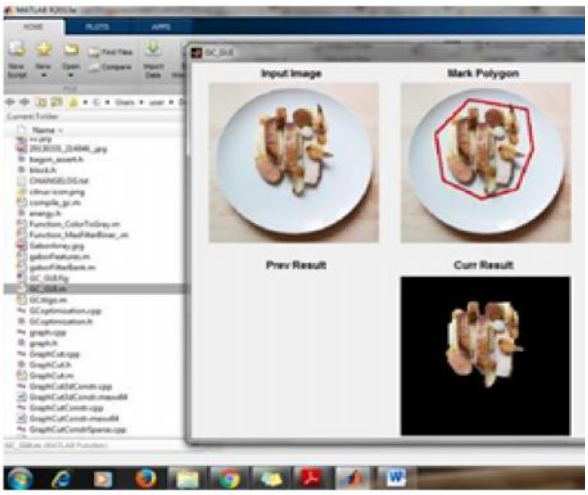

CALCULATING COLOR HISTOGRAM

6. CONCLUSION

In this project, AutoDietary a comprehensive and preliminary solution for food intake recognition in daily life system is presented. Health monitoring application is developed with the use of built in camera in smartphones. Food recognition is done by image processing techniques which provide comfortable results compared with other existing system. Images are segmented and features extractions are carried out. Using SVM based techniques food classification is performed. Developed application on the smartphone which not only aggregates food intake recognition results but also displays the information in a user-friendly way and provides suggestions on healthier eating.

REFERENCES

[1] Yin Bi, LV. Mingsong, Chen Song, Wenyao Xu, Nan Guan and Wang Yi., "AutoDietary: A Wearable Acoustic Sensor System for Food Intake Recognition in Daily Life", Sensors Journal, Vol.16, No.3, Feb-2016.

[2] Lopez-Meyer Paulo *et al* Sazonov Edward and Schuckers Stephanie, "Noninvasive Monitoring of Chewing and Swallowing for Objective Quantification of Ingestive Behavior", Physiological Measurement, Vol. 29, No.5, 2008.

[3] Oliver Amft, "A Wearable Earpad Sensor for Chewing Monitoring", IEEE Transactions on Sensors, Vol.1, No.5, Nov. 2010.

[4] Sebanstian Pabler and *et al* Matthias Wolff, "Food intake Monitoring: An Acoustical Approach to Automated Food intake Activity Detection and Classification of Consumed Food", 2012.

[5] Mike Wilson Eric, Muth Yujie Dong, Jenna Scisco and Adam, "Detecting Periods of Eating during Free Living by Tracking Wrist Motion", Biomedical and Health Informatics, 2013.

[6] Jiang Gao, Alexander G.Hauptmann, Ashok Bharucha and Howard D.Wactlar, "Dining Activity Analysis Using a Hidden Markov Model", ICPR, Vol.2, 2004.

[7] Wen Wu and Jie Yang., "Fast Food Recognition from Videos of Eating for Calorie Estimation", 2009.

[8] Yoshiyuki Kawano and Keiji Yanai., "Real-time Mobile Food Recognition System", 2015.

[9] Taichi Joutou and Keiji Yanai, "A Food Image Recognition System with Multiple Kernel Learning", 2009.

[10] Hao-hua Chang, Shih-yen Liu and Polly Huang., "The Diet Aware Dining Table: Observing Dietary Behaviors Over a Tabletop Surface", Pervasive Computing. Springer Berlin Heidelberg, 2006.

[11] Mathias Bo Zhou, Jingyuan Cheng, "Smart Table Surface: A Novel Approach to Pervasive Dining Monitoring", IEEE International Conference on Pervasive Computing and Communications, 2015.

Performance Analysis of a Dynamic Weighing System in Labview

V. Prabhu and S. Kiruthika
Electronics and Instrumentation Engineering,
M.Kumarasamy College of Engineering, Karur - 639 113, Tamil Nadu
E-mail: prabhuv.eie@mkce.ac.in, kiruthikas.eie@mkce.ac.in

Abstract

Beltweigher is an instrument used to measure and control the solid flow rate in industries. It allows the continuous weighing of materials as they are transported through the conveyor. It usually form a part of the conveyor equipment where it replaces a particular section of the conveyor belt. There are various factors such as belt tension, belt stiffness, location and alignment which affect the accuracy of the equipment. Hence it is necessary to simulate the process conditions and check the performance of the equipment before commissioning in the field. This paper discusses the performance analysis of a continuous beltweigher under different loading conditions using Labview.

Keywords: *Beltweigher, Flow rate, Labview, Load, Performance, Solid*

1. INTRODUCTION

Beltweighers are used to determine the mass flow rate of materials with high accuracy. They are predominantly used in power plants to weigh the coal which has been purchased. Since it is used to estimate the consumption of raw materials, the accuracy of the beltweigher should not be compromised. The challenging part in this equipment is to compensate for the external disturbances which affect the accuracy of the instrument. Also periodic calibration will lead to interrupts in plant process. The beltweigher not only measures the mass flow rate but also controls it by varying the speed of the conveyor or the opening of a feeder.

The measurement of mass flow rate gives the edge over the accuracy since the volumetric flow rate needs to be compensated for density changes due to pressure and temperature. Some of the factors which affect the mass flow rate measurement in beltweighers are belt tension, belt stiffness, alignment and tracking. With predetermined requirements for a load capacity the causes for these disturbances can be simulated in Labview and the compensation required to overcome these disturbances can be obtained. This provides the advantage of designing the equipment without testing it directly in the field thereby reducing the overall cost. It also provides an opportunity to enhance the performance of the weigher by considering the factors affecting the accuracy. This paper proposes a performance analysis method in labview which allows the engineer to identify the errors in weighing using a beltweigher and design the equipment appropriately.

2. LITERATURE SURVEY

Authors have utilized the Labview software to simulate virtual SCADA system and study the effects of bus parameter changes in loading conditions [1]. An automatic speed assistant system was designed for various road conditions to pave way for a safe transportation system [2]. The performance of an induction motor was performed under different motor parameters [3]. A temperature digital control system was designed to check the performance of electronic devices under different temperatures [4]. The position control of a DC motor using Fuzzy and PID control was realized using Labview [5].

3. BACKGROUND REVIEW

3.1 Beltweigher

The belt load or the material to be weighed is measured by a load cell and the speed of the conveyor is measured by a proximity probe. The product of the two values provides the mass flow rate in tons per hour or kilograms per hour. The beltweigher replaces a part of the conveyor belt and measures the flow rate through that length. They can be configured as counterbalanced type, pivoted type, single roller or multiple rollers etc. Each has its own advantages and disadvantages. The pivot system is rigid but is subjected to wear in corrosive environments. The speed of the conveyor is calculated from the pulses received from the proximity probe and is controlled by varying the input frequency of the supply. An important factor to be considered during installation of beltweigher is that it should not be placed at the point of feeding.

Accuracy will be high if it is placed near the point of discharge.

3.2 Labview

Labview is a graphical programming environment predominantly used for data acquisition and Industrial automation and control simulation. It has a user friendly interface and graphical coding language which makes it popular even about beginners in programming. It allows users to test the individual VI before compiling it into a large program using subVI. Dynamic characteristics of a process can be analyzed using mathematical models which accelerates the development of a product. It features a control design and simulation module to construct control models using transfer functions and analyze the system using step response and various plots. Labview also allows interfacing hardware devices with the software to store data as well as control devices. Using these features a performance analysis system was developed and its performance was analyzed.

4. IMPLEMENTATION

The beltweigher chosen for the analysis purpose uses two idlers for weighing as shown in fig.1. The maximum flow rate and belt speed is taken to be 100 kg/m and 0.2 m/s. This type of system is generally preferred in industries and hence this design has been taken into consideration. Some of the problems in the continuous weighing section are due to wear and tear of the roller, dust accumulation, varying belt thickness and alignment. By understanding the sources of error it is possible to eliminate its effect and improve the accuracy. Other possibility of errors may originate from the load sensor, speed probe and the controller electronics. The effect of these errors on the belt weigher and how it is compensated are discussed below.

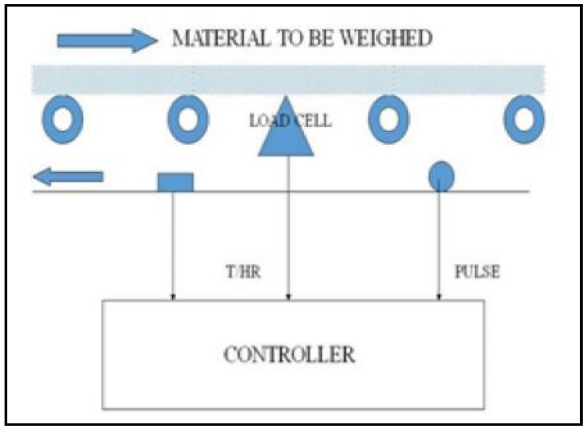

Fig.1 Belt weigher with multi idlers

4.1 Idler Alignment

For idlers which are aligned perfectly and negligible belt thickness the force acting on the idler is given by

$$F = M*g*P,$$

where M–belt load, g-acceleration due to gravity, P-idler pitch. When any misalignment occurs the weighing idlers are displaced by a distance x form the nearby idlers an additional force of magnitude

$$Fo = 2*T*x/P$$

is introduced. The ratio of these forces gives the effect of belt tension and idler pitch on the weigher readings. The values of maximum belt load, acceleration due to gravity and belt stiffness are provided through a numeric constant as shown in fig.2 as these values are fixed. The values for idler pitch and displacement are provided through a random generator. Plotting the value of these two forces over a XY graph we obtain a relationship that clearly states that the belt tension should be low and idler pitch should be high. The value of error plotted over a graph for x and P as shown in fig.3 helps to attain the proper idler alignment conditions.

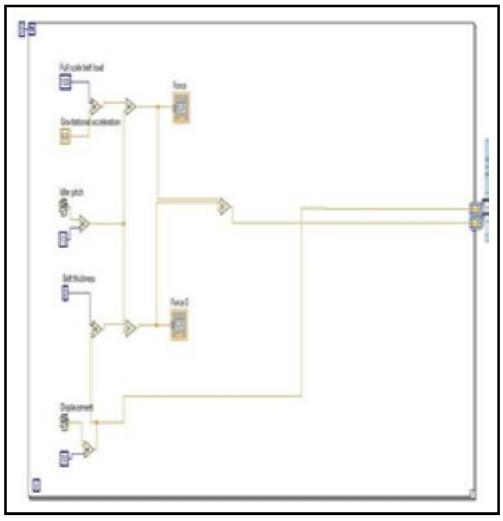

Fig.2 Block diagram for idler alignment

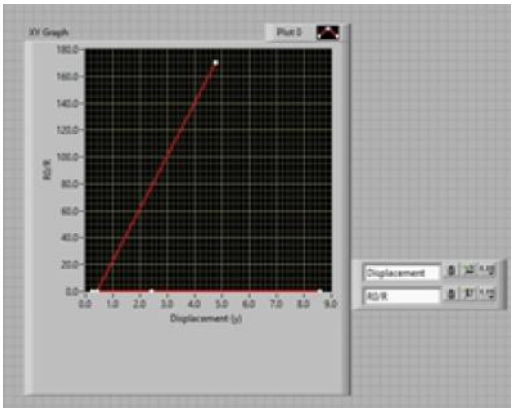

Fig.3 Performance analysis for idler displacement

4.2 Belt Stiffness

For the previous error compensation the condition was that the belt stiffness was negligible. However conveyor belts contain varying belt thickness which causes an additional force on the weighing idlers. A stiffness factor Kt was given by Cutler as

$$Kt = 1+12[1/P*"E*l/T]^2$$

By simulating the values in labview using constants as shown in fig.4 and operators we can generate a graph relating the stiffness factor and percentage of error. Obtaining the graph as shown in fig.5 for the belt stiffness factor and the belt pitch suggests that a stiff belt will produce less error compared to a loose belt. It also says that the accuracy not only depends on the weighing idlers but also on the idlers nearby to the weighing idlers. Additionally the belt stiffness also varies with the troughing angle and property of materials.

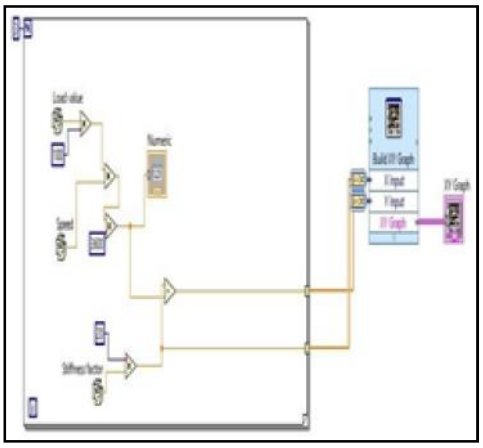

Fig.4 Block diagram for belt stiffness

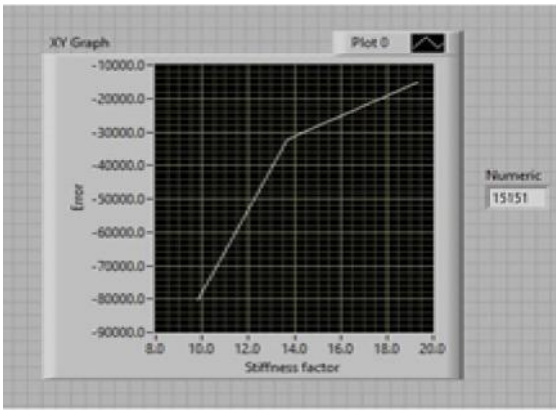

Fig.5 Performance analysis for belt stiffness

4.3 Skirt Plate

Errors are introduced due to the usage of skirt plates as the friction between the conveyed materials and the skirt plate induces an additional force on the weighing idlers. Since this error is nonlinear it is difficult to compensate. The force exerted by the conveyed materials on the weighing idlers is reduced by the frictional forces generated by the skirt plates. The correct value of weight acting on the weighing section is calculated using the variables such as specific weight of the material (y), belt depth (h) and belt width (b) as follows:

$$W = b*h*y$$

The frictional forces are calculated from the wall friction angle and corrected weight. The graph obtained shows the performance of the weigher with the inclusion of skirt plates. The obtained results clearly show that the inclusion of skirt plate increases the percentage of error.

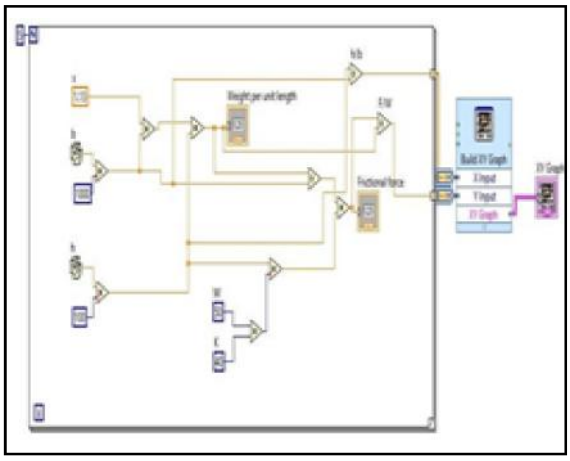

Fig.6 Block diagram for skirt plate

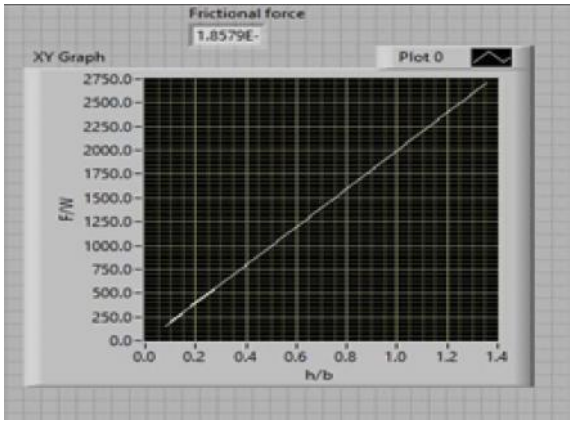

Fig.7 Performance analysis for skirt plate

4.4 Calibration

Calibration is the process of comparing with a known standard to ensure that the instrument is operating within its predefined limits. It is a critical process when the instrument is used for measuring the raw material consumption in a plant. Calibration of a weigher can be done by two ways:

- Chain calibration: In this method a roller chain of known length and mass is placed over the weighing section. This type of calibration ensures only the effects of load over the particular section of the belt where the chain is placed. It does not ensure the effects of load over the remaining belt sections. Hence its accuracy is very low and is used for weighers with low capacity.
- Dead weight calibration: In this method a dead weight which is calibrated against a standard weight is placed on

  the load cell platform. The theoretical value is calculated manually using the belt speed and the weight applied. This value is compared with the value displayed by the controller. This type of calibration is very simple and should be considered only for short period calibrations.

5. RESULTS AND DISCUSSION

The performance of a multi idler based system with a load capacity of 100 kg/m and belt speed of 0.2 m/s was analyzed. The graph obtained for individual factors like idler alignment, belt stiffness and skirt plate shows how the weigher can be designed such that these effects can be reduced without affecting the accuracy of the instrument. Figure shows that the idler pitch needs to be high in order to reduce the weighing error. Figure shows that a stiff belt will produce less error. Figure shows that the percentage of error increases with the increasing dimensions of a skirt plate.

6. CONCLUSIONS

This paper presents a performance analysis method using labview where the accuracy of the weigher with respect to various parameters is analyzed graphically with minimal programming effort. This system has been designed in such a way that it can be used by engineers with minimum programming knowledge. By means of this simulation, optimum parameter for a weigher design has been obtained.

REFERENCES

[1] Narendra Kumar and Uttam Kumar, ''Simulation of Virtual SCADA System using Labview,'' IEEE International Conference, December 2012.

[2] P. Ramani Ranjan Senapati and J. Sam Jebakumar, ''Labview Based Automatic Speed Assistance System in Uncertain Road Conditions'', IEEE International Conference, March 2016.

[3] Qianxiang Li, Jingtao Hu, "Simulation Model of Induction Motor Based on LabVIEW", International Conference on Intelligent Networks and Intelligent Systems, 2010, pp. 273-276.

[4] P. Joao Bazzo, C. Jean, C. Silva, G. Emerson, Carati, Marcio Vogt and Tiago Lukasievicz, "Digital Control System using a Thermoelectric Cell for Temperature Electronic Devices Testing", IEEE Latin American Symposium, February 2010.

[5] Jamal and Qun Xiong, "Real Time DC Motor Position Control by FPID Controllers and Design using Labview Software Simulation," International Conference on Computer and Automation Engineering, February 2010.

[6] Savas Sahin, Mehmet Olmez and Yalcin Isler, "Microcontroller Based Experiments for SCADA Education", IEEE Trans. on Education, Vol. 53, No.3, August 2010.

[7] Zafer Aydogmus and Omur Aydogmus, "A Web-Based Remote Access Laboratory Using SCADA", IEEE Trans. on Education, Vol.52, No.1, February 2009.

[8] P. M. Anderson and A. A. Fouad, "Power System Control and Stability", The Iowa State University Press, AMES, IOWA, U.S.A., 1977.

[9] Tom A. Short, James R. Stewart, David R. Smith, James O'Brien and Kenneth Hampton, "Five Wire Distribution System Demonstration Project", IEEE Trans. on Power Delivery, Vol. 17, No. 2, April 2002.

[10] Khalid M. Darwish, A.R.Al Ali, Rached Dhaouadi, "Virtual SCADA Simulation System for Power Substation".

[11] Savas Sahin, Mehmet Olmez and Yalcin Isler, "Microcontroller Based Experiments for SCADA Education", IEEE Trans. on Education, Vol.53, No.3, August 2010.

Power Factor Improvement in Consumer Side Through Power Line Carrier Using RFID Technology-Smart Grid

B.Rajesh Kumar and P.Ranjani
Assistant Professor, Department of Electrical and Electronics Engineering
M. Kumarasamy College of Engineering, Karur- 639 113, Tamil Nadu
E-mail:rajuae2011@gmail.com

Abstract

Smart grid is a grouping of information and communication technology and intelligent common infrastructure. Talking about smart grid the consumers and suppliers are very much important inorder to manage,monitor and control all energy issuses smartly. Easy instalation and high reliablity data communication over power line carrier is an important requirment to make a smart grid more constructive than fixed grid system.Therefore a latest RFID based power line technology has been developed unlike conventional system carrying data through antenna. RFID based power line carrier technology is used for detection and payment inorder to keep up the grid smart. With this technology, power factor correction and maintanance techniques are included inorder to improve the power system stability. Whenever the non-linear load is connected in load side, the proposed system will automatically detect and connect the power factor correction circuit(capacitor bank) for maintain the power factor in consumer side.

Keywords: *Capacitor bank, Power factor, Power Line Communication (PLC), Radio Frequency Identification (RFID), Smart grid*

1. INTRODUCTION

Today's electrical infrastructure have remained electrical grid has been ageing infrastructure, the demand for electricity has gradually increased. The demand and utilization of electricity increased by 2.5% annually over the last 20 years. Today the electric power distribution network be very complex. Among the deficiencies are a lack of some ideas and switching mechanically causes slow response system, due to lack of system response blackouts were occurred over past few years. The various factors are the growing population, the demand for the energy, the global climate condition, equipment failures problem, the capability limitations of electricity generation, energy storage problems, one-way communication and decrease in fossil fuels.

Consequently, a new grid infrastructure is straight away needed to address these challenges. Smart grid is a new trend in electric power grid infrastructure to improve the overall efficiency and reliability of the system.Smartgrid is the best technique for smooth integration of renewable energy sources through automated control and modern two way communications technologies [9].

The wireless RFID (Radio Frequency Identification) technology is widely used throughout the world. Its high-security system, used in a wide range of applications such as cashless payment ticketing systems for transportation and home appliances. For example in departmental stores, the people be able to pay the payments more easier, by holding an RFID card over a reader/writer. Radio-Frequency Identification (RFID) be an automatic identification system, relying on storing and retrieving data using devices called RFID tags otherwise transponders. RFID includes RFID reader and RFID tag[8].

In conventional electricity billing system, a person from electricity office has to come to the consumers premises and note down the reading of the electricity kWh. The consumer must pay the required amount to the electricity board. If the consumer did not reimburse the amount, the person from electricity board again has to come and trip the supply to consumers. Inorder to avoid human required to do the billing and tripping process, a new technology were developed to enhance the grid to be real smart. This paper proposes a new technique to make the present electrical grid system into very smart by by means of RFID based power line carrier technology with power factor maintenance and correction in load side. The proposed system suggests

the RFID tag which can be used for data transmission between the consumer and suppliers.With this technology,whenever nonlinear load is connected in the consumer side,the powerfactor can be automatically corrected by the power factor correction circuit to avoid penalty to consumers. The user should buy one RFID card from electricity board. The card number have to be registered in the data base of the electricity board.

The power factor plays an significant role inorder to design an energy saving scheme in load side. The power losses in the electrical network is increased due to lagging power factor in the output power[7].The non -linear load will be the major cause for lagging power factor. The designed scheme is concerning about maintaining the power factor of load side.

Power factor be the cosine of the angle between the voltage and current. The current and voltage is sensed by with current and voltage transformer. The phase angle between the voltage and the current is calculated and the result will be compared in the microcontroller. These processes are continuously carried out by microcontroller and maintain the power factor automatically [1-2][5].

2. HARDWARE DESCRIPTION

2.1 Smart Grid

Smart grid has been a recent phenomenon which has attracted the attention of engineers and researchers of both the electric power and communication sectors. The idea of smart grid has appeared in recent literature in different techniques used to control the power grid operation. It has been called as the 'grid of the future', while some refer to it as the 'intelligent grid'. The primary objective of the smart grid concept is to provide the consumers with more efficient and reliable power supply, which the power grids of today may not be able to supply in future. Smart grid can be used a two-way communication among the suppliers and consumers of electric power. The bi-directional communication indicates the ability of smart grid to accept the end users and their power requirement demands to the utility suppliers.

A smart grid can be rightly defined as a modernized electrical grid which uses the information and communication technology to collate and assimilate ideas and behavior of the suppliers and consumers automatically in order to enhance the efficiency and uniqueness in the production and distribution of electricity. The efficient and real time information of the smart grid becomes the most notable factor for the reliable delivery of power to the consumers from the suppliers. The impact of apparatus failures or damage, capacity constraints, and natural accidents which creates some problems in monitoring, diagnostics and protection of power system [9]. The communication system is the most significant component of the smart grid infrastructure. Different communications technologies are used for data transmission between measuring equipments and electric power utilities. In some cases wired communications have some advantages over wireless technologies such as low-priced and maintenance. The transmission path may cause the signal to attenuate. On the other hand, wired solutions do not include interference problems and their functions are not dependent on batteries, as wireless solutions often do.

It could be said that two types of information infrastructure are required for information transmission system of smart grid, the one is from the electrical appliances to smart meter and the other is from the smart meter to the utility's data center. As suggested in [9], the data transmission can be accomplished by power line communication or wireless communications, such as ZigBee, RFID, Z-wave etc,.

2.2 Power Line Communication

Smart Grid functions include the integration of intermittent renewable energy sources into the electricity supply chain, affording reliable electricity delivery to the consumers, and using the existing electrical infrastructure more effectively. Power line communication (PLC) carries data going on a conductor that can also be used for AC electric power transmission or electric power distribution to customers. Power line communication (PLC) is a unique technique in the transmission system that can handle data signals from one device to the other.

It has been the first choice for communication with the electricity meter owing to the direct connection with the meter and successful implementations of AMI (Automatic Metering Infrastructure) in urban areas whereas other solutions struggle to meet the needs of utilities. PLC systems based on the low voltage distribution network have been one of the research topics for smart grid applications in China [9].

2.2.1 Features of PLC

- PLC is an innovative and dedicated technology for smart grid applications. It is so because of the fact that the existing infrastructure significantly decreases the installation cost of the communication infrastructure.
- The efforts on standardization on power line communication networks, the high cost, ubiquitous nature, and is used in wide applications. It is also to be noted that the home area applications is one of the biggest areas where PLC technology has been applied.
- Smart metering, monitoring and control application can be well suited for urban areas by this technology, since the PLC infrastructure covers the areas that are in the range of the service territory of utility companies.
- Although there are strong wireless and wire line communication competitor, it is believed that power line communications (PLCs) will complete various communication tasks in upcoming Smart Grid deployments as PLC provides the natural upgrade from simple electricity conductors to mixture and bidirectional electricity and data communication solutions.

2.3 Radio Frequency Identification

The one automatic identification method is the Radio-frequency identification (RFID), relying on storing and remotely retrieve data by means of strategy called RFID tags or transponders. An RFID tag can be applied to a product and radio waves is used for identifying and tracking the users. The RFID tag is able to read from several meters away and beyond the line of sight of the reader. Electronically program with unique information. Many types of RFID systems are available in the bazaar. Depending upon the frequency range they are classified as follows:

- Less-frequency (30 KHz to 500 KHz)
- Medium-Frequency (900KHz to 1500MHz)
- High Frequency (2.4GHz to 2.5GHz)

The above frequency ranges mostly depends on the length of the tag. For example, low frequency tag ranging from 3m to 5m, mid-frequency tag ranging from 4m to 16m and high frequency tag ranging from 5ft to 95ft. There are different types of frequencies or spectra by using that RFID tags communicates with readers. For illustration, low-frequency tags are incredibly cheaper and better than Ultra High- Frequency (UHF) tags that is it uses a little amount of power and are it has the ability to penetrate in non-metallic substances. Scanning the objects is also possible with high water content, for example fruit, are at close range. The data transfer is faster in ultra high frequencies which have a better range, when compare to every other frequencies. More power is needed to pass through the materials. So UHF tags are used into wood, paper, cardboard or clothing
products.UHF tags were very much useful for scanning goods in ware house.

2.3.1 Data Capacity

The amount of bits stored on the tag can varying from 16 bits on the low end to as much as several thousand bits on the high end. Of course, if the storage capacity is high the price per tag is high.

2.3.2 Passive Versus Active

Passive and active tags are different from each other. There is no battery for “Passive” tags and it “broadcast” their data at only after energized by a reader.”Active” tags are having batteries so it use its own battery power to broadcast their data .Another difference is that the ranges of read are much greater for active tags than for passive tags. The read range of active tags and the extra capability are higher however, this will be more cost where as passive tags read ranges is less than the active tags but cost effective.

For high-value objects active tags are much more likely to be used that may be trailers, where the cost is minimal compared to the item value, and very long read ranges are required. The passive tags are mostly used in conventional supply chain applications, such as RFID-based track and agreement programs emerging in the consumer goods retail chain and it is cost effective than active tag.

2.3.3 Typical Applications of RFID

- Automatic Vehicle identification
- Payment system
- Access management
- Tracking animals

2.3.4 RFID Merits over Bar coding

- No "line of sight" requirements: Bar code read can sometimes be limited or problematic due to the need to have a direct "line of sight" among a scanner and a bar code. RFID tags are able to read through materials without line of sight.
- More automated reading: RFID tags can be able to read automatically when a tagged product comes past or near a reader, reducing the manual labor required to scan product and allowing more proactive, real-time tracking.
- Improved read rates: RFID tags finally offer the promise of higher read data rates than bar codes, particularly in high-speed operations such as container sortation. Larger data capacity: RFID tags can be easily encoded with item details such as cluster and batch, weight, etc.
- "Write" capabilities: since RFID tags can be rewritten with new data as supply chain actions are completed, tagged products carry updated information as they move throughout the supply chain.

D. Power Factor

The main purpose of this proposed system is to develop an energy efficient scheme in load side. Due to this proposed system, network losses are decreased and system stability level is improved. The designed topology is mainly concerned for improving the power factor in the load side. Industrial power distribution networks encounters increase in power losses and raise in the type of load is accompanied with low power factor which leads to huge transfer of reactive power from the utility through the network. The main limits of presence of non linear load are increase in the network losses and reduce the voltage magnitude. It can result in poor reliability and higher energy costs.

Power factor is defined as the ratio linking real power or actual power to apparent power. The general definition can be applied to all cases. The actual amount of power being used by a circuit is called true power. The power being used by the capacitors and inductors is called reactive power. The linear combination of real power and reactive power is called apparent power.

Three major loads in the power system are resistive, inductive, capacitive loads. Some of the resistive loads are kettles electric radiators and electric heaters. In the same way Inductive loads are arc furnance, induction motors and reactors and at last capacitive loads are various capacitors, capacitor banks and over excited synchronous motor. Inductive loads are mainly used in industry sectors than domestic area. This industry load value can be changed time to time due to the presence of inductive load and it causes power factor problem more than the domestic area. So that there is a requirement of power factor correction [7]. In an AC circuits there exist a phase angle difference between voltage and current. The term be also known as power factor of the circuit.

Power factor=Active power (kw)/Apparent power (kvar)

A purely resistive load (kettles ,electric radiators and electric heaters) would include a power factor of 1.0 (unity).If the circuit is inductive, the current value lags voltage value with 90 degree and the power factor is called as lagging power factor. If the circuit is capacitive then current value lead to the voltage value by 90 degree and power factor is said to a be leading power factor. The average power in an AC circuit is uttered in terms of rms current and voltage, P= VI cosΦ.

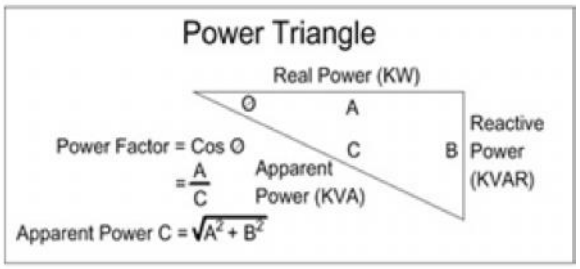

Fig.1 Power Factor Triangle

E. Non-Linear Load Power Factor

In present scenario electrical power utility companies have been increased a quantity and magnitude of nonlinear loads being linked to their power systems. Loads such as induction motor, microprocessor-driven equipment, fluorescent lights, power supplies and variable speed drives are well dispersed to cause a major negative impact on the power system. This paper deal about the concept of nonlinear load. Subsequently, non linear load power factor is discussed with practical example. In AC power distribution systems, harmonics occur during the normal electric current waveform is unclear by non-

linear loads. Most loads in modern electrical distribution systems are inductive. Examples include transformers, motors and induction furnaces. The induction motor may operate at a lagging power factor. This power factor value may vary between 85 to 90 percentage of the load. Due to the of air- gap between the stator and rotor of an induction motor increases the reluctance of the magnetic circuit, so induction motor draws a large magnetizing current to produce the required flux in the air-gap. The power factor of the electrical power system is represented by the equation:

Power factor=cosΦ (1)

The power factor can also be calculated by using activepower and apparent power of the system. When the load consumes low delivered power as a working power and reactive power, causes the power factor get reduced. The reactive component of the power generated should be reduced to achieve the good efficiency. The displacement angle of the voltage and current should be maintain inorder to maintain the power factor or else reactive component in the total power get increases.

Power factor maintenance is a technique which involve in the concept of controlling the power factor of the load. The requirement of Power factor modification is necessary for an electrical power transmission utility to improve the constancy and efficiency of the transmission network or correction may be installed by individual electrical customers to reduce the cost charges to them by their electricity suppliers [7]. Power factor maintenance is also reducing the penalty cost to the customers. Auto transformer is used as a inductive load for varying the power factor.

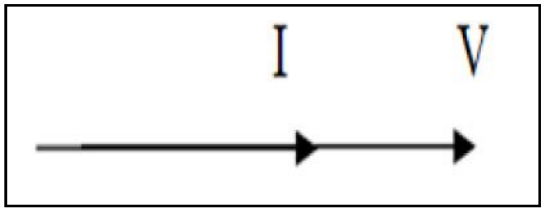

Fig. 2 Phasor diagram for resistive load

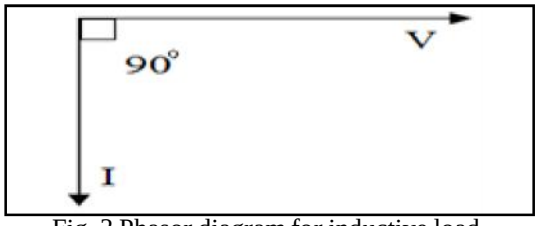

Fig. 3 Phasor diagram for inductive load

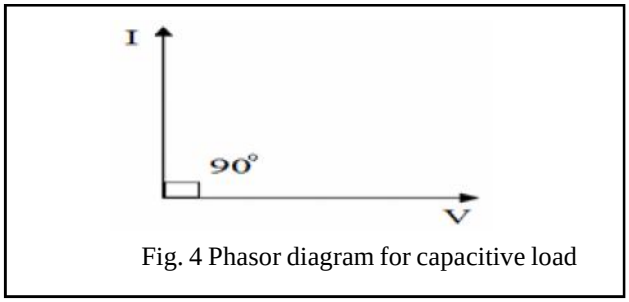

Fig. 4 Phasor diagram for capacitive load

3. EXISTING SYSTEM

Easily installable and greatly reliable data communications over power line is a requirement to make Smart Grid more convenient and helpful than fixed grid systems. Therefore RFID (Radio-Frequency Identification) over Power Line technology be developed. Unlike conventional RFID carrying data wirelessly by antenna, radio-frequency signals for identification and payment runs from side to side the power line in Smart Grid. The appliances embedded with IC card chips are detected and recognized when their electrical plug connectors are insert into the outlets in the electrical grid equipped by reader/writers. This system has the potential to revolutionize the practice of Power Line Communications with applications such as automatic detection, power control, and payment/ticketing all the way through the power lines.

RFID over Power Line is the applied technology of usual RFID, NFC (Near Field Communication), or contactless IC card. It is also Power Line Communication transfer high frequency signals of RFID over power line to detect appliances which are connected to the electrical grid and to pick up their encrypted data.An RFID tag chip or contactless IC card chip is embedded in an appliance and is connected to the power line. It holds written data and thus holds identity information. The RFID tag chip or contactless IC card chip is read by a reader/writer connected to the power line in Smart Grid. The reader/writer transmits scanned signals into the power line, and scans an area of Smart Grid continuously.When the plug (connector) of the appliance is inserted to the electrical outlet (i.e. when the appliance joins Smart Grid), the IC chip is activated by electromagnetic waves transferred from the reader/writer, and the high-speed data transmission is induced. It can provide secure and convenient prepayment of electricity and other utilities.

The existing block diagram which uses the principle of power line carrier technology for electricity billing and

recharge for making the system to be smart.Existing system can be extended for power factor detection circuit in the previous work.Further the system is applied for the new concept of power factor correction and compensation purpose.

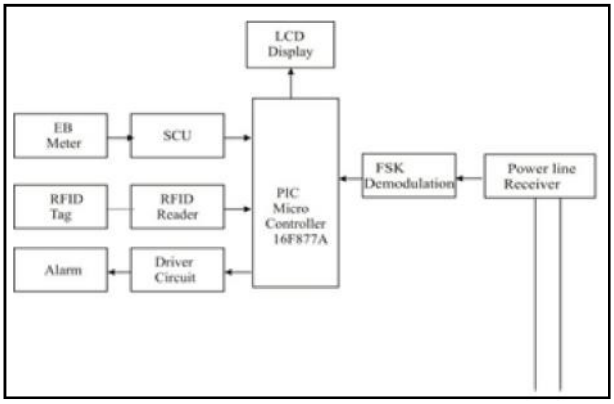

Fig.5 Block diagram for existing system

4. PROPOSED SYSTEM

4.1 Proposed System Block Diagram

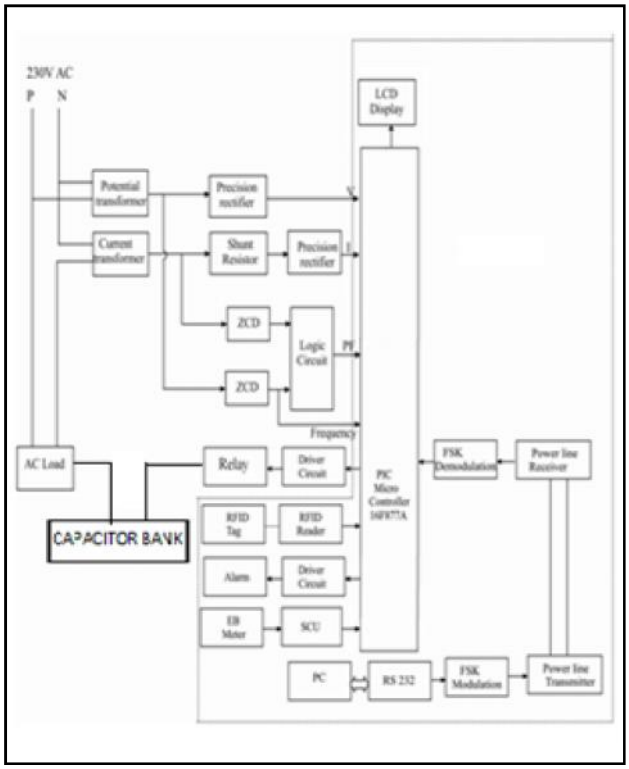

Fig.5 Block diagram for proposed system

4.2 Performance of the Proposed System

This proposed system is separated into two parts: consumer and supplier. The consumer side consists of a energy meter, logic circuit, an RFID reader base on a microcontroller, and the supplier consists of a PC with data base of consumers. Credit id which is read by RFID reader is verified by the supplier and sent to the consumers from which microcontroller take action based on that information. The microcontroller manages all the system work in the consumers. The ID and its information can be transmitted among each consumers and the supplier through Power Line Communication(PLC) and also this proposed system perform the operation based on the signals are obtained from instrument transformers like potential and current transformers. The square waveform is converted into compatible waveform with the help of suitable logic circuit. The Counter is located in the microcontroller and converted wave form is fed into the counter. The counted pulses are distorted into corresponding value of phase angle
Φ.Relay mainly performs the opening and closing of a connection of load from side to side supply mains depending upon the amount present in the RFID card and the presence of non-linear load (inductive load) at a moment.

4.3 Experimental Setup

Energy Meter will be generally used to show the electrical pulses proportional to the power consumed by the consumer. Microcontroller obtains the details of energy consumed by the consumer through the output of Energy Meter and act according to the programs full on the microcontroller. RFID Card interfaces with the microcontroller unit in which the amount recharged by the customer are written. When the amount is reduced below 10 percentage, the alarm circuit will get on. Relay primarily performs the operation that connecting and disconnecting the load through supply mains depending upon the account balance present in the smart card at a moment whenever the non-linear load is come into play. The voltage and current magnitude are given as data into the microcontroller inorder to find the phase angle difference between the voltage and current. The cosine of the phase angle difference between the voltage and current is known as displacement factor. According to the displacement factor the relay will connect or disconnect the non-linear load. The signal on or after microcontroller (either 0 or 1) is used to operate the relay.

4.4 Hardware Snapshot

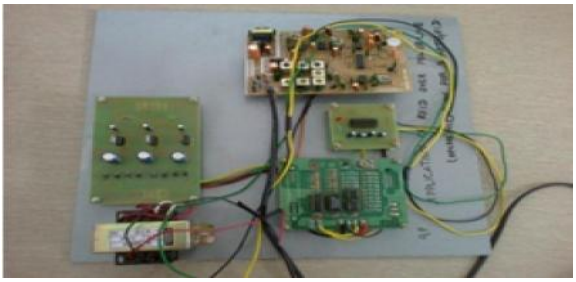

Supplier Side

Consumer Side

4.5 Features of Proposed System

- Remotely Connect / Disconnection of Power supply from side to side PLC. Automation of all features including communication from the sub - station to the customer.
- It involve less cost to communicate. PLC is a quick reaction. Once the power line is connected, identification and transaction can be done within
- 0.1 second. This system increases productivity.
- The power factor maintenance is used to increase the stability of power system.

4. CONCLUSION

In this modern era various technologies were available all over the world for calculating and collecting the electricity billing process in India appears to have become very absolute and is still lagging behind and is unable to meet the latest available technology. However in this project above mentioned process is completely automated and the communication is entirely made possible through the power line communication. The communication between the transmitter and receiver is bi-directional and data rate will be fast for long distance. When the system is user friendly it will be more beneficial to the customers. The EB billing procedure has the ability of fulfilling a set of needs for the user and the EB workers. This proposed power factor detection and maintanance circuit experimentally tested with auto transformer. Electric energy is very much essential to our daily life. It is used in Industry applications. The power factor adjustment is primarily used to maintain the stability of the power system.

REFERENCES

[1] András Fehér, Dr. ZoltánPuklus, “Definitions and Measurement of Power Factor”, 8th International Symposium of Hungarian Researchers on Computational Intelligence and Informatics.

[2] Fawzi Al-Naima, Bahaa Jalil, “ Building a Prototype Prepaid Electricity Metering System Based on RFID”, International Journal of Electronics and Electrical Engineering ISSN : 2277-7040, Vol.1, No.1.

[3] G.Venkatesan, R.Arumugam, M.Vasudevan, S.Paramasivam and Vijayan 2006, “Modeling and Simulation of Novel Switched Reluctance Motor Drive System with Power Factor Improvement, American journal of Applied Sciences, ISSN 1546-9239, Science Publications, Vol.3, 1, 2006, pp.1649-1654.

[4] J. Vales-Alonso, V. Bueno-Delgado, E. Egea-Lopez, F.J.Gonzalez-Castano, J.Alcaraz, “Multiframe Maximum-Likelihood Tag Estimation for RFID Anti- Collision Protocols”, IEEE Transactions on Industrial Informatics, Vol.7, 2011, pp.487.

[5] Md. MejbaulHaque, Md. Kamal Hossain, Md. Mortuza Ali, Md. Rafiqul Islam Sheikh “Microcontroller Based Single Phase Digital Prepaid Energy Meter for Improved Metering and Billing System”, International Journal of Power Electronics and Drive System (IJPEDS), Vol.1, No.2, December 2011, pp. 139-147.

[6] M.Ravindran, V.Kirubakaran, “Electrical Energy Conservation in Automatic Power Factor Correction by Embedded System”, Energy and Power 2012, Vol.2, No.4, pp.51-54.

[7] SapnaKhanchi, Vijay Kumar Garg, “Power Factor Improvement of Induction Motor by Using Capacitors”, International Journal of Engineering Trends and Technology (IJETT), Vol.4, No.7, July 2013.[8] Takanori Washiro “Applications of RFID Over Power Line for Smart Grid” 2012 IEEE International Symposium on Power Line Communications and Its Applications.

Design and Fabrication of Waking Leg Module Using Theo Jansen Mechanism as an Alternate for Conventional Tyres

K.Ponraj, D.Mytheeshwaran, R.S.Mohan Kumar and K.Vijayanand
Department of Mechanical Engineering,
Kumaraguru College of Technology, Coimbatore - 641 049, Tamil Nadu
E-mail: pon94864@gmail.com,waranmytheesh@gmail.com

Abstract

In linkage based locomotive systems, Theo Jansen mechanism is gaining extensive attractiveness among the designers of legged robotics. Its major attractiveness includes scalable design, energy efficiency, low payload-to-machine-load ratio, deterministic foot trajectory and bio inspired locomotion. For few effortless applications, like climbing tiny uneven rock piles, conventional wheel models are preferably used. For complex applications such as sudden instantaneous elevation changes like stairs, use of wheel will not provide desired result. As a replacement for the conventional tyres, Theo- Jansen Mechanism (Strandbeest) that overcomes the drawbacks of tyres is comparatively appreciable. The mechanism converts a rotation movement into walking pattern. It has a smooth walking pattern and easy controlling on any given uneven terrain. The main intention of our work is to propose an idea for replacing the conventional wheels with a walking leg mechanism. This paper deals with the design and fabrication of a walking four- legged robot which is based on Theo Jansen mechanism.

Keywords: *All terrain motion, Theo Jansen Mechanism, Walking robot*

1. INTRODUCTION

In this technologically advancing world, for sophisticated jobs in challenging environment robots are deployed to do the tasks as per the instruction given to it. In recent days employing robots are increasing in almost all fields such as military, rescue, space exploration, medical, industrial sector, agricultural sector etc., Basically, a robot consists of following parts sensors, controllers and mechanisms. The mechanisms include parts such as arm, joints, end effectors, legs (mostly wheels) etc., Kinematics of the mechanisms permits robot to perform desired job by allowing relative motion between the links at pre-determined angle and distance. The robots are machines that functions autonomously with certain Artificial Intelligence (AI). In most of the applications, robots are moving from one place to another to complete the given task. The operating surface may be flat or with lot of obstacles i.e. uneven surfaces. For example, consider a military robot or rescue robot. It will be deployed at all terrain, where the surface is inclined with loose soils and rocks. Most of the robots are moved using the wheels mounted to its base. Controlling the wheel kind of mechanisms (rolling) is easier than other mechanisms such as leg based mechanisms. With the wheels dominating the robots, engineers and innovators trying better replacement for wheels which would work in any kind of an environment. Adding legs to robots might be a solution for robots which runs on unprepared terrain.

Legs resemble humans or animals but making legs for robot is a quite challenging task. Extensive research is going on to develop legs, so that the robot can be move with controlled rate and stable in both static and dynamic conditions. The advantages of legged robot over wheeled robot are (i) legged robots or vehicles can navigate on any kind of surfaces which is inaccessible for robots with wheels, (ii) wheels are designed to work on prepared surfaces like smooth surfaces, roads, rails, etc., (iii) legged robots can jump or step over obstacles whereas wheels need to somehow travel over it, or take a different path, (iv) wheels require a continuous path to travel whereas legs can step over isolated paths and move on. For example, if a particular city is hit by an earthquake, then the surface with the obstacles of continuous path. This is where legged robots come into picture, although tracked wheels can manage up to a "certain" extent, (v) legged robots can avoid undesirable footholds which cannot be avoided in a wheeled robot.

There are different kind of legged robots in use based on the number of legs. One- legged robot is the minimum number of legs for a robot to have a ground contact is

one. Two legged robot (Biped) is the beginning of building robots, studies on biped robots (robots with two legs) have been continuously carried out, especially towards developing humanoids. Biped Robot Creating a robot which resembles a human would mean that they can be used in the same human working environment without making any changes. This means they are built to imitate humans and human behaviour. Three legged robots (Tripod) are statically stable since there are three contact points to ground. Strider - Three legged Robot for a robot to be statically stable, it requires a minimum of three contact points to ground. Four legged robot (Tetrapod) walking with four legs is common for most animals and there is a good reason to replicate this in robots. Four legged robots are statically stable and the walking pattern of a four legged robot can be designed in different ways: one leg at a time or alternating Pair. In this approach, alternate legs are moved as if two biped robots are connected together. Six legged robots having more number of legs provides greater stability. Hexapods (robots with 6 legs) possess greater static stability while moving and standing. These robots are also biologically inspired as there are many insects with 6 legs.

2. LITERATURE SURVEY

In linkage based locomotive systems, Klann mechanism that actually mimics the motion of the biological organism is used as replacement for the conventional tyre mechanism. But due to its few drawbacks being jerky motion and difficulty in vehicle turning, Theo-Jansen mechanism (Strandbeest) which had a smooth walking pattern on any uneven terrain and could easily function as per requirements is selected [1]. The free fall model of walking mechanism is designed and realize the position control based on the LYAPUNOV stability theory. [2]

Klann and Theo Jansen mechanisms are used for legged robots. Though Klann mechanism has less number of links than Jansen mechanism, Klann mechanism has very high step height in compare with Jansen's. In terms of stability Jansen mechanism has more stable than the Klann due to its nominal step height. [3]

Theo Jansen mechanism is chosen for walking patterns. In order to walk in a road with bumps such as ups and downs, the mechanism should have a capability to change the elliptic leg orbit depending on surface conditions. An additional cyclic motion of the linkage centre is added in the Theo Jansen mechanism which is never going to move in the original system but for preventing rising instability, alters the original walking pattern into orbits systematically with various functional aspects. Modelling and analysis of four legged Theo Jansen walking machine driven by only one input using projection method. [4]

Though Theo Jansen mechanism is a simple in structure, the main absence in the mechanism when compared to human leg is muscles. Electrolytic polymer can occupy the importance of muscles in the mechanism. It acts as the artificial muscles. Mowgli which is a frog like robot developed in Japan has six pneumatic muscles. It has touch sensors on its feet, potentiometers at each joint and a pressure sensor on each muscle. Artificial muscles are probably the future in robotics and also it is very much useful in legged robots to compete the wheeled ones. [5]

Based on the work of Theo Jansen, the design of a crank-based leg linkage was fabricated and simulated in Mathematica that includes both the analysis of foot path and centre of mass. The comparison results discussed that though the new proposed design is more flatter and with more constant velocity when it is in contact with the ground, but its step height is about 33% less than the Theo Jansen mechanism. [6]

The linkage configuration of the walking mechanism is essential for obtaining a stable motion. Computer aided design process will be very much helpful for the designer to complete the model with fewer errors in short span of time. The shapes of trajectory described by the feet during walking phase and the optimal leg configuration in order to walk smooth and stable. [7]

The dynamic analysis is done for the optimization of Theo Jansen mechanism using the superposition method was conducted [6], but this work is incomplete, without details on the analysis and discussions of equivalent Lagrange's equation. In fact, the complete dynamic analysis involving constraint forces and equivalent Lagrange's equation of motion is necessary for any meaningful extension and/or optimization of legged systems based on Theo Jansen mechanisms. [8]

Additionally Theo Jansen mechanism can walks well in even surfaces but Klann mechanism is less stable in even surfaces. Reducing the number of actuators and driving sources in the legged robots will results in lighter

structure and simpler control. Six legged robots with a six-bar watt's chain forms the kinematic chain for the legs and is actuated by a cam mechanism and transmission bar and controlled by the PLC [9]. A new model of walking machine which is entirely different from Theo Jansen walking machine. The model is created by connecting a pantograph with four bar linkage using a common link between them. [10]

3. PROBLEM IDENTFICATION

In many locomotives, the vehicles are designed up to the certain environment lands, but in some important applications like defence, spying the robot should be capable of move in any terrain.so, the main problem identified and solved in this paper is all terrain motion. In general robot are equipped with wheels for the motion. But in certain lands the wheel becomes wear and lead to slippery in motion.so the tire slippery is one more problem and solved by this model.

Most of the wheeled robots can only be turned in the radius of turning, if the path doesn't have much space it could not turn. But legged robots can easily turn in the constraint path by disable the inner side leg of the robot.

4. OBECTIVES OF THE PROJECT

- Higher energy efficiency
- Greater mobility
- Improved isolation from terrain inconsistencies
- Less environmental damage (both from paving and erosion)
- Ability to avoid obstacles by stepping over them
- Statically stable during entire locomotive cycle
- Durable joints/hinges/moving parts
- Inexpensive materials

5. PRINCIPLE OPERATION OF THEO JANSEN MECHANISM

The principle operation of this mechanism is converting the rotational motion into the walking pattern. This conversion is done by the two four bar mechanisms and one parallel bar mechanism which are integrated in the Theo Jansen mechanism as shown in the figure 1. The two four mechanisms are linked by a common link which acts as a crank for the input rotational motion. The two four bar mechanism and the parallel bar mechanism are coupled by the coupler link. The desired walking pattern is obtained as the output from the output coupler link which is attached to both the parallel bar mechanism and the lower four bar mechanism. As the crank turns, the foot traces out a cyclical path relative to the body of the walker; this path is known as the locus.

In this paper the chassis for the robot is designed as a symmetric component and two legs are assembled in each side of the robot which is also symmetric about the chassis. The crank link of the two legs in one side of the robot is hinged into a common pivot and connected to the centre axle of the robot. The two ends of the axle shaft are provided with eccentric type circular crank. The axle shaft is driven by the DC geared motor.

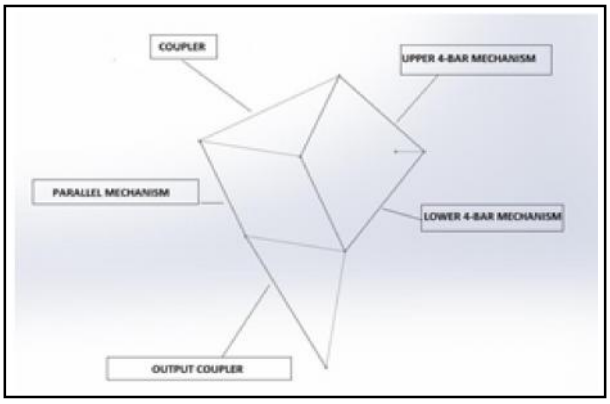

Fig.1 Mechanisms incorporated in Theo Jansen mechanism

6. CALCULATION OF THE PROJECT

The main calculation done for this model is scale reduction of the links from the dimensions given by Theo Jansen. The original dimensions are shown in Figure 2 and the scaled dimensions are shown in Figure 3.

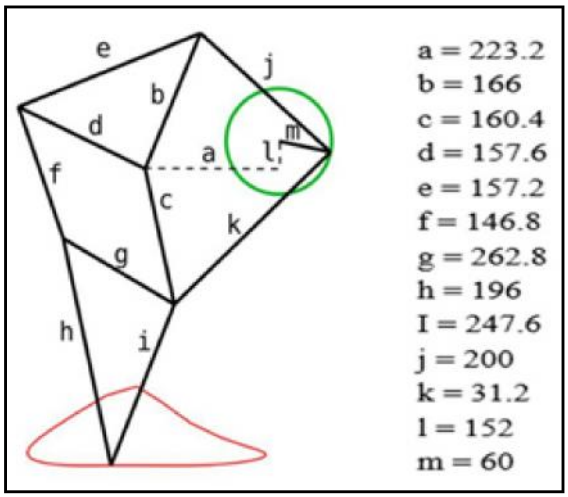

Fig.2 Dimensions mentioned in the reference

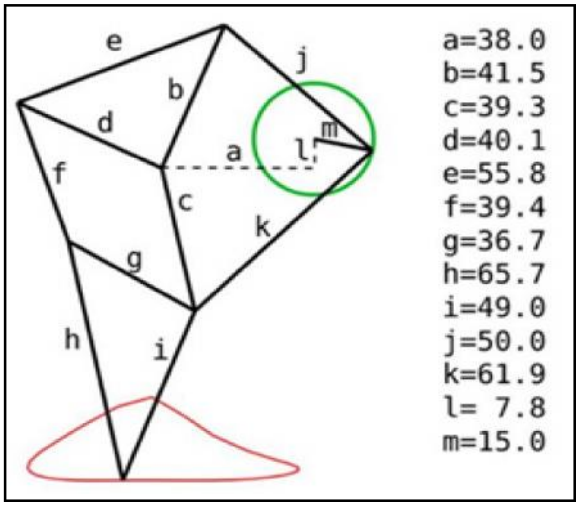

Fig. 3 Dimensions after scale reduction

All dimensions are in mm.

7. DESIGN OF THE ROBOT

The dimensions of the leg links shown in the Figure 3 was modelled in the Dassault systems Solid Works 2016. The dimensions of the chassis are found from the offset required for the mechanism and the chassis is a symmetric part by which four legs are assembled in the symmetric way.

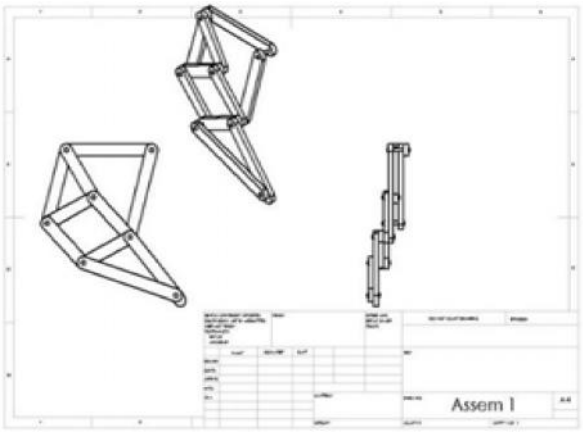

Fig. 4 Drafted view of the leg

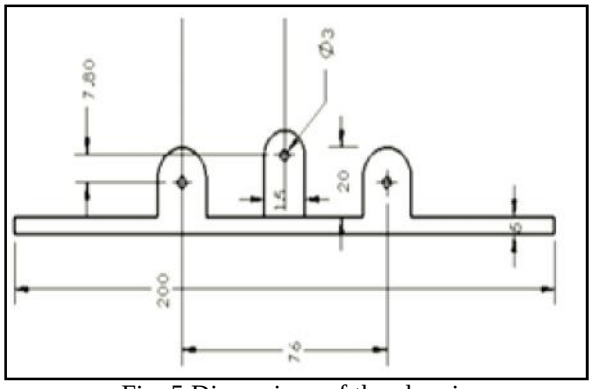

Fig. 5 Dimensions of the chassis

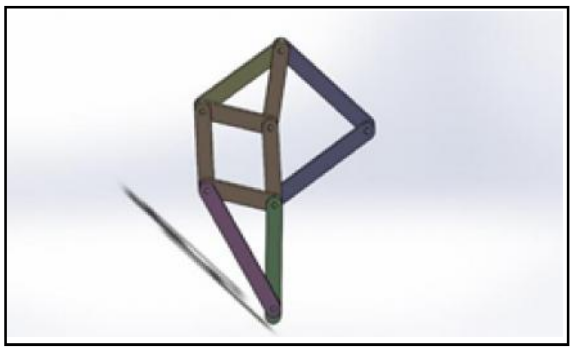

Fig.6 3D assembly view of single leg

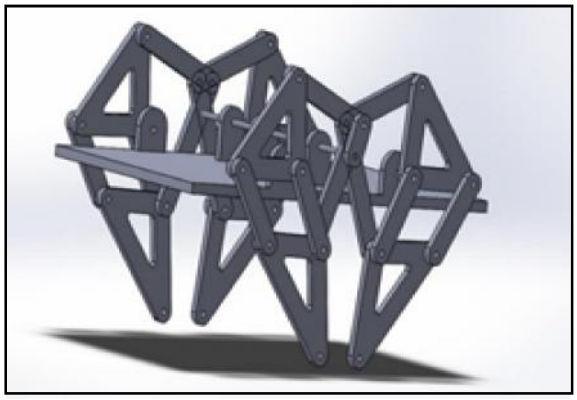

Fig.7 3D assembly view of the robot

8. CALCULATION OF THE ROBOT MOVEMENT

It is based on the Rotational speed of Motor that is given as an input crank Rotation. The motor drive is given to the centre axle through small spur gears. Number of teeth in the gear mounted on the motor shaft (Z1) = 24 Number of teeth in the gear mounted on the centre axle (Z2) = 50.

The motor speed (N1) = 60 rpm

$$\frac{N_1}{N_2} = \frac{Z_2}{Z_1}$$

N_2 = 29 rpm

When crank rotates 29 rotations per minute, the corresponding length of movement of the Robot is 29 times of the stride length.

Stride length	67.9
Step height	22.4

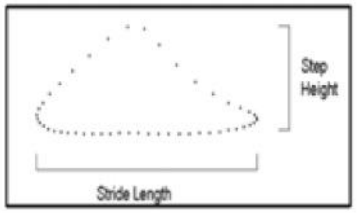

Linear speed of robot = (rotational speed) (stride length)
= (29) (67.9)
= 1969.1 mm/min
Linear speed of robot =1.969 m/min
Actual Linear speed of robot = (75-80) % of Theoretical Speed of the Robot (approx. = 1.47 m/min)

9. FABRICATION OF THE MODEL

The whole robot is fabricated in the acrylic material. Links and chassis are made in 5mm thickness acrylic sheet. By designing the linkages in the solid works it was drafted to the scale of 1:1 in the drawing sheet. The drawing sheet is pasted on the 5mm acrylic sheet and cut down the linkages as mentioned in the drawing sheet using table jig saw machine.

After cutting the outer profiles of the links the pivot points are drilled to 3 mm diameter. Then the links are assembled to make a complete leg. For making the joints between the links custom aluminium pins are used.

Likewise the chassis was also made in the acrylic sheet in the dimensions shown in the figure [5]. The centre axle in the robot is made up of 6mm screw rod.

Two discs made up of wood in which the eccentric holes are provided. This disc acts as an eccentric crank for the leg motion.

Small plastic spur gears are used between the motor and the centre axle shaft. The four legs are individually made as mentioned in the previous process and assembled in the chassis. The crank link of the legs are connected to the eccentrically drilled disc which is mounted at the ends of the centre axle shaft.

10. FUTURE SCOPE OF THE PROJECT

- By replacing the acrylic sheet by light weight metal accuracy of the robot can be increased.
- By manufacturing the robot in large scale we can use it for the defense application.
- By using micro controllers for control it can be used for many industrial applications.

11.COST OF THE MODEL

The cost for making this prototype is tabulated in the table 1.

Table 1 Cost of the Model

Sl.NO	PART NAME	MATERIAL	QUANTITY	PRICE/piece (Rs.)	PRICE(Rs.)
1	Legs	Acrylic (5"x 5")	4	150	600
2	Chassis	Acrylic (6" x 8")	1	200	800
3	Motor	Dc motor	1	250	250
4	Wires	Cooper	4 m	15	60
5	Rivets	Aluminum	25	2	50
Total					**1760**

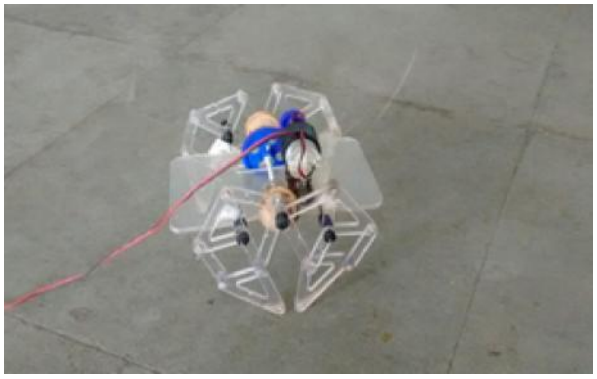

Fig.8 Fabricated model in acrylic material

12. CONCLUSION

In the present work, a legged mechanism is used for a robot. The mechanism is replica of Theo Jansen mechanism. This mechanism finds a numerous application in robotic fields. Theo Jansen walking robot has been developed for the use of robots in different terrain where robots with wheels cannot able to find its application. This mechanism is more suitable for robot because it does not contain any complex structure and cost for manufacturing is also low. The mechanism has been tested in different terrains. The stability of robot is acceptable, with varying speed. The performance of the legged mechanism of robot is tested in inclined surface and uneven surfaces. The legged mechanism is to be improved for moving the robot at different directions.

REFERENCES

[1] Patnaik, Swadhin, "Analysis of Theo Jansen Mechanism (Strandbeest) and its Comparative Advantages Over Wheel Based Mine Excavations System", IOSR Journal of Engineering Analysis, Vol.5, No.7,2015.

[2] Nansai, Shunsuke, *et al*., "Dynamic Modeling and Nonlinear Position Control of a Quadruped Robot with Theo Jansen Linkage Mechanisms and a Single Actuator", Journal of Robotics, 2015, pp.4.

[3] U.Vanitha, V. Premalatha, M. NithinKumar and S. Vijayaganapathy, "Mechanical Spider Using Klann Mechanism", Scholars Journal of Engineering and Technology (SJET) , ISSN 2321-435X (Online), 2015.

[4] Komoda, Kazuma and Hiroaki Wagatsuma, "A Proposal of the Extended Mechanism for Theo Jansen Linkage to Modify the Walking Elliptic Orbit and A Study of Cyclic base Function", Proceedings of the 7th Annual Dynamic Walking Conference (DWC'12). 2012.

[5] Ignell, Nils Brynedal, Niclas Rasmusson and Johan Matsson, "An Overview of Legged and Wheeled Robotic Locomotion", Available from: Mälardalen University, Website: http://www. idt. mdh. se/kurser/ct3340/ht12/MINICONFERENCE/ FinalPapers/i rcse12 sub mission, Vol.21, 2012.

[6] Ghassaei, Amanda, Professors Phil Choi and Dwight Whitaker, "The Design and Optimization of a Crank-Based Leg Mechanism", Pomona, USA 2011.

[7] Florina Moldovan1, A.Valer Dolga, "Analysis of Jansen Walking Mechanism Using CAD", Solid State Phenomena, Vol.166-167, 2010, pp.297-302.

[8] Giesbrecht, Daniel, and C. Qiong Wu. "Dynamics of Legged Walking Mechanism "Wind Beast", Department of Mechanical and Manufacturing Engineering, University of Manitoba, California 2010.

[9] Soyguder, Servet and Hasan Alli, "Design and Prototype of a Six-legged Walking Insect Robot", Industrial Robot: An International Journal, Vol.34, No.5, 2007, pp.412-422.

[10] Anthony James Ingram, "A New Type of Mechanical Walking Machine", A Dessertations Submitted to University of Johannesburg, November 2006.

Series Combination of Hybrid Filter With Distorted Source Voltage

J.Priyanka Devi and A. Saranya
Dept of Electrical and Electronics Engineering
M.Kumarasamy College Of Engineering, Karur - 639 113, Tamil Nadu
E-mail: priyanka.jey26@gmail.com, saranyaa.eee@mkce.ac.in

Abstract

The use of power electronic devices in industry and domestic applications such as adjustable speed drives, inverters, furnaces, computer applications and other electronics devices let to the injection of harmonics and reactive power in the power system. So harmonic filter is important one for filtering harmonics in the power system. The shunt active and shunt passive filter is designed for compensating 5th and 7th harmonics. Hybrid filter performance was verified through MATLAB/SIMULINK where the source voltage having 3rd harmonic component. Thus the hybrid filter provides an effective harmonic compensation and reactive power compensation.

Keywords: Hybrid power filter, Nonideal mains voltage

1. INTRODUCTION

The power electronic devices are used for ac power control in the power system. The harmonics injection and reactive power cause disturbance to the customer and interference in the communication line with low system efficiency and poor power factor. Many researchers have provided solutions for harmonic and reactive power compensation [1] and they imposed specific limitations of current harmonics and voltage notches. Passive filter is used for eliminating lower order harmonics and capacitors used for compensating reactive power demand in the system. They have some drawback such as fixed compensation and resonance problems. Then the fundamental frequency reactive power may affect the system voltage regulation. Here the increased harmonic pollution leads to the development of active filters. The active filter rating depends on harmonics and reactive power to be compensated. Generally active filters required high current rating and higher bandwidth requirement that do not constitute cost effective solution for harmonic mitigation.

Hybrid filter with series combination of shunt active and shunt passive filter can overcome the demerits of active and passive filter [2]. The hybrid topology with series combination of active and passive filter reduces the rating of active filter, improves the filtering characteristic of passive filter and greatly reduces the precise tuning of passive filter. It supplies reactive power as per demand and maintains voltage regulation.

Many control strategies, starting from instantaneous reactive power compensation, evolved since the inception of shunt active filters. One of the control strategy based on DC link voltage was discussed [4] [5]. In this method the shunt active filter is to compensate the load side harmonics and reactive power, thereby making the load linear. Therefore the supply side distortions are imposed on the line current. Even though this method meets the reactive power requirement of the load when the supply voltage distortion occur and the same are imposed on the line current also, where the line current still remains non-sinusoidal even after compensation.

In this paper the instantaneous reactive power algorithm has been used for shunt active filter with some modification that can effectively compensates the harmonics caused by source side distortion also. This proposed method overcomes this drawback by preprocessing supply voltage using park's transformation for that we are using only the fundamental positive sequence component of source voltage for reference current calculation. Control block diagram and operational principles are discussed below. This proposed method can effectively compensate the harmonics and reactive power even when the source voltage is unbalanced.

2. CONTROL STRATEGY

Most of the active filters are designed based on the instantaneous reactive power algorithm. The instantaneous reactive power algorithm is derived based

on the dq0 transformation, where they can calculate the current compensation based on a two-axis system [6]. In this method, the voltage and load current were first transformed into two-axis representation. The instantaneous real and instantaneous reactive power consumed by the loads was calculated based on this representation system. After compensation, the post compensated current in the two-axis system was required to inversely transform back to the three phase system from the grid; from this the reference signals of compensation current can be obtained.

$$I_a^* = I_m^* \sin(\omega t)$$

$$I_b^* = I_m^* \sin(\omega t - 120°)$$

$$I_c^* = I_m^* \sin(\omega t - 240°)$$

The control strategy proposed here is for making the compensated line current to be sinusoidal and balanced. Therefore the objective includes a sinusoidal reference current calculation and the current control technique for generation of switching pulses to the VSI for a sinusoidal and balanced line current. Where is the amplitude of the desired line current, the phase and frequency of the line current are obtained from the supply voltage. The magnitude of reference line current can get by regulating the DC bus voltage of VSI. The DC-link capacitance of VSI is used as an energy storage element in the system. For a lossless active filter in the steady state, the real power supply from the supply should be equal to the real load demanded, and no more real power passes through the power converter into the capacitor. Therefore the averaged dc- capacitor voltage can be maintained at the reference voltage level. For a balanced line current under unbalanced source voltage the proposed method to use one phase of source voltage as phase reference and 120 shifter. By this method the harmonics present in the source voltage are reflected in the reference line current. Therefore, a modified algorithm, by preprocessing the source voltage template is proposed to make the compensated the line current sinusoidal.

The source voltages are transformed into d-q reference frame using park's transformation. After transformation nth order positive sequence component becomes (n-1)th order component becomes (n-1)th order component and nth order component becomes (n+1)th order component in d-q reference frame. The fundamental component of source voltage becomes a dc component in d-q reference frame which should be filtered out using a low-pass filter. This filtered dc value after counter transformation into 3-phase component can be used for unit templates for reference current calculation. Thus this modification filters out the effect of source side distortion in the line current.

In order to drive the line currents to trace the reference currents an effective current control technique has to be used for generating the switching pulses of the VSI. Hysteresis control is implemented here for this purpose. In this control line currents are sensed and compared with the reference currents. The error in each phase is sent to the hysteresis control, Where in a switching pulse is generated to the upper switch of the VSI, if this error s less than the lower hysteresis band and a switching pulse is generated to the lower switch of the VSI if the error is found more than the upper hysteresis band.

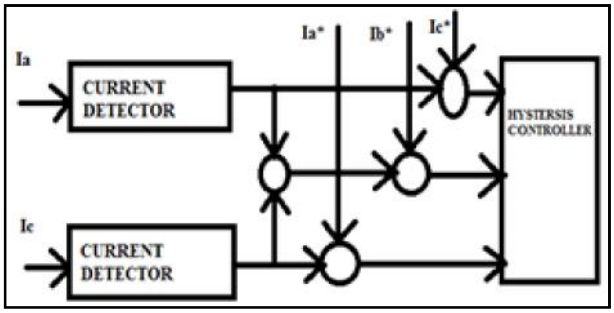

Fig.1 Block diagram for control strategy

3.PROPOSED METHOD

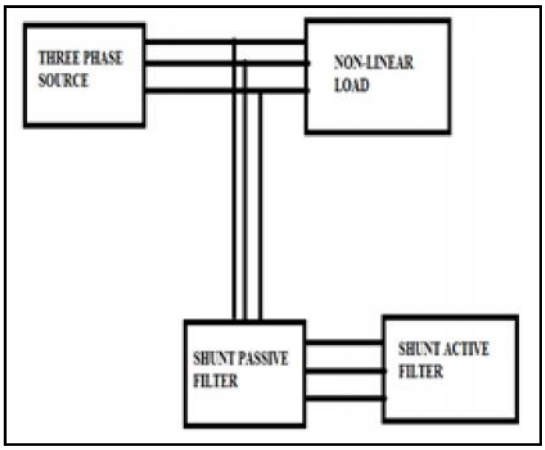

Fig.2 Block diagram for series combination of shunt active and passive filters

The Figure 2 represents three-phase source and non-linear load. Where the shunt passive filter and shunt active filter are connected in series with the line. Passive filter provides cost effective mitigation for harmonics and reactive power from supply. Active filter can effectively

compensate the harmonics and can meet the reactive power demand. The hybrid filter with series combination of active filter and passive filter reduces the rating of active filter, which also improves the filtering characteristics and reduces the precise tuning of passive filter.

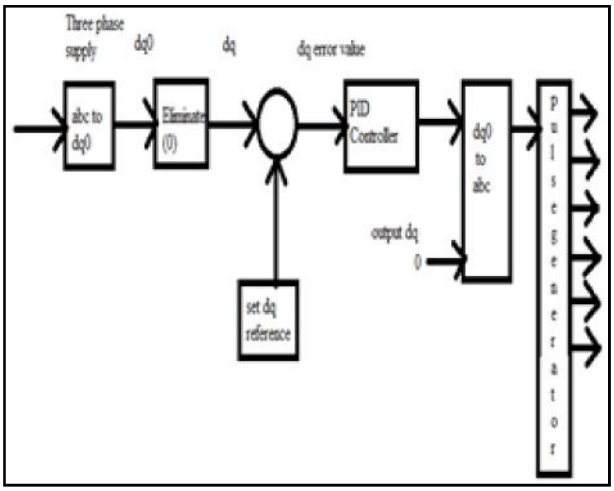

Fig.3 Block diagram for controller

The Figure 3 represents the controller block diagram. Where three phase supply from the grid and they are converted into dq0 transformation. By eliminating the 0th term we get dq alone, setting dq reference value by comparing the actual value and reference value we get dq error value.PID controller output depends on the erroneous value. Then converting dq0 to abc value they are given as input to the pulse generator, by varying the amplitude can generate six pulse and given as input to the three-phase inverter.

4. SIMULATION RESULTS

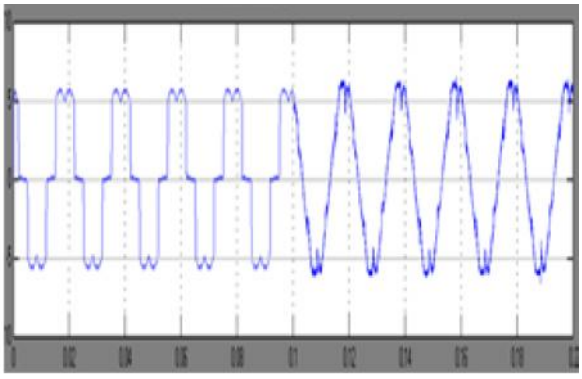

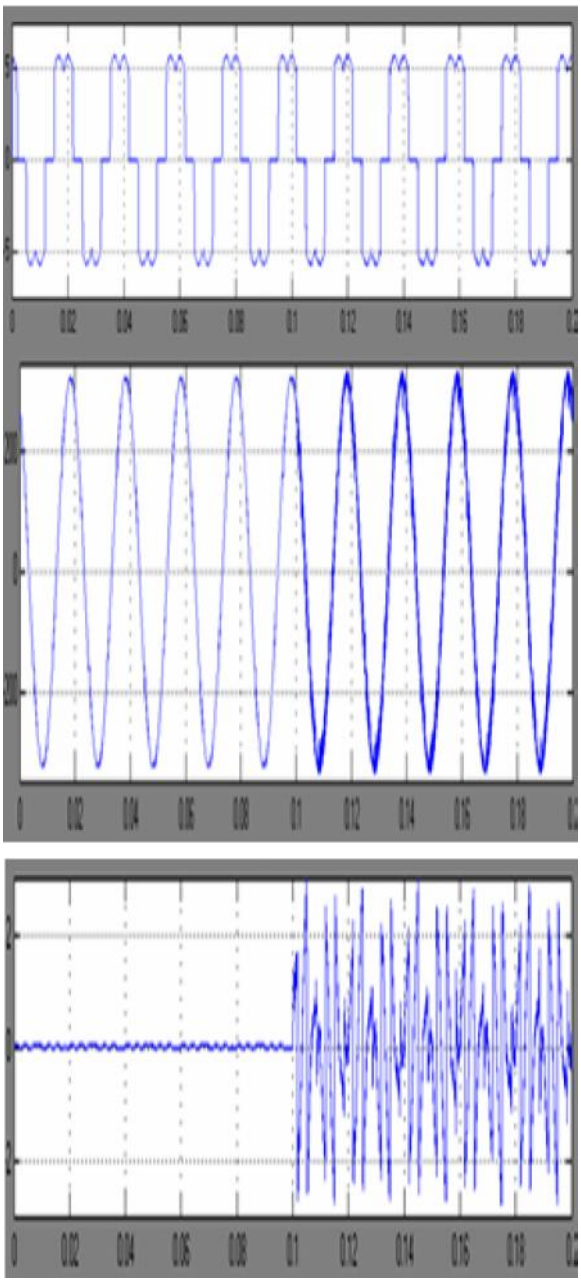

Fig.4 simulation result for series combination of hybrid filter

Table 1 TDD Values for Various Parameters

	Reactive Power (KVAR)	Filter Inductance (mH)	Filter Capacitance (μF)
5^{th} harmonics (Q=40)	0.5	40	10
7^{th} harmonics (Q=40)	0.5	20.4	10
11^{th} harmonics (Q=50)	1	4.2	20

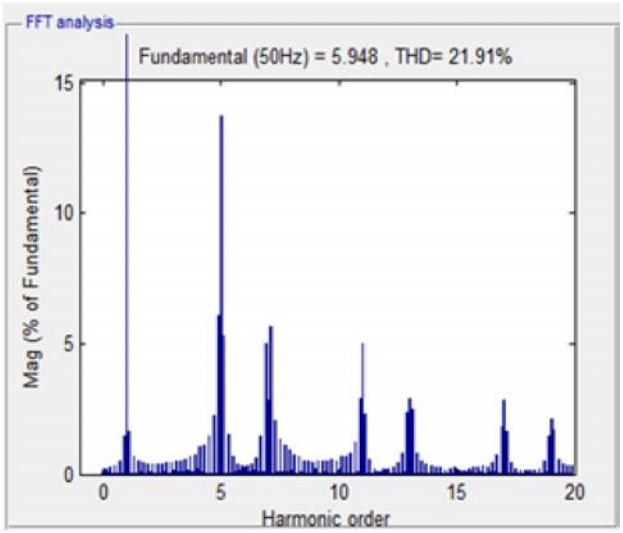

Fig.5 FFT analysis for hybrid filter in series combination

The active filter parameters are Lc=3.35mH, Rc=0.4 Ohms, DC-link capacitance CDC= 2200µF, DC-link reference voltage Vdc,ref= 400Volts for series Hybrid filter topology. Fig1.3 shows the simulation results for series combination of passive and active filter. The source voltage (Vs) is having aTHD of 12.21%, and the load current (Iload) having a THD of 21.91%. The line current(Is) after compensation is having 7.33%. The peak value of supply current is found less than the peak value of load current that shows the supply current is carrying only the active component of load current and active component of compensating current. The DC-link voltage of the VSI is maintained at 400Volts.

To drive the line currents to trace the reference currents an effective current control technique has to be used for generating the switching pulses for the VSI. Hysteresis control is implemented for this purpose. In this control the line current are compared and sensed with the reference current. Therefore this modification filters out the effect of source side distortions in the line current.

Table 2 Passive Filter Parameters

	Source Voltage (Vs)	Load Current (I_{load})	Line Current (I_{line})	Compensating Current (I_c)
Series Combination of Hybrid Filter	25.23	30.65	21.91	25.18

The topology of hybrid filters are simulated using MATLAB/SIMULINK and the results are compared under non-ideal supply voltage with a 0.1pu 3rdm harmonic negative sequence component in the source voltage. The rms value of the fundamental component is 230Volts. The various design values of passive filter are shown in Table2.

5. CONCLUSION

The results show the use of hybrid filter topology for harmonic and reactive power compensation. However, hybrid filter topology with a series combination of active and passive filters is installed in place of an already existing passive filter, to make efficient. The passive filter performance might have affected due to changes in the system parameters. This topology helps in improving the performance of passive filter and the active filter can be used at a lower rating. In this paper, a new algorithm has been proposed to improve the active filter performance under nonideal main voltages. The performance of control strategy used here is simple and effectively compensates the load generated harmonics and nullifies the effect of source voltage harmonics in the line.

REFERENCES

[1] Bhim Singh, Kamal Al-Haddad and Ambrish Chandra, “A Review of Active Filters for Power Quality Improvement”, IEEE, Vol.46, No.5, Oct.1999.

[2] Bhim Singh and Vishal Verma, “An Indirect Current Control of Hybrid Power Filter for Varying Loads”, IEEE Vol.21, No.1, Jan.2006.

[3] Adil M. Al-Zamil and David A. Torrey, “A Passive Series, Active Shunt Filter for High Freedom”, in Modern Mechanical Engineering, 2011, Vol.1, pp.47-55.

Indian Journal of Engineering, Science, and Technology (IJEST)

(ISSN: 0973-6255)
(A half-yearly refereed research journal)

Information for Authors

1. All papers should be addressed to The Editor-in-Chief, Indian Journal of Engineering, Science, and Technology (IJEST), Bannari Amman Institute of Technology, Sathyamangalam - 638 401, Erode District, Tamil Nadu, India.
2. Two copies of manuscript along with soft copy are to be sent.
3. A CD-ROM containing the text, figures and tables should separately be sent along with the hard copies.
4. Submission of a manuscript implies that : (i) The work described has not been published before; (ii) It is not under consideration for publication elsewhere.
5. Manuscript will be reviewed by experts in the corresponding research area, and their recommendations will be communicated to the authors.

Guidelines for submission

Manuscript Formats

The manuscript should be about 8 pages in length, typed in double space with Times New Roman font, size 12, Double column on A4 size paper with one inch margin on all sides and should include 75-200 words abstract, 5-10 relevant key words, and a short (50-100 words) biography statement. The pages should be consecutively numbered, starting with the title page and through the text, references, tables, figure and legends. The title should be brief, specific and amenable to indexing. The article should include an abstract, introduction, body of paper containing headings, sub-headings, illustrations and conclusions.

References

A numbered list of references must be provided at the end of the paper. The list should be arranged in the order of citation in text, not in alphabetical order. List only one reference per reference number. Each reference number should be enclosed by square brackets.

In text, citations of references may be given simply as "[1]". Similarly, it is not necessary to mention the authors of a reference unless the mention is relevant to the text.

Example

[1] M.Demic, "Optimization of Characteristics of the Elasto-Damping Elements of Cars from the Aspect of Comfort and Handling", International Journal of Vehicle Design, Vol.13, No.1, 1992, pp. 29-46.

[2] S.A.Austin, "The Vibration Damping Effect of an Electro-Rheological Fluid", ASME Journal of Vibration and Acoustics, Vol.115, No.1, 1993, pp. 136-140.

SUBSCRIPTION

The annual subscription for IJEST is Rs.600/- which includes postal charges. To subscribe for IJEST a Demand Draft may be sent in favour of IJEST, payable at Sathyamangalam and addressed to IJEST. Subscription order form can be downloaded from the following link http:// www.bitsathy.ac.in./ ijest.html.

For subscription / further details please contact:

IJEST
Bannari Amman Institute of Technology
Sathyamangalam - 638 401, Erode District, Tamil Nadu Ph: 04295 - 226340 - 44
Fax: 04295 - 226666 E-mail: ijest@bitsathy.ac.in Web:www.bitsathy.ac.in

Indian Journal of Engineering, Science, and Technology

Volume 11, Number 1, January - June 2017

CONTENTS